



No. 94 – December 1998

Successful Commissioning of FORS1 – the First Optical Instrument on the VLT

I. APPENZELLER¹, K. FRICKE², W. FÜRTIG¹, W. GÄSSLER³, R. HÄFNER³, R. HARKE², H.-J. HESS³, W. HUMMEL³, P. JÜRGENS², R.-P. KUDRITZKI³, K.-H. MANTEL³, W. MEISL³, B. MUSCHIELOK³, H. NICKLAS², G. RUPPRECHT⁴, W. SEIFERT¹, O. STAHL¹, T. SZEIFERT¹, K. TARANTIK³

¹Landessternwarte Heidelberg, ²Universitäts-Sternwarte Göttingen, ³Universitäts-Sternwarte München, ⁴ESO Garching

1. Introduction

1.1 The Project

FORS, the **FO**cal **R**educer/low dispersion **S**pectrograph, was the first VLT instrument to be designed and built outside ESO. Following a Call for Proposals in 1990, the contract to realise the project was awarded in 1991 to a consortium of three German astronomical institutes (Landessternwarte Heidelberg and the University Observatories of Göttingen and Munich). Due to its large variety of observing modes, a heavy demand for observing time was expected for the envisaged instrument. Therefore, ESO decided from the beginning to order two nearly identical instruments from the consortium. An account of the start of the project is given in [1]. In April 1992 the Preliminary Design Review was held followed by the Final Design Review in February 1994. Immediately afterwards, the consortium started to transform the approved design into hardware. The performance of the instrument and its components was continuously tested in the laboratory during the different stages of

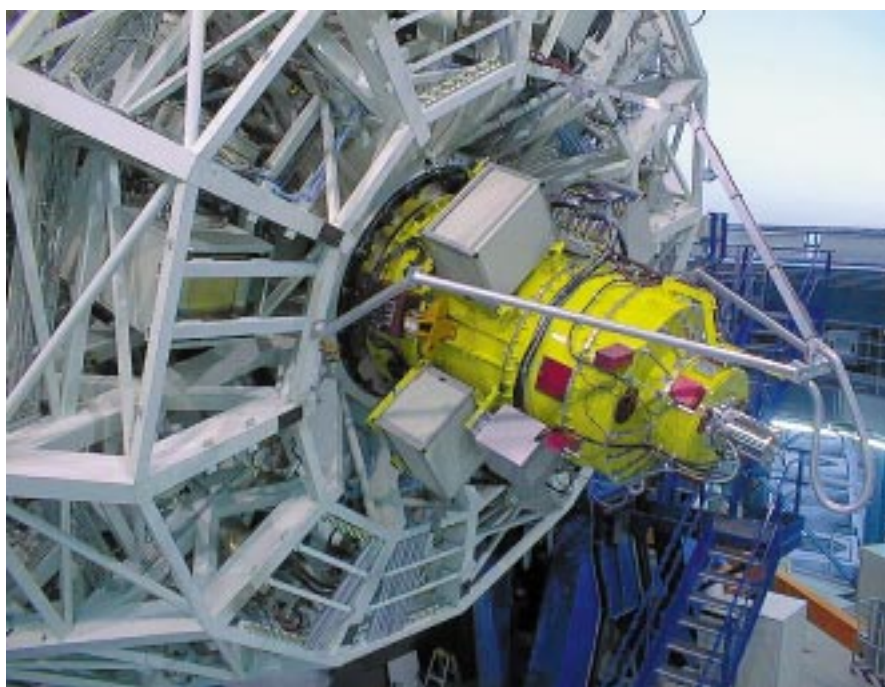


Figure 1: FORS1 installed on UT1. The instrument with the electronics boxes is well visible as well as the tripod on the M1 cell that carries the cable hose. This cable hose (a flexible metal hose) contains all electric power, LAN and cooling water lines for FORS.



Figure 2: FORS1 on the telescope simulator during flexure tests in the integration hall of DLR at Oberpfaffenhofen near Munich.

manufacturing and assembling. In November 1996 extensive tests of the integrated FORS1 instrument were started in an Integration Facility of the Deutsche Forschungsanstalt für Luft- und Raumfahrt (DLR) in Oberpfaffenhofen near Munich. A telescope and star simulator allowed to tilt and rotate the instrument and to simulate stars in the field of view. Electro-mechanical functions, image motion due to flexure, optical performance, the calibration units and the instrument-related software were checked for their conformity with the specifications given by ESO and were optimised if deemed necessary. For details see [7] and [8].

Within the consortium the tasks were distributed as follows:

- Heidelberg: optics, data reduction software, telescope and star simulator
- Göttingen: mechanics, auxiliary devices
- Munich: instrument-related software, electronics, project management

The detector system, based on a SiTe 2048 × 2048 CCD with 24- μ m pixel size, was developed by ESO.

The manufacturing of the twin instrument FORS2 will be completed by the end of 1998. After the performance tests, which will take about half a year, FORS2 will be shipped to Paranal in summer 1999. It will be installed on VLT UT2 at the end of 1999 and released for observation in March 2000.

1.2 Design Parameters

FORS has been designed as an all-dioptic Cassegrain instrument for the wavelength range from 330 nm to 1100 nm and it will cover the following observing modes:

- Direct imaging with two image scales (0.2 and 0.1 arcsec/pixel, corresponding fields of view of 6.8' × 6.8' and 3.4' × 3.4', respectively)

- Low-dispersion grism spectroscopy (resolutions between 200–1800 for 1 arcsec slit width, reciprocal dispersion 44–228 Å/mm)

- Multi-object spectroscopy (MOS) of up to 19 targets with individually adjustable slits

- Long-slit spectroscopy (mask with 9 slits with fixed widths between 0.3 and 2.5 arcsec)

- Imaging polarimetry and spectro-polarimetry (linear and circular; FORS1 only)

- Echelle spectroscopy (FORS2 only), with resolutions up to about 5000 for 1 arcsec slit width, reciprocal dispersion 15–40 Å/mm

- Multi-object spectroscopy with slit masks (FORS2 only), for survey-type programmes where more than 19 objects are observed or special slit shapes are needed.

A more comprehensive description of the instrument performance is given in [2], [3] and [4]. The grisms used in FORS are described in [5].

The main scientific objective of FORS was to extend ground-based spectroscopy and photometry to significantly fainter objects than could be reached so far. Among the tasks of FORS will be the quantitative analysis of the properties of galaxies at distances up to 10 billion light-years and beyond. Thus it will become possible to obtain information on the universe in its early phases resulting in fundamental insights into the creation and development of galaxies. Investigations of clusters of galaxies and of single stars in galaxies may shed light on the nature of the dark matter. Spectroscopy of luminous stars, supernovae and planetary nebulae in remote galaxies will allow us to obtain a better knowledge of the expansion of the universe and will provide information on the origin of chemical elements outside our own Galaxy. Even in

our Galaxy new discoveries concerning e.g. the late phases of stellar evolution or the creation of stars and planetary systems are to be expected (see also [6]).

2. The Final Steps

By the beginning of 1998 the FORS project started to home in on the final round. The instrument had already been tested extensively in the DLR facility. In January ESO's Optical Detector Team delivered the final scientific CCD system, together with one of the first copies of the newly developed FIERA CCD controllers.

Another round of tests followed which also served as the "First Verification Test" specified in the contract to be done before shipping the instrument to Chile. During these tests particular attention was paid to proving that the image quality in all observing modes conformed to the specifications. During another extensive set of measurements we checked for image motion due to instrument flexure (Fig. 2). This is particularly important for FORS as a Cassegrain instrument that is subjected to wide variations in spatial orientation during tracking. The results are published in [8] and fully comply with the finite element calculations done during the design phase. Other tests included the setting accuracy of the slitlets for the multi-object spectroscopy, which is crucial for the successful use of that mode. Moreover, we tested already in Europe the complete control system, from the workstation software through the local area network connection to the software running on the three instrument local control units ("board computers") and their co-operation with the FIERA detector controller. In addition, the interface to the Telescope Co-ordination Software (TCS) was tested with the TCS simulator at ESO/Garching. All tests were passed successfully, and by the middle of June FORS was removed from the telescope simulator to be packed for shipping.

It had been decided to transport FORS by air to Chile. This meant first a transport by truck from Oberpfaffenhofen to Frankfurt airport and from there by airplane to Santiago de Chile. The packing therefore had to take into account the specific requirements of this multiple transport: The instrument was taken apart as far as necessary to allow safe packing in dedicated boxes. The boxes for the major instrument sections consisted of sturdy frames on which wooden boxes were sitting, damped by specially dimensioned coiled steel springs. All other components like drive units, electronic racks, filters, grisms, etc. were packed in aluminium containers. Altogether the shipment consisted of 22 boxes. After the transport had arrived in Santiago they were loaded onto two climatized trucks with air suspension for the final 1200-km journey to the VLT Observatory on Paranal. Thanks to the very professional way this was handled by the truck drivers, also this 2-day trip passed without problems – under the



Figure 3: Re-assembly in the Auxiliary Telescope Hall on Paranal with FORS1 on the integration stand in the background, the control cabin at right and the Cassegrain carriage (foreground left) which is used for all major transport and handling operations.

watchful eyes of the accompanying project manager.

In the meantime, the preparations on Paranal for the re-assembly of FORS1 were nearly complete: erection of a specially designed integration stand, setting up of a local-area network for our workstation and many other little things which would allow us to start integration of the instrument immediately after its arrival on the mountain.

Re-assembly in the Auxiliary Telescope Hall (ATH, Fig. 3) in the Paranal base camp went very smoothly. The instrument sections were unpacked, transport locks and dampers removed, and the main optics inserted. In parallel the electronics were activated. Finally, all instrument sections were put together on the integration flange and the detector system attached. Another round of tests involving functional checks of all motors and series of screen flats and pinhole exposures followed which proved that we were really ready for installation on the telescope.

In the morning of September 10, the ATH crane was used to put FORS1 (well packed in plastic foil to protect it against dust during the following 3-km journey) onto the loading area of the large Paranal air suspension truck. It is a strange feeling to watch the work of the past 9 years hover 5 metres above the ground, supported only by a couple of thin wires!

Very slowly and carefully, the truck moved up to the top of the mountain, accompanied by an escort of cars forcing all other traffic out of the way, and some colleagues constantly having an eye on the truck with its precious load (Fig. 4). After nearly one hour, the convoy arrived in front of UT1. The following operation proved to be the most time consuming of the whole transport and installation: get-

ting FORS1 and the carriage down from the transport truck using the huge M1 cell lifting platform. The carriage with FORS1 on it was then lifted through the trap door opening onto the telescope fork base with the enclosure crane and soon afterwards FORS1 was mounted at the UT1 Cassegrain flange! Finally the CCD detector in its cryostat was attached at the FORS1 bottom end as well as the tube tripod carrying the cable hose with the electrical power, LAN and cooling water lines. The next day saw the first test of the complete FORS1 system in the telescope environment (Fig. 1) which also went with-

out problems. Next was the loading of all auxiliary optics (filters, grisms, Wollaston prism) in the corresponding openings of the filter and grism wheels.

3. At Last: First Light!

On the evening of September 15 finally everything was ready: The sky over Paranal was clear, the enclosure was opened, the telescope pointed to a photometric standard star field close to zenith, the image analysis was performed by the active optics system and the instrument shutter opened for a 10-second exposure through the Bessell V filter. The excitement in the control room was growing while the image appeared on the Real Time Display station: the stars looked neatly small and round – we had successful First Light! The camera focus had been pre-set to the value calculated according to the current temperature, and as the following series of exposures showed this was exactly the right setting.

The rest of this night and the subsequent ones were used to conduct a quick series of observations in all instrument modes to confirm that the overall performance was as expected. In the fourth night a thorough verification programme began during which we made exposures in all observing modes, with all available filters and grisms. Altogether about 20 Gb of data were taken during the 21 nights of the first commissioning period. Some of these data were reduced in a preliminary way and made public immediately (see <http://www.eso.org/outreach/press-rel/pr-1998/pr-14-98.html> and <http://www.eso.org/outreach/press-rel/pr-1998/phot-38-98.html>); now work is going on with the remainder to prove that the instrument indeed fulfils the specifications. A preliminary assessment is given in the following section.



Figure 4: FORS1 on its way to the telescope.

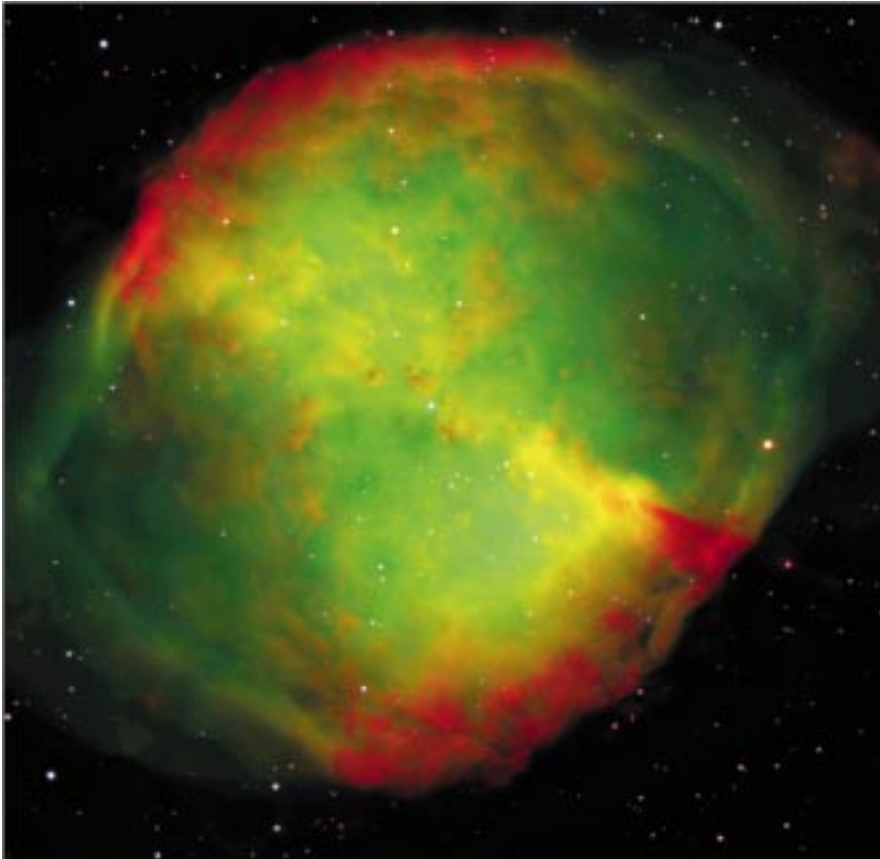


Figure 5: Colour image of the Dumbbell planetary nebula (M 27), obtained on September 28, 1998. This is a three-colour composite based on two interference ([OIII]) at 501 nm and 6 nm FWHM – 5 min exposure time; H-alpha at 656 nm and 6 nm FWHM – 5 min) and one broadband (Bessell B at 429 nm and 88 nm FWHM; 30 sec) filter images. North is up; East is left.

4. Preliminary Results

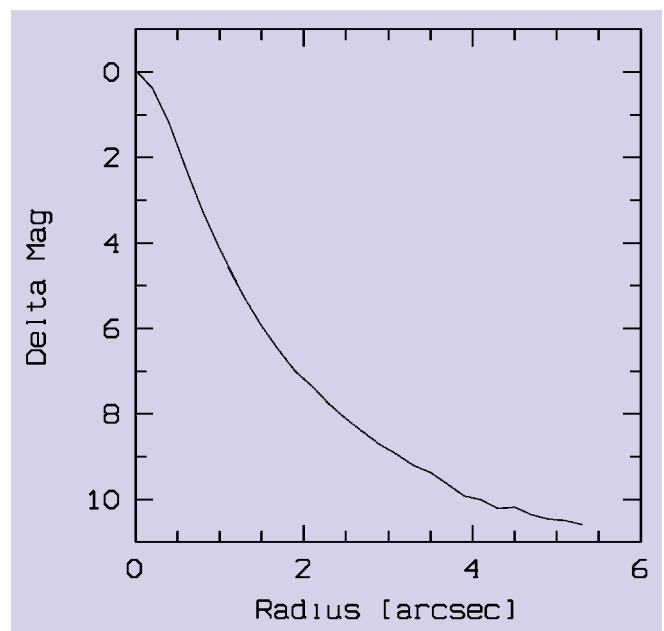
During the first commissioning phase, all observing modes of FORS1 were systematically tested with astronomical targets. The commissioning tests span a very wide range from photometric calibration through astrometric tests to extensive polarimetric observations. The second main topic during this phase was the proper interaction between telescope, instrument and the software user interfaces (see below). Most optical tests were done both in high and standard resolution mode and for a large number of optical components. Although these repetitive tests dominated our work we also obtained some eye-catching souvenirs, e.g. observing the splendid face-on spiral galaxy NGC 1232 and the Dumbbell nebula M27 (Fig. 5), both of which fit very well in the field of view in standard resolution mode.

After attaching FORS1 to the telescope, the standard maintenance procedures for preparing the instrument for astronomical work were executed. They include an automatic check of all electromechanical functions, insertion of optical components as well as the alignment of CCD, gratings and Wollaston prism. At the end of this stage the instrument was ready for the "first astronomical light". This first light was used for some initialisation procedures like telescope/instrument focusing or deter-

mination of the angle between the CCD rows/columns and the telescope axes. After this was done, the instrument was ready for astronomical work. The first observations were performed with an engineering Instrument Control Panel which allows the execution of single exposures. Later on, FORS templates as executed by BOB (the broker of observation blocks) were used.

The Telescope Control Software with the real telescope behind it and real sky images constituted two new interfaces for the FORS Software. They introduced modifications in its uppermost layers, i.e. in the Observer Support Software (OSS), in the FORS templates and in the Observation Software (OS). The remaining software modules i.e. the

Figure 6: Profile of a stellar point spread function in standard resolution mode.



Maintenance and Instrument Control Software were working perfectly almost without any modifications.

The Observer Support Software is a Graphical User Interface based on ESO SKYCAT, which will be used for the preparation of observations in all observing modes. It allows e.g. the preparation of the MOS set-up, i.e. it specifies the telescope pointing position, the telescope rotator position and assigns targets and MOS slits. The astronomer will use this tool in advance for preparation of the observations.

The FORS templates provide support for the following observing modes: imaging (IMG), imaging polarimetry (IPOL), long-slit spectroscopy (LSS), multi-object spectroscopy (MOS) and multi-object spectropolarimetry (PMOS). For each mode two templates exist: one for internal calibration (screen flat and wavelength calibration) and the other for science observation and external calibration (sky flat and standard stars). Templates necessary for all modes are collected in the category ALL (e.g. dark, focus or acquisition templates). The templates are built in such a way that all features of FORS can be used in their full variety.

Observation Software is triggered by the FORS templates to perform the set-up of instrument, detector and telescope and to execute the exposure. It writes also the header information in the output FITS file. In interaction with FORS templates, this module is also responsible for the alignment of targets and slits for spectroscopic observations.

One of the main characteristics of FORS is the very high stiffness of the instrument. Any motion of the image on the detector would degrade the instrument performance.

Therefore, a passive flexure compensation scheme was part of the FORS design. The passive system compensates any motion of the collimating optics by tilting the camera.

Tests with our telescope simulator confirmed that the internal image motion from the focal plane of the telescope to the focal plane of FORS is smaller than a quarter of a pixel during long exposures of one hour in standard and two hours in high-resolution mode.

External flexure and motions of FORS relative to the guide probe and the guiding accuracy were tested with a long time series observation of an empty field, which showed that the external flexure and the guiding can be kept within a fraction of a pixel during several hours of observing time and thus complies with the contractual specifications.

In direct imaging, the image quality measured on the detector was always limited by the outside seeing. Most of the time it was better than the values indicated by the DIMM seeing monitor and always compatible with the measurements by the adapter guide probe. The best FWHM values achieved range from 0.48" for a 4-min. exposure in the U band to 0.35" in the I band (1 min.). No image degradation due to the FORS1 optics could be detected over the whole field of view. The variation of the stellar FWHM over the field is less than 3% with both collimators. A composite PSF profile for the standard resolution collimator is shown in Figure 6. The radius of the PSF 10 mag below the peak bright-

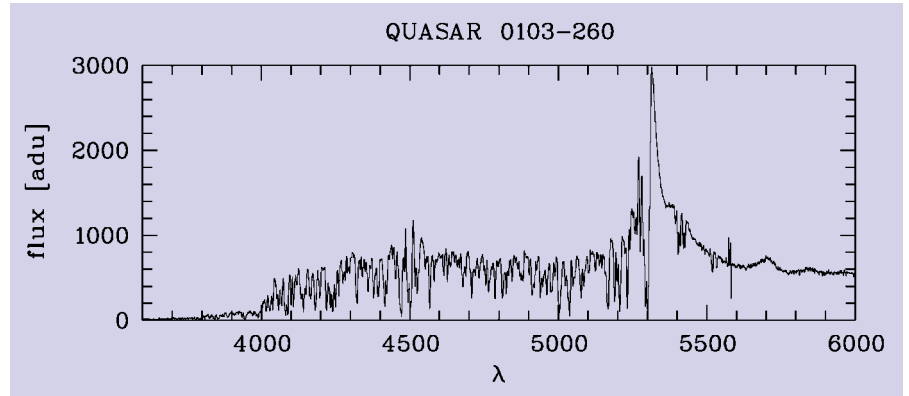


Figure 7: A spectrum of the quasar Q0103-260. The quasar shows a prominent Lyman alpha forest.

ness is about 4", an excellent value.

The characteristics of all grisms were analysed in long-slit and multi-object mode using test observations of various different types of targets. The measured spectral resolutions were found to match very well the theoretically calculated values for two-pixel sampling. As an example we present in Figure 7 a section of the spectrum of the distant quasar Q0103260 (visual magnitude $V = 18.8$, redshift $z = 3.36$). This spectrum is based on a 30-minute FORS exposure taken with a 1.0" slit and the 600B grism (600 lines/mm blazed in the blue spectral range). The

prominent emission line at 530 nm is the Lyman- α resonance line of atomic hydrogen, redshifted from 122 nm to 530 nm. To the left of the Lyman- α emission line we see clearly the "Lyman- α forest" formed by numerous Lyman- α absorption lines of hydrogen clouds of lower redshift located between the quasar and us. Q0103-260 is a particularly interesting object for studying the Lyman forest since this quasar is in a region close to the south galactic pole with its exceptionally low density of foreground stars and foreground galaxies. Therefore, it will be possible to obtain with FORS on the VLT very deep images and spectra of faint very distant objects in the field around this quasar in order to search for objects that may be connected to the hydrogen absorption features in the spectrum of the quasar.

Several multi-object spectra were also taken to test the functionality of the object acquisition and the instrumental behaviour in the MOS mode. In Figure 8 the spectra of 19 stars (including several Be stars) in the open star cluster NGC330 in the Small Magellanic Cloud are shown.

Imaging polarimetry was done for a sample of unpolarised and polarised standard stars, both for linear and circular polarimetry. Systematic errors due to the fact that our retarder plates are built as mosaics are less than $2 \cdot 10^{-4}$. Also linear and circular spectropolarimetry was done to calibrate the angular zero point of the half-wave plate as a function of wavelength and to evaluate possible cross-talk between the Stokes parameters. As an example, the circular polarisation of the 14.8-magnitude magnetic white dwarf GD229 is shown in Figure 9. The sharp features in the polarisation spectrum around 420 nm, 530 nm, 630 nm and 710 nm correspond also to broad 'absorption' features in the flux spectrum. Most of those can be explained by stationary Zeeman transitions in a magnetic field of 25 to 60 MG. The very low noise of 0.15% was reached with two exposures of 10 minutes. At this level the noise is in good agreement with the photon noise and no systematic effects appear.

As pointed out above, FORS was developed mainly to do spectroscopy

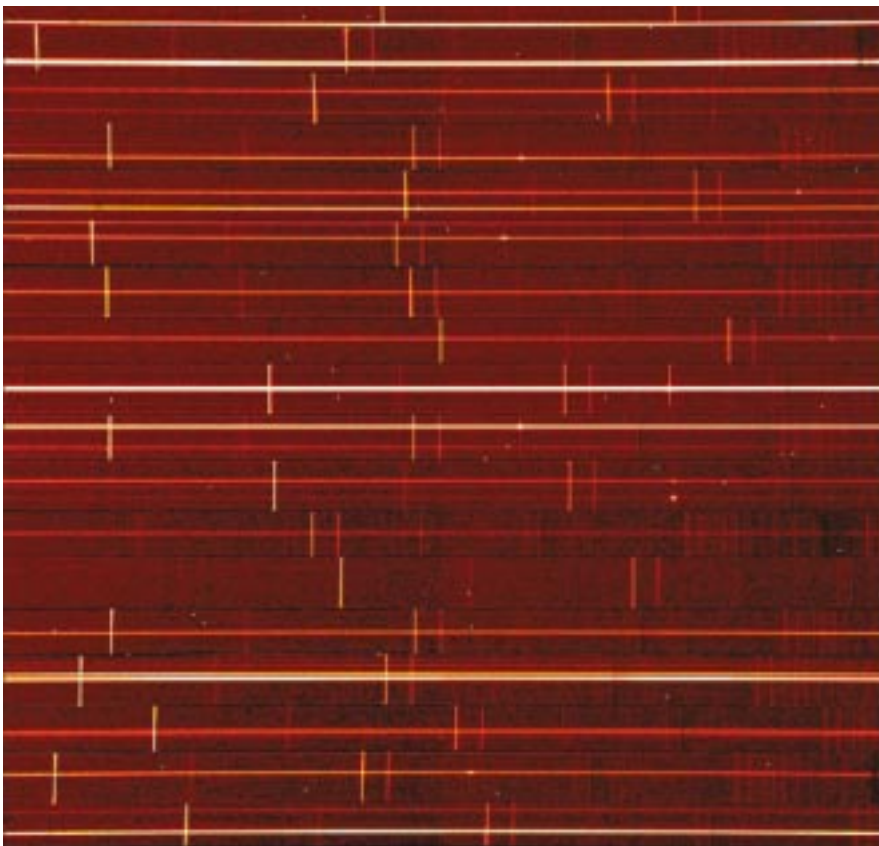


Figure 8: Multi object spectroscopy of stars located in the open cluster NGC330 of the Small Magellanic Cloud, exposure time 6 minutes. The spectra appear as bright lines spanning the full field in horizontal direction. The shorter, bright vertical lines are spectral emission lines originating in the terrestrial atmosphere (airglow); they show the extent of the individual slits. Note that in some slits more than one star spectrum has been registered, thus further increasing the observing efficiency.

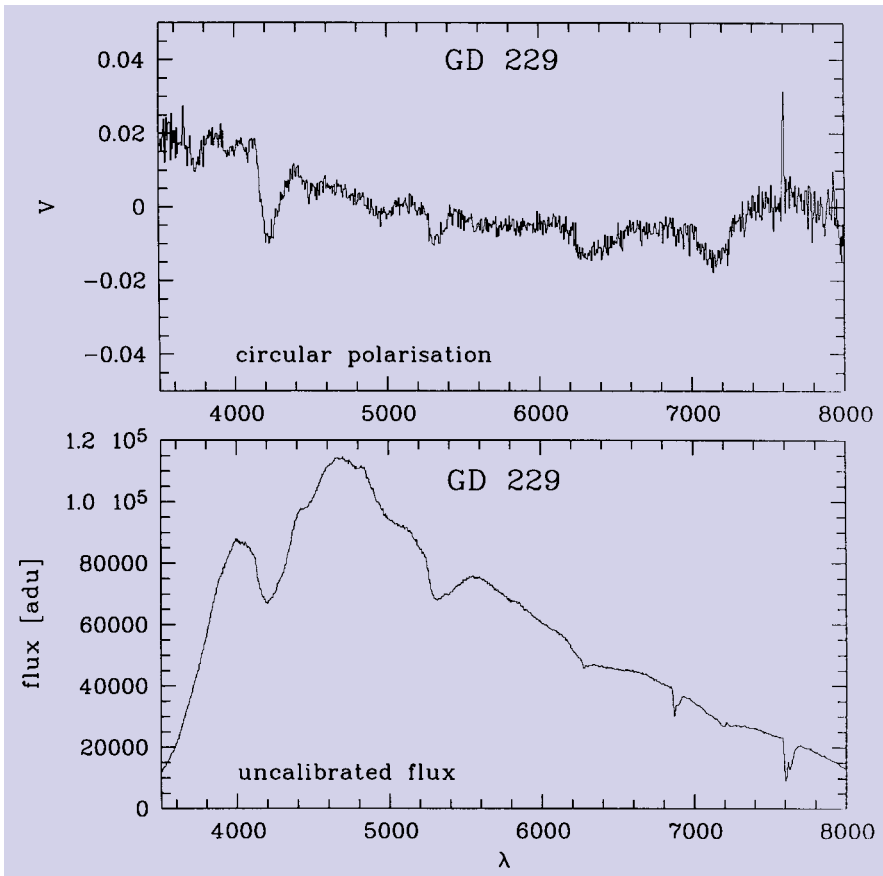


Figure 9: Circular spectro-polarimetry of the magnetic white dwarf GD229. The amount of circular polarisation is shown on the top and compared to the flux spectrum below.

on very faint objects. Therefore, we made spectroscopic test observations of distant galaxies up to 25 magnitude in R and I. Moreover, we successfully obtained spectra of faint gravitational arcs around two galaxy clusters. The reduction and evaluation of these data is still in progress.

5. A Bright Future Ahead

The FORS schedule foresees a second commissioning period after the assessment of the data from the first commissioning; after this the instrument is officially handed over to ESO who performs one week of Science Verification in January 1999. The beginning of Observing Period 63 on April 1, 1999 marks the start of regular observations of FORS on UT1 and the arrival of the first Visiting Astronomers on Paranal. By that time also a core team of telescope and instrument operators will have taken up duty to carry out the approved observing programmes. 182 proposals have been submitted for observations with FORS1 alone during its first 6 months of service – proof of trust that the instrument will live up to the expectations! And the extrapolation of our experience gained during the commissioning truly lets us expect that FORS1 on the VLT will be a world-class facility for the exploration of the very faintest objects.

6. Acknowledgements

The FORS project would not have been possible without the contributions of numerous people in the VLT Instrument Consortium and in ESO. We would like to thank all those who have contributed to this ambitious project, especially the members of the workshops of the participating observatories. The project would not have been successful without a co-operation between the VIC and ESO teams which was, through the entire duration, dominated by the common goal of delivering a superb instrument to the astronomical community of ESO's member countries and characterised by an excellent personal relationship between all team members.

Our special thanks are due to our former collaborators in Heidelberg (C. Hartlieb, S. Möhler, R. Östreicher, L. Schäffner), Göttingen (F. Degenhardt, K.-H. Duensing, U. Duensing, S. Gong, T. Nguyen, R. Pick, V. Radisch, H. Renziehausen, M. Ronnenberg, T. Töteberg, W. Wellem) and Munich (H. Bönnhardt, H. Geus, A. Hebenstreit, S. Kieseewetter-Köbinger, W. König, W. Mitsch, F. Mittermeier, M. Roth, P. Well).

The valuable contributions by ESO staff during the FORS development phase (A. Balestra, J. Beletic, C. Cumani, S. Deiries, B. Delabre, S. D'Odorico, R. Donaldson, R. Dorn, G. Filippi, R. Gilmozzi, G. Hess, O. Iwert, H. Kotzlowski, M.

Kraus, J.-L. Lizon, G. Monnet, W. Nees, R. Reiss, G. Raffi, R. Warmels, G. Wieland) and the installation and commissioning phase (H. Bönnhardt, J. Brynnel, M. Cullum, F. Franza, H. Gemperlein, P. Gray, G. Ihle, I. Osorio, P. Sansgasset, J. Spyromilio, A. van Kesteren, A. Walander, K. Wirenstrand) are gratefully acknowledged.

The Instrument Science Team (S. Cristiani, S. di Serego Alighieri, Y. Mellier, P. Shaver, J. Surdej) gave many constructive recommendations.

The FORS test team benefited from the DLR management (H. Holzach) and the local workshop. Last but not least: The FORS project could not have been realised without the financial support by the German Federal Ministry of Education, Science, Research and Technology (BMBF grants 05 3HD50A, 053 GO10A and 053 MU104).

References

1. Appenzeller, I., Rupprecht, G.: FORS, The Focal Reducer for the VLT, *The Messenger* No. 67, p. 18, 1992.
2. Mitsch, W., Rupprecht, G., Seifert, W., Nicklas, H., Kieseewetter, S.: Versatile multi object spectroscopy with FORS at the ESO Very Large Telescope, in: *Instrumentation in Astronomy VIII*, eds. C. Crawford and E.R. Craine, SPIE Proceedings Vol. 2198, p. 317, 1994.
3. Bönnhardt, H., Möhler, S., Hess, H.-J., Kieseewetter, S., Nicklas, H.: Design Benchmarks of the FORS Instrument for the ESO VLT, in: *Scientific and Engineering Frontiers of 8-10m Telescopes*, eds. M. Iye and T. Nishimura, Universal Academic Press Inc. Tokyo, p. 199, 1995.
4. Möhler S., Seifert, W., Appenzeller, I., Muschielok, B.: The FORS Instruments for the ESO VLT, in: *Calibrating and Understanding HST and ESO Instruments*, ed. P. Benvenuti, ESO Conference and Workshop Proceedings No. 53, p. 149, 1995.
5. Fürtig, W., Seifert, W.: A set of grisms for FORS, in: *Tridimensional Optical Spectroscopic Methods in Astrophysics*, eds. G. Comte and M. Mercein, ASP Conference Series Vol. 71, p. 27, 1996.
6. Appenzeller, I., Stahl, O., Kieseewetter, S., Kudritzki, R.-P., Nicklas, H., Rupprecht, G.: Spectroscopy of faint distant objects with FORS, in: *The Early Universe with the VLT*, ed. J. Bergeron, ESO Astrophysics Symposia Proceedings, Springer-Verlag, p. 35, 1997.
7. Seifert, T., Appenzeller, I., Fürtig, W., Seifert, W., Stahl, O., Bönnhardt, H., Gässler, W., Häfner R., Hess, H.-J., Mantel K.-H., Meisl, W., Muschielok, B., Tarantik, K., Harke, R., Jürgens, P., Nicklas, H., Rupprecht, G.: Testing FORS – the first Focal Reducer for the ESO VLT, in: *Optical Astronomical Instrumentation*, SPIE Proc. Vol. 3355, p. 20, 1998.
8. Nicklas, H., Bönnhardt, H., Fürtig, W., Harke, R., Hess, H.-J., Jürgens, P., Muschielok, B., Seifert, W., Stahl, O., Tarantik, K.: Image motion and flexure compensation of the FORS Spectrographs, in: *Optical Astronomical Instrumentation*, SPIE Proc. Vol. 3355, p. 93, 1998.

I. Appenzeller
iappenze@mail.lsw.uni-heidelberg.de

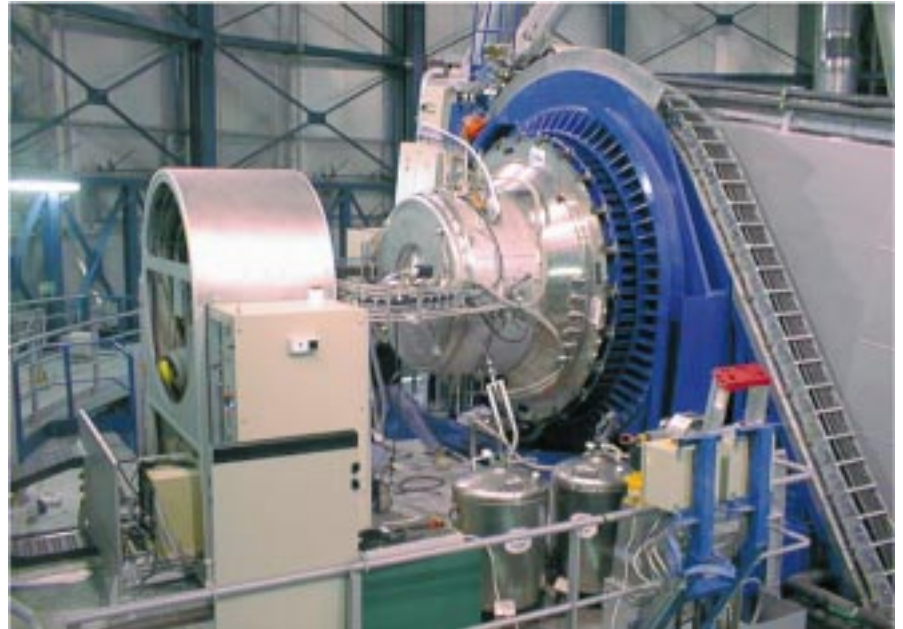
ISAAC Sees First Light at the VLT

A. MOORWOOD, J.-G. CUBY, P. BIEREICHEL, J. BRYNNEL, B. DELABRE, N. DEVILLARD, A. VAN DIJSSeldonk, G. FINGER, H. GEMPERLEIN, R. GILMOZZI, T. HERLIN, G. HUSTER, J. KNUDSTRUP, C. LIDMAN, J.-L. LIZON, H. MEHRGAN, M. MEYER, G. NICOLINI, M. PETR, J. SPYROMILIO, J. STEGMEIER

ESO, Garching and Paranal

ISAAC, the cryogenic infrared spectrometer and array camera developed by the Instrumentation Division at ESO (<http://www.eso.org/instruments/isaac/>) saw first light on the VLT on the night of 16/17 November 1998. Figure 1 shows the instrument mounted on the Nasmyth B focus of Unit Telescope 1. Visible are the 1.6-m diameter vacuum vessel surrounding the 350-kg cooled optical assembly and the co-rotator system which carries the electrical cables and closed-cycle cooler hoses to the instrument and rotates with the telescope adapter as the telescope tracks objects on the sky. ISAAC has 0.9–2.5 μm (SW) and 2–5 μm (LW) 'arms' providing imaging and spectroscopic capabilities over a maximum field of 2.5' with a variety of pixel scales and resolving powers.

The moment of first light was preceded by intense activity by the ISAAC team from Garching, assisted by their Paranal colleagues, to install this complex in-



▲ Figure 1: ISAAC as it is now mounted on the UT1 Nasmyth B adapter-rotator. The 1.6-m-diameter vacuum tank houses the 350-kg cryogenic optical assembly which is cooled by means of two closed-cycle coolers. Various gas and liquid hoses plus all the electrical cables are carried by the co-rotator system visible on the left which rotates with the adapter as objects are tracked on the sky.



◀ Figure 2: Colour composite image of the RCW38 star-forming complex obtained by combining short Z(0.9 μm), H(1.65 μm) and Ks(2.16 μm) exposures. Stars which have recently formed in clouds of gas and dust in this region about 5000 light-years away are still heavily obscured and cannot be seen at optical wavelengths but become visible at infrared wavelengths where the obscuration is substantially lower. The diffuse radiation is a mixture of starlight scattered by the dust and atomic and molecular hydrogen line emission. The field of view is 2.5 \times 2.5' with North at the top and East to the left and the image quality is set by the FWHM seeing of 0.4".

Figure 3: A Ks (2.16 μm) image centred on the distant radio galaxy MRC0316-257 ($z = 3.14$) obtained primarily to locate other distant galaxies for future spectroscopic observations with ISAAC. This image was obtained by combining 45 1-min exposures, taken with the telescope randomly offset by small amounts in between ("jittering") to allow subtraction of the bright sky emission. The field measures 2.5×2.5 arcmin with North at the top and East to the left. The seeing was 0.5 arcsec and the limiting magnitude is Ks ~ 22 . ▶

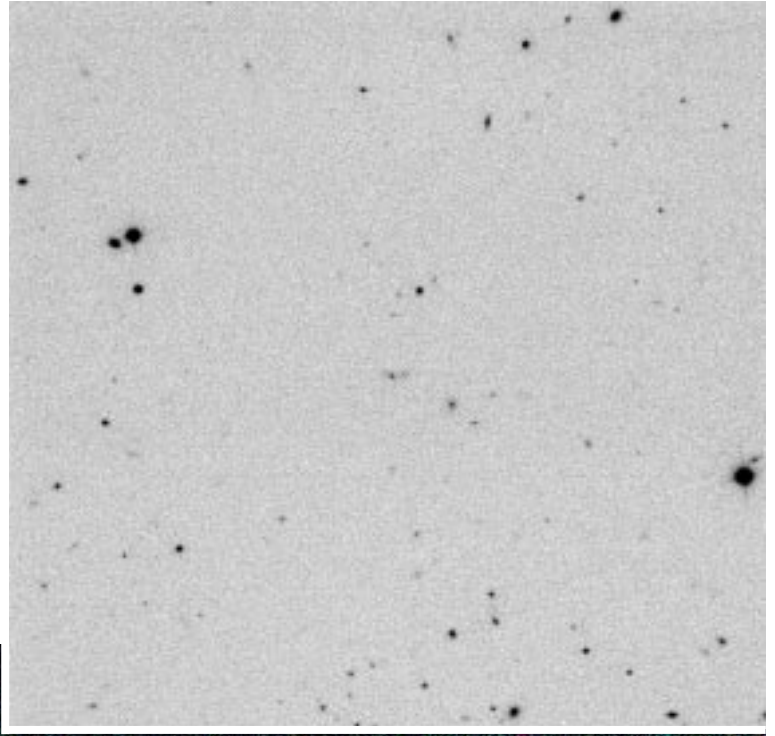
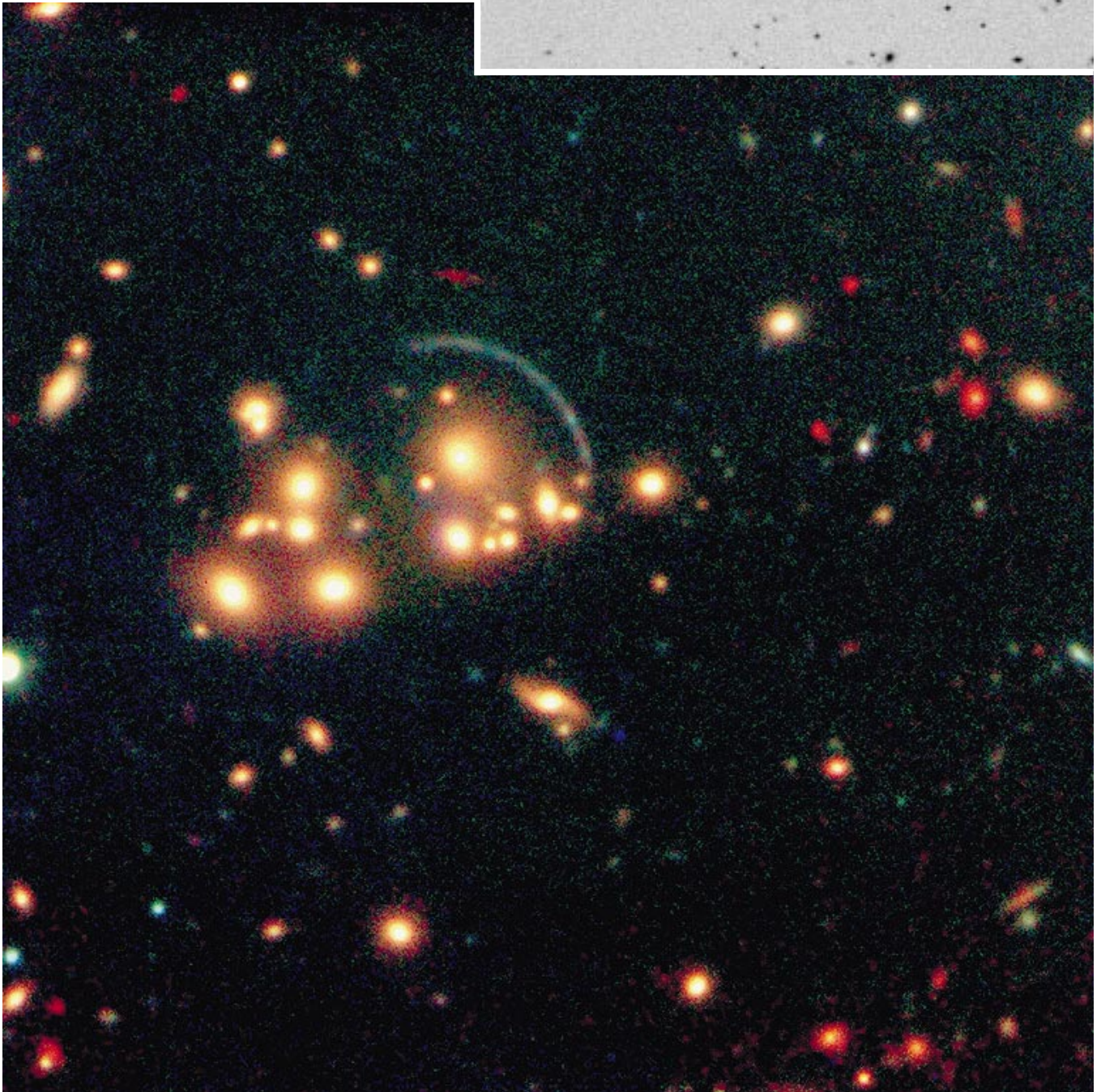


Figure 4: Colour composite image of the galaxy cluster CL2244-02 ($z = 0.33$) obtained by combining a 20-min jittered ISAAC Ks (2.16 μm) exposure with 15-min V and R exposures made with the VLT Test Camera at the UT1 Nasmyth focus. In addition to the prominent blue arc, produced by gravitational lensing of a galaxy at redshift $z = 2.24$, there are also notable, very red arcs, both closer to the centre and further out which were only detected in the infrared image indicating that these lensed galaxies are either not forming stars or are much more distant. The field size is about 1.5×1.5 arcmin with North at the top left and East at the lower left corner. The average seeing was around 0.5 arcsec. ▼



strument on the telescope and start the evacuation and cool-down procedure. Despite its large mass, cooling is actually achieved in only 24 hours by using a liquid-nitrogen pre-cooling circuit in addition to the closed-cycle coolers. Once operational and after focussing and aligning the instrument and telescope pupils, short exposures in the 1–2.5 μm filters quickly demonstrated the excellent combination of Paranal seeing and telescope plus instrument optical quality by delivering images with around 0.3" FWHM across the 2.5' field. During the next several nights, test images and spectra of a variety of astronomical targets were made to exercise and establish the performance of the various SW instrument modes. Due to a few technical problems encountered in this period, it was then necessary to dismount and open the instrument which, although unfortunate, was a possibility for which contingency had already been foreseen in the planning of this first test. Four days later, testing of the long-wavelength arm started and is continuing as this short report is being written in the control room on Paranal.

A first impression of the capabilities and performance offered by this new instrument is provided by Figures 2, 3, 4 and 5, which show a small selection of the images obtained so far. More images plus the first spectra obtained can be viewed at <http://www.eso.org/outreach/press-rel/pr-1998/pr-19-98.html>



Figure 5: Combination of 15-min Ks (2.16 μm) and L(3.8 μm) band images of the central region of the galaxy NGC1365 made with the Long Wavelength arm plus chopping at the telescope secondary mirror. The field is 16 \times 16" with North at the top and East to the left and shows the prominent Seyfert nucleus plus a rich complex of star forming regions extending over a region about 1 kpc across and including one almost at the nucleus to the East.

News from VLT Science Verification

The data from the UT1 Science Verifications (SV) have been released to the ESO community on October 2, 1998, with the data relative to the Hubble Deep Field South being available worldwide. The SV data can be retrieved either from the ESO Web server at <http://www.eso.org/paranal/sv> or ask the library of your institution for the CD-ROM set containing the combined and the raw data. These CD-ROM sets were mailed in October to all astronomical institutes within ESO member states (addressed to the institute's library). Since some sets are still available, interested people may get one by contacting ESO through the above Web page.

A widely publicised editorial of the Board of Directors of *Astronomy and Astrophysics* has called for papers based on the UT1 SV data, with those submitted by November 30, 1998, and passing the peer referee process, being published in a special issue of *A&A Letters* on March 1, 1999.

With the successful installation and commissioning of FORS-1 at UT1 and the

forthcoming commissioning of ISAAC, the plans for the SV observations with these instruments are in an advanced stage of preparation. The FORS-1 SV Team has been formed (based largely on a new set of astronomers compared to UT1 SV Team), and the ISAAC SV Team is being assembled. The target selection for SV will reflect the expectations of the community, with an attempt being made to cover as far as possible the large variety of astronomical areas in which ESO astronomers are currently active.

FORS-1 SV observations will take place during the dark time in January (14–21 January, 1999), while ISAAC SV observations are planned for 18–25 February, 1999. The astronomical targets of SV will be advertised through the above SV Web in advance of the observations. The two SV data sets should be released about one month after they were obtained, as it was done for the UT1 SV data obtained with the Test Camera. The SV Teams will make every effort to provide combined and flatfielded data.

Along with the SV data, also science grade data obtained during instrument commissioning may be released. Keep watching the Science Verification Web pages for any news.

The instrument SV observations will include some of the observations for which the VLT was specifically built. With FORS, the optical spectroscopy of faint objects – especially in multi-object mode – as well as the deep imaging on a respectable field of view will demonstrate the capabilities of the VLT to a much larger degree than could be achieved by the Test Camera images.

With ISAAC, the start of near-infrared observations with a large telescope in many ways will open up completely new capabilities. By having prompt access to FORS and ISAAC science grade data astronomers in the community will have yet another, even more exciting opportunity of using and familiarising with VLT data, specifically of the kind that will be provided by UT1 to the community of successful investigators in ESO observing Period 63.

Performance of the First Two Beryllium Secondary Mirrors of the VLT

S. STANGHELLINI, A. MICHEL, ESO

During the month of September 1998 REOSC Optique in Paris successfully completed the mechanical mounting and the optical tests of the second VLT M2 mirror in Beryllium. The secondary mirror was accepted by ESO and shipped to Dornier Satellitensysteme for integration in the second Electromechanical Unit, undergoing its final dynamic acceptance testing.

The secondaries of the VLT, with their diameter of 1116 mm, are amongst the largest Beryllium mirrors ever produced. The manufacturing process, set up for the first mirror by REOSC and its subcontractor Brush Wellmann, is optimised to achieve the low mass and inertia demanded by the steering capability of the mirrors, without compromising the optical quality and the long-term optical stability. The manufacturing process, already described in a previous issue of *The Messenger* (No. 86 of December 1996), has been further optimised after the production of the first mirror. The blanks are made out of a Beryllium billet obtained by Hot Isostatic Pressing of structural grade Beryllium powder (I-220H) lightweighted by machining pockets in the back surface. Due to the hardness of the material and the depth of the pockets, there is the risk of vibration of the tool, possibly leading to its rupture. Therefore,

the material removal is done at very slow rate.

The total machining time of the back and front faces – the latter up to less than 20 μm tolerance from the final asphere – takes approximately 9 months. After the generation of the asphere by grinding, the blank is Nickel plated on both sides. The polishing is done on the Nickel layer. As the secondary mirror of the VLT is undersized, the optical surface extends up to the mechanical edge. To polish up to the edge, a lip was left at the outer rim of the first mirror, that was later cut by electromachining discharge (EDM). Although the internal stresses in the mirror were very low (estimated around 5 MPa), their release, after cutting off the lip, generated a warping which demanded further polishing.

For the second mirror REOSC has developed a method to polish up to the border without producing a turned down edge. The lip was therefore cut before Nickel plating and the subsequent polishing.

Some of the most relevant physical data of the mirrors are provided in Table 1.

The lower mass of the second mirror is due to a stricter control of the dimensional tolerances during machining and to a slight difference in the values of thickness of the Nickel plating. The vari-

ation of the mass and inertia are well within the tuning capability of the control system for the steering mechanism of the secondary unit, so that mechanical adjustment is not needed. The third and fourth mirrors (presently in production) will have characteristics similar to the second one.

The mirrors have been tested after integration in their cells and with the optical face down, therefore under conditions similar to those encountered in the telescope. The mirrors are tested against a Zerodur matrix. The measurements are performed with the mirror mounted in its cell, and with the cell fixed onto a template simulating the electromechanical unit. The radius of curvature and the conic constant of the matrix were previously measured with a Hartmann test using a null-lens, and then with a second independent null-lens for cross-check.

The specification demanded by ESO contains requirements for the so-called passive and active modes. In the passive mode the full pupil of the mirror is tested and the optical quality is deduced after removal of the effects of mirror curvature (focus error) and conic constant (3rd order spherical aberration). The slope errors are obtained after measurement against the matrix.

The active mode quality is expressed in Central Intensity Ratio (CIR) which compares the performance of the telescope to that of a diffraction-limited telescope in well-defined atmospheric conditions. The CIR is evaluated after removal of the 16 first natural modes of the primary mirror, which are corrected by the active optics of the VLT. The effects of high spatial frequency errors are calculated with a sub-pupil test (mask with sub-apertures on a mirror diameter), and their effect subtracted from the CIR to obtain the final minimum value of the CIR.

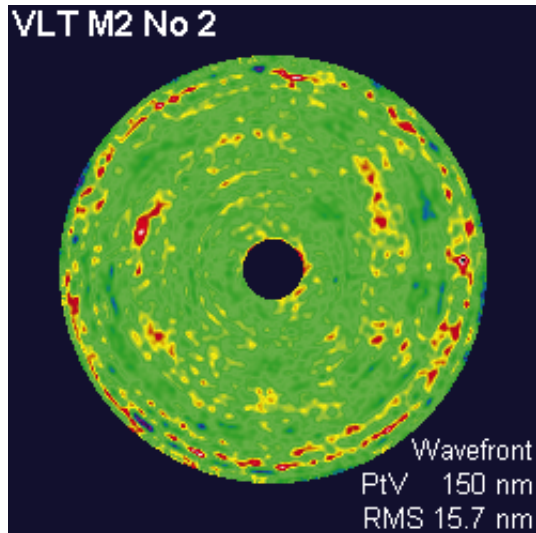
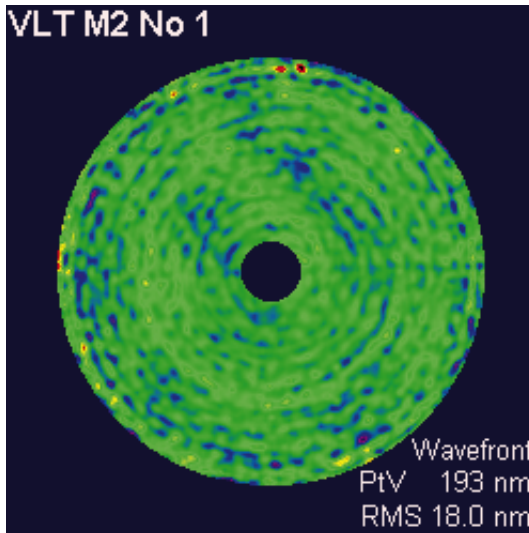
Classical checks such as micro-roughness, cleanliness and other in-

Table 1. Mechanical characteristics of the first two VLT secondaries

Characteristics	M2 Mirror #1	M2 Mirror #2
External diameter	1116 mm	
Diameter of centre hole	46 mm	
Height at mirror centre	170 mm	
Dimension of bevel at edge	< 0.2 mm	
Mirror mass	43.1 kg	41.8 kg
Total mass (M2 + mounts +cell)	52.5 kg	51.2 kg
Total moment of inertia	4.17 kg m ²	4.07 kg m ²
First eigenfrequency on three rigid points	> 635 Hz	
First eigenfrequency on the three mounts	> 365 Hz	

Table 2. Optical performance of the first two VLT secondaries

Performance	M2 Mirror #1	M2 Mirror #2
Radius of curvature	4554.62 mm	4554.91 mm
Conic constant	-1.66980	-1.67046
Optical Quality in Passive mode	0.32 arcsec RMS slope error	0.20 arcsec RMS slope error
Optical Quality in Active mode	18.0 nm RMS (Wavefront)	15.7 nm RMS (Wavefront)
Central Intensity Ratio (min.)	CIR = 97.4%	CIR = 98.1%
Microroughness	1.5 nm RMS	1.8 nm



spections were also performed. The surface quality of both mirrors is excellent and within specification.

Table 2 provides the major optical performance of the first two secondary mirrors. The two mirrors are extremely similar, with only a fraction of the budget of error allocated for the radius of curvature and the conic constant being used. REOSC was also able to improve the op-

tical quality with the polishing of the second mirror.

It is possible to conclude that while the feasibility of the Beryllium technology used had been demonstrated with the delivery of the first secondary mirror and the excellent images already obtained by the first VLT telescope, a further advance in the manufacturing process was achieved by REOSC with the recently

delivered second mirror, leading to an improvement of the optical performance and to a shorter production time. The total production of the first mirror demanded more than two years, while the second mirror was produced in around 20 months.

sstanghe@eso.org



The La Silla News Page

The editors of the La Silla News Page would like to welcome readers of the twelfth edition of a page devoted to reporting on technical updates and observational achievements at La Silla. We would like this page to inform the astronomical community of changes made to telescopes, instruments, operations, and of instrumental performances that cannot be reported conveniently elsewhere. Contributions and inquiries to this page from the community are most welcome.

(J. Brewer, O. Hainaut, M. Kürster)

News from the NTT

O. R. HAINAUT

During the last three months, the operation of the NTT has been particularly smooth; we did not experience any major problem, and the weather has been fairly cooperative. The technical downtime was of the order of 2%.

On August 12 and 13, the NTT and its team passed a very detailed "Acceptance Review", during which all the technical and operational aspects of the telescope were presented. This review constituted the formal return of the NTT from the VLT Division to the La Silla Observatory after

the Big-Bang. The review board found the technical and operational status of the telescope to be more than satisfactory; the staff, system, operation, and procedures all received excellent reviews.

The dewar of SUSI2 was suffering from vacuum losses since the installation of the instrument (cf. last issue of *The Messenger*). It has been exchanged by a new, improved dewar, which immediately worked perfectly. Also, we identified the source of a mysterious light contamination which occasionally affected the im-

ages: the lamps of the rotator and altitude encoders were not perfectly shielded. In some positions of the rotator, a part of the instrument which was not correctly blackened was reflecting the encoder light to the detector. Additional light baffles have been mounted, and the blackening of the instrument completed, resulting in the complete removal of the contamination. SUSI2 is now performing at its expected level.

Over the past couple of months, the Observation Block (OB) database in La

Silla, the OB repository in Garching, and the communication between these two have caused many problems, sometimes resulting in a degradation of the operation. While these problems were efficiently tackled by the Data Management Division, they nevertheless revealed some weaknesses in the system, which have already been partially solved by improving the structure of the OB database. A more robust version of the P2PP software (used at the telescope for the preparation of the OBs) will soon be delivered.

Since the "Big-Bang", the operation of the NTT is performed according to detailed and optimised procedures and check-lists; these have helped ensure the high reliability of the system. While these

procedures are in constant evolution, the vast majority of the NTT operation is now documented as an extensive collection of WWW-based procedures. The next step is to tackle the maintenance plan of the system; while most of the maintenance tasks are regularly performed, their execution and the corresponding procedures are currently mostly left to the experience of the team's technicians (fortunately, their experience is extensive). The maintenance plan and its corresponding procedures are now being documented in the same way as was done for the operation procedures. In addition, a vast collection of "templates" (scripts that can be automatically executed by the whole system) has been developed to measure the various para-

meters needed for the maintenance, such as the current consumed by the various motors of the rotators, the instrumental flexures and focus variations, etc. A first calibration plan will soon be implemented, and will continue to be developed and expanded in 1999. This will allow us to detect problems at an early stage, and take corrective actions before they lead to a loss of observing time.

Finally, let me announce that new versions of the EMMI and SOFI user's manuals have been released and are available on the NTT web page. They are very detailed, and include recent throughput measurements of all observing modes, as well as notes for the preparation of the observations with the "neoclassic" system (Observation Blocks, etc.).

2.2-m Telescope Upgrade: a Status Report

T. AUGUSTEIJN

The hardware modifications and the installation of the VME-based telescope control system (TCS) were finished according to schedule on the 1st of October 1998. In addition, the telescope cabling has been cleaned, the control room refurbished, and the TCS and the instrument control system (DAISY+) workstations have been installed and integrated into the local network.

At the time of writing, a direct camera is mounted at the Cassegrain focus for test purposes. We are currently in the process of testing the TCS user interface and verifying the telescope performance in preparation for the arrival of the Wide Field Imager (see previous issue of *The Messenger*). Although the current set-up is not optimal, we regularly obtain sub-arcsecond seeing and on various occasions have obtained seeing below 0.5 arcsec-

onds, demonstrating the excellent optical quality of the telescope. In combination with the well-sampled half-degree field of the WFI, the 2.2-m Telescope will be a major asset to the observing facilities at ESO. Updated information on the 2.2-m Telescope and the WFI is available on the 2p2 Team Web Page (see URL: <http://www.lis.eso.org/lasilla/Telescopes/2p2T/2p2T.html>).

Performance of CES 3.6-m Fibre Link and Image Slicers

M. KÜRSTER

Three new image slicers for the fibre link from the Coudé Echelle Spectrometer (CES) to the Cassegrain focus of the 3.6-m telescope have arrived. Their properties are summarised in the following table which compares the measured and planned resolving powers, and lists the number of slices produced by each slicer as well as the extent on the CCD of the total spectrum (all slices) in the direction perpendicular to the dispersion.

Even though the goal for the maximum resolving power has been missed by 12%, the high-resolution image slicer does make the CES by far the highest-res-

olution facility among all ESO instruments. Using the spectrograph entrance slit instead of an image slicer even higher resolving powers up to $R = 284,000$ can be achieved, albeit at the expense of a large loss in throughput.

During the commissioning period (3–7 November 1998) strong and variable cirrus clouds hampered the determination of reliable measurements of the efficiency of the whole optical train (telescope, fibre link, image slicers, spectrograph and detector). Nevertheless, it was possible to obtain some encouraging lower limits for a few wavelengths that were not

much lower than the expected values. As an example, the efficiency near 6100\AA is listed in the table for CCD #38 and less efficient CCD #34 (values in brackets). Within a few percent, all slicers yield the same throughput. Results from final efficiency measurements will be communicated when they are available.

The CES instrument is currently undergoing a refurbishment which we expect to be finalised by the end of July 1999. The major modifications foreseen for the CES include:

- An upgrade of the instrument control system to VLT standards (second VLT compliant 3.6-m instrument after EFOSC2).
- Stabilisation of the predisperser via a new drive system.
- Improving the turntable drive.
- Stabilisation of the thermal environment of the instrument by modifying the coude room.

We will continue to report all important changes on these pages.

Slicer	Resolving power		# Slices	Extent (pixels)	Efficiency at 6100 Å	
	Achieved	Planned			Lower limit	Expected
High res.	194,000	220,000	12	400	7.2% (3.6%)	8% (4%)
Medium res.	138,000	110,000	8	265	"	"
Low res.	88,000	80,000	6	168	"	"

European Site Testing at Chajnantor: a Step Towards the Large Southern Array

A. OTÁROLA¹, G. DELGADO², R. BOOTH³, V. BELITSKY³, D. URBAIN³,
S. RADFORD⁴, D. HOFSTADT¹, L. NYMAN², P. SHAVER¹, R. HILLS⁵

¹European Southern Observatory; ²SEST/Onsala Space Observatory; ³Onsala Space Observatory;
⁴National Radio Astronomy Observatory; ⁵Mullard Radio Astronomy Observatory

Abstract

The Large Southern Array is one of the highest priority projects in European astronomy today. The planned submillimetre operating wavelengths and the need to maximise the efficiency of observing time make the selection of the observatory site a fundamental issue.

1. Introduction

The last decades have seen great progress in (sub-)millimetre astronomy, leading to the design and construction of new and powerful instruments. There are now many very good 10–15-m-diameter (sub-)millimetre telescopes available to the astronomical community. In particular, the 15-m-diameter *Swedish-ESO Submillimetre Telescope* (SEST) is unique in the Southern Hemisphere. This telescope has opened the southern skies to millimetre astronomy, achieving outstanding scientific results during the last ten years (see articles in *The Messenger* No. 91, 1998).

The continuing quest for higher resolution and greater sensitivity calls for ra-

dio telescope arrays. In 1995, European interest in a millimetre array sparked the *Large Southern Array* project (LSA) with an agreement between ESO, the *Institut de Radio Astronomie Millimétrique* (IRAM), the *Onsala Space Observatory* (OSO), and the *Netherlands Foundation for Research in Astronomy* (NFRA). With the aim of achieving a total collecting area of 10,000 m² and an angular resolution better than 0.1 arcsec at a wavelength of 3 mm, this project was at the time the most ambitious plan considered for millimetre astronomy. Since the early 1980s, the US *National Radio Astronomy Observatory* (NRAO) has planned another array, the *Millimeter Array* (MMA) which is a 2000-m² array capable of working at sub-millimetre wavelengths. Both projected instruments would be sited in northern Chile, naturally suggesting collaboration.

In 1997, ESO and NRAO agreed to work together to explore a common millimetre/submillimetre array, to be financed jointly by Europe and the US. The LSA/MMA project is a compromise array with 64 telescopes, each of 12 m diameter, giving a total collecting area of

7,000 m², with baselines up to 10 km, and with sub-millimetre capabilities. It will be located on Llano de Chajnantor, a 5000-m-high plateau near the village of San Pedro de Atacama in the Atacama Desert area. This will be the most powerful (sub-)millimetre telescope in the world, opening completely new horizons in astronomy.

The LSA/MMA will be the natural complement, in its wavelength range, to the HST and VLT, with equivalent resolution and sensitivity and the additional capability to observe the inner part of the dust-obscured regions of star formation and dust enshrouded galaxies.

At (sub-)millimetre wavelengths, the atmosphere presents natural limits to the sensitivity and resolution of astronomical observations. Pressure-broadened molecular lines, in particular of water vapour, are the cause. The atmosphere adversely affects observations both by attenuating the incoming signal and by increasing the system noise, since it radiates thermally. Furthermore, inhomogeneities in the water vapour distribution change the electrical path length through the atmosphere. These random variations result in



Figure 1: Partial view of the site-testing equipment deployed in Llano de Chajnantor. The LSA container is to the left, while the MMA container is to the right. In the background Cerro Chascón.

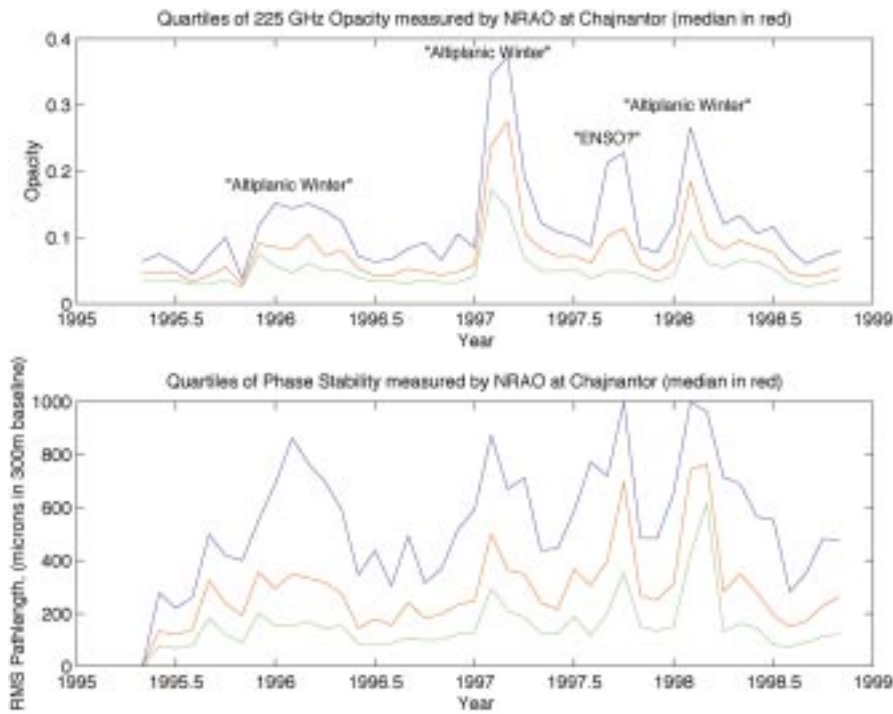


Figure 2: Quartiles of the zenith optical depth – opacity – at 225 GHz (upper plot) and the phase stability (lower plot) observed by NRAO during the years 1995–1998. The global weather conditions Altiplanic Winter and one El Niño – Southern Oscillation (ENSO) event can be seen in the cumulated data.

data, as can be seen in Figure 2. However, the Chajnantor site provides excellent observing conditions, perhaps amongst the very best in the world for sub-millimetre wavelengths. The high atmospheric transparency allows high-efficiency telescope operations.

Moreover, the whole area around Cerro Chascón, including Llano de Chajnantor, has recently been declared to be of “scientific interest” by a presidential decree. A land concession has been granted to the *Comisión Nacional de Investigación Científica y Tecnológica* (CONICYT), the agency in charge of evaluating, supporting and funding scientific and technological research in Chile. The area around the LSA/MMA is

phase errors between the array elements which degrade the sensitivity and resolution of the images. To minimise such atmospheric degradation, then, the ideal site should be a dry plateau at high altitude.

For several years the European collaboration has been exploring the northern area of Chile searching for potential sites (Otárola et al., 1996). The experience has helped not only our own efforts, but also other groups conducting site studies and/or astronomical projects in the same area. NRAO began site characterisation measurements at Llano de Chajnantor in 1995. In 1998, after more than a year of measurements at another candidate site (Pampa Pajonales), the European measurements started at Chajnantor as well. Several instruments are deployed alongside those of NRAO (Fig. 1). The goal is to share the infrastructure and to correlate the data obtained at the same place and time with the different instruments.

The work done at Chajnantor by NRAO shows that the median zenith optical depth at a frequency of 225 GHz is about 0.06 (see Fig. 2). This is significantly better than that measured at the CSO on Mauna Kea with an identical instrument. Also, there is less diurnal variation in transparency on Chajnantor than on Mauna Kea. These data span the period 1995 to 1998. The main meteorological events (“Altiplanic Winter” and “El Niño – ENSO”) have had an adverse effect on the



Figure 3: Map of the Atacama Desert region in Chile (scale 1:3,000,000). To the east of “Salar de Atacama” can be seen the location of Llano de Chajnantor, while to the south of Antofagasta Paranal can be seen (adapted from “Atlas de la República de Chile”, Instituto Geográfico Militar, 1983).

now protected from third parties and from possible mining claims or other such activities.

In this report an overview of the site, the instruments used to characterise it, their scientific rationale and some preliminary results are presented.

2. Chajnantor

Llano de Chajnantor is the selected site for the combined LSA/MMA project. The atmosphere at Chajnantor and the nearby plateau "Pampa La Bola" have been studied extensively by NRAO and the *Nobeyama Radio Observatory* (NRO), respectively. Measurements have shown that this area is among the driest in the world, with conditions that excel for astronomical research at several wavelengths.

Chajnantor is a 5000-m-high plateau about 60 km ESE of San Pedro de Atacama. This village is a place of great ethnological and archaeological importance, being the oldest continuously inhabited site in Chile. It is also one of the most important tourist attractions of the region because of the impressive mountain and desert landscapes, the pre-Columbian archaeological sites, the fine archaeological museum, and the relaxing atmosphere given by the rustic nature of its centuries old adobe houses and narrow streets.

2.1 Geomorphology

Three north-south mountain ranges dominate the geomorphology of the Atacama Desert area (see Fig. 3): the Coastal mountains, with peaks over 3500 m, the Domeyko mountains, located at middle longitudes, and the Andes, with peaks well above 5000 m.

The 25 km² Chajnantor plateau is located on the western edge of the Andes at 67°45' west and 23°01' south, about 380 km NE of Paranal. This plateau is open to the west and north-west, but several 5600-m peaks border the site in other directions.

2.2 Logistics

Prom Pedro de Atacama an international highway to Argentina, "Paso de Jama", allows an easy access to the site. By March 1999 this road will be paved through the CONICYT land concession, ensuring access by a good paved road.

A power source is essential for the development of the LSA/MMA. The nearest existing power lines are 180 km NW in Calama. Due to the growing commercial relations with Argentina, however, several projects are being carried out to bring natural gas from Argentina to produce electrical power for the Atacama region. One of these gas pipelines crosses the Chajnantor plateau. NRAO and GasAtacama, the pipeline owner, have signed an agreement to install a gas tap at the north edge of the Chajnantor area. This will allow the



Figure 4: One of the 183-GHz water vapour monitors to the right of the antennas of the 11.2-GHz interferometers.

LSA/MMA to generate electrical power as needed.

A few years ago, when we first started exploring this area, Chajnantor was a very isolated place. By early 1999, the site will have a good paved road running nearby and natural gas on site.

2.3 Climate

Weather conditions in the Atacama Desert are dominated by a high-pressure anticyclone, an inversion layer on the coast, the north-south coastal mountains, the Andes mountains, the high

insolation, and the high ventilation.

The whole area is extremely dry and lies in the meridional transition region. To the north, the Altiplano convective summer rains predominate, where frontal winter rains prevail to the south. The aridity originates in the prevailing anticyclone conditions associated with a slow downward air motion (Fuenzalida et al. 1996). Over the coast this subsidence is responsible for an inversion layer several hundred metres thick that starts about 1000 m. The inversion layer separates the moist air of the lower marine boundary layer from the dry subsiding air and acts as

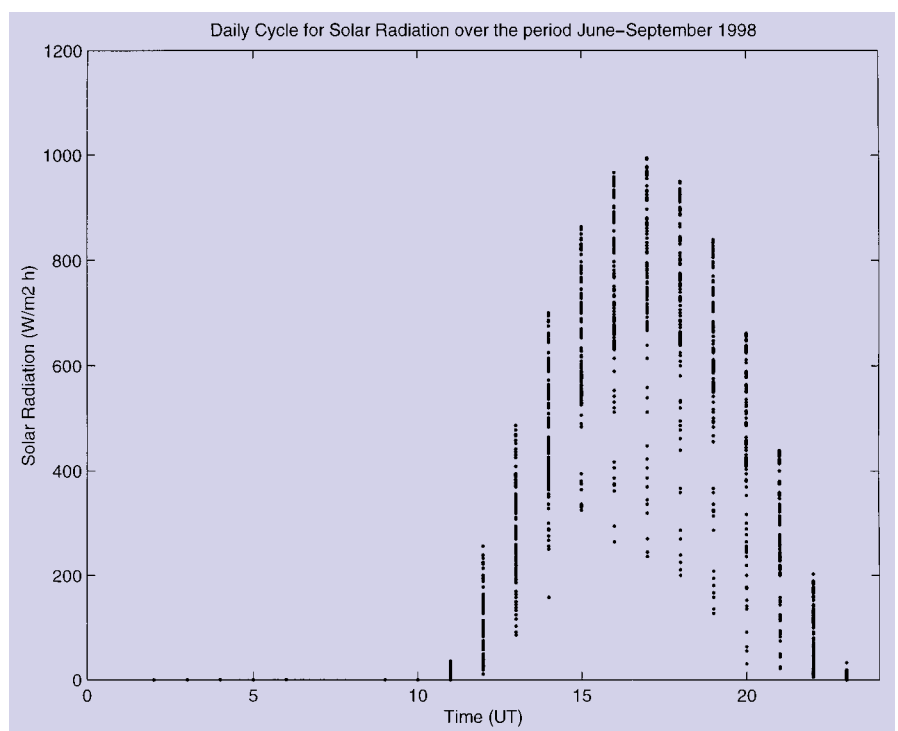


Figure 5: Diurnal cycle of the solar radiation for the period June–September 1998 in the Chajnantor area.

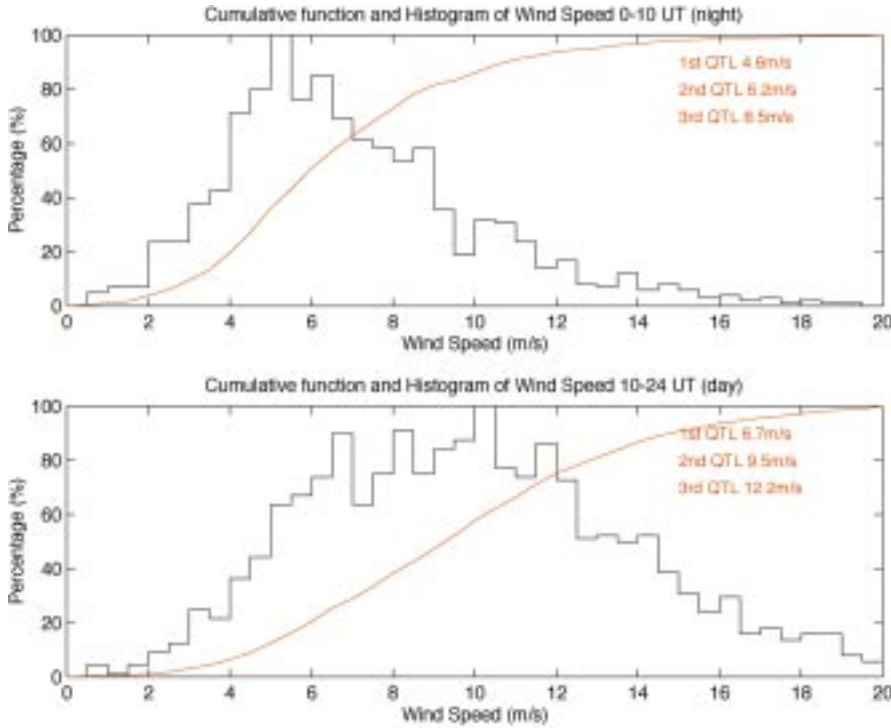


Figure 6: Cumulative function and histogram for the wind speed over the period June–September 1998 in the Chajnantor area. Upper plot shows night-time while lower one is day-time.

a barrier to any mixing process that might transport moisture evaporating from the sea to upper levels. The well-mixed marine boundary layer is restricted to lowlands along the coast on the west slope of the coastal mountain range.

As humid air masses moving westward from the Atlantic zone rise up the east slope of the Andes they cool and precipitate. Hence, very little humid air gets over to the west side of the Andes. The exception is during summer, when the high-pressure system over the Pacific weakens and, at the same time, moves southward (Fuenzalida et al. 1987, Aceituno et al. 1996). This change in atmospheric circulation allows warm humid air from the Amazon to reach the Altiplano in northern Chile and produce rain. This is known locally as “Bolivian or Altiplanic Winter”.

The driving force behind the climatological processes is the extremely high solar radiation. The daily and yearly maxima, averages and ranges of the insolation are amongst the highest recorded in the world. The average daily maximum reaches almost 1300 W/m^2 during summer. Only convective and advective

processes can remove the absorbed heat because the extreme aridity means that the evaporating water cannot dissipate the heat. The wind then is the main energy carrier. The strong thermal contrast between the Pacific and the Andes drives a constant sea-mountain airflow. Almost every climatic process within the boundary layer is controlled by this regional wind system. At night the boundary layer regularly disappears so the climate near the ground is directly influenced by the upper atmosphere winds (Schmidt 1997).

3. Site Testing Equipment

At the beginning of June 1998, the Onsala-ESO European site-testing group deployed equipment to characterise the atmospheric conditions at Chajnantor for (sub-)millimetre astronomy. Our instrumentation and measurements complement the measurements carried out by the other groups (see Fig. 4).

3.1 Container

The computers and other ancillary equipment are installed in a 20-foot in-

ulated ocean-shipping container. About 18 m^2 of photovoltaic panels are mounted outside to charge a battery bank that provides about 700 W around-the-clock. The computers housed in the container control the instruments and store the data. Communications are maintained with an analogue cellular telephone. Data for all the instruments are retrieved about once a month during routine visits.

3.2 Weather stations

Two weather stations have been installed on the plateau. They measure air temperature, solar radiation, atmospheric pressure, relative humidity, and wind speed and direction. Their main characteristics are detailed in Table 1.

The weather stations include a data logger that, with the actual sampling rate, can store 42 days of data. The wind sensors are atop a 4-m mast and the other instruments are installed in a ventilated shelter to protect them from direct solar radiation.

Analysis of these data improves our understanding of the climatology of the site, with emphasis on the wind speed and direction and the diurnal and seasonal patterns. These data also provide information on the environmental constraints which will influence the design of the LSA/MMA antennas, and it is a basic calibration input for the analysis of the data obtained with other instruments at the site.

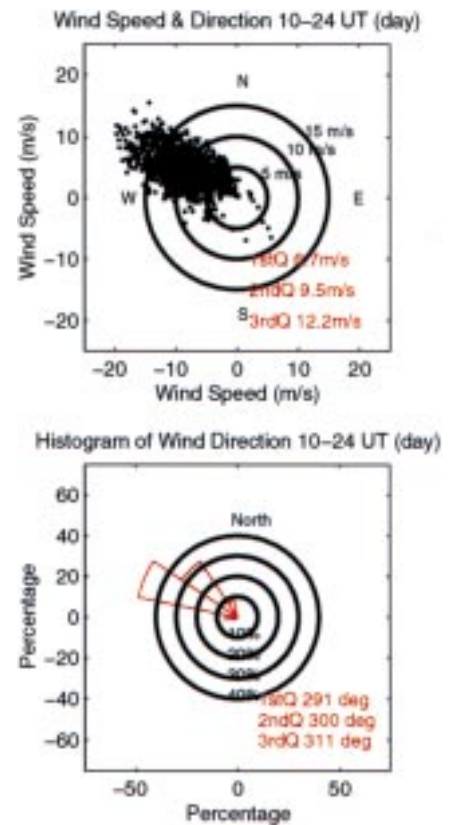


Figure 7: Wind speed and direction over 14 hours during the day (upper plot), and histogram with the percentage of time that the wind blows in a particular direction during this same time period (lower plot). The distribution for night-time is similar.

Table 1: Main characteristics of the sensors available in the weather stations deployed in Chajnantor

Sensor	Operating range	Accuracy
Air temperature	$-30 - +70 \text{ }^\circ\text{C}$	$0.2 \text{ }^\circ\text{C}$
Relative humidity	5–95%	1.5% in the range 5% to 60%
Solar radiation	$0-1100 \text{ W/m}^2$	$\pm 5\%$ per MJoule, spectral response 400–1100 nm
Anemometer	0–150 km/h	0.5 m/s
Wind direction	0–360 degrees	3.0 degrees
Barometric pressure	740–490 mbar	$\pm 5 \text{ mbar}$

3.3 Interferometer

Atmospheric phase stability, or “seeing”, is a crucial issue for the LSA/MMA. Because radio waves travel more slowly in wet air than in dry air, fluctuations in the water vapour distribution will cause variations in the electrical path length through the atmosphere. Path length variations across the array aperture will degrade both image quality and array sensitivity. These path length fluctuations, which are almost independent of observing frequency at millimetre wavelengths, correspond to phase fluctuations that scale linearly with frequency. Simulations suggest that phase fluctuations less than 10 degrees rms at the observing wavelength will have little impact upon most images, phase errors of 30 degrees rms will permit imaging with up to 200:1 dynamic range, albeit with somewhat reduced sensitivity, and image reconstruction becomes all but impossible when phase errors exceed 60 degrees rms (Holdaway and Owen 1995b). Although the LSA/MMA will undoubtedly use a correction technique to overcome atmospheric image degradation (either fast switching or radiometric phase calibration), the better the natural stability, the better these correction schemes will work (Holdaway et al. 1995c, Woody et al. 1995).

Atmospheric phase stability at Chajnantor is monitored with two 300-m baseline interferometers observing 11.2 GHz tracking beacons broadcast by geostationary communications satellites (Radford et al. 1996). One instrument was installed by the MMA project in May 1995 and another was installed by the LSA project at Pajonales in April 1997 and later moved to Chajnantor in June 1998. Because the atmosphere is non-dispersive away from line centres, these measurements can be extrapolated to characterise the atmospheric phase stability up to at least 350 GHz and, with care, throughout the submillimetre region. These interferometers sense atmospheric structures on 300-m and smaller scales. The phase stability is characterised by the rms phase fluctuations calculated over 10-minute intervals. This interval is twenty times longer than the time it takes an atmospheric feature to move the length of the baseline at 10 ms^{-1} , which is the median wind speed aloft. Thermal instrumental phase noise is on the order of 0.1 degree rms at 11.2 GHz, while the smallest observed atmospheric phase fluctuations are – after correcting for instrumental noise – 0.3 degree rms (Holdaway et al. 1995c).

The two interferometers are collocated along the same east-west 300-m baseline, but observe different satellites separated by about 5° . As the (quasi-static) pattern of atmospheric turbulence passes over the interferometers, they will record similar signals that are delayed from one to the other. From this delay, some estimate of the wind speed aloft, and the geometry, we can deter-

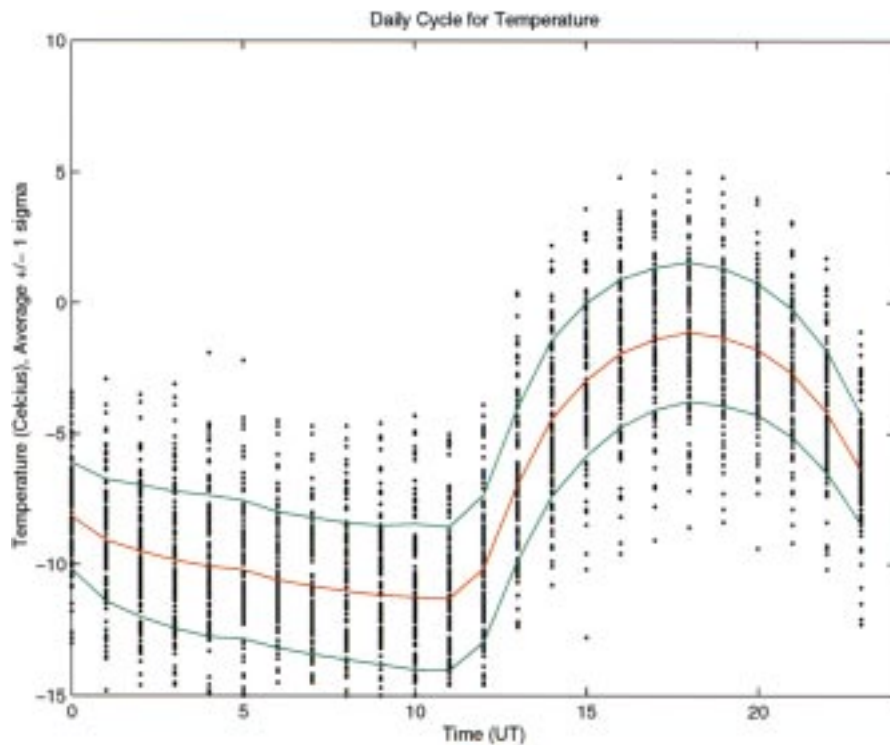


Figure 8: Diurnal temperature cycle over the period June–September 1998 in the Chajnantor area.

mine the effective height of the turbulent layer. Differences in the interferometer signals, on time scale shorter than the delay, provides a measure of the evolution of the turbulence (Holdaway and Radford 1998). The effectiveness of fast switching at overcoming atmospheric image degradation depends on both the height and the time scale for evolution of the turbulence (Holdaway and Owen 1995b).

3.4 183 GHz water vapour monitor

Now under development at several observatories, water-line radiometry is a promising technique for overcoming the effects of atmospheric phase fluctuations. The varying depth of the water vapour column is determined by continuously monitoring the intensity and shape of a water-vapour emission line. Changes in the atmospheric phase delay are then

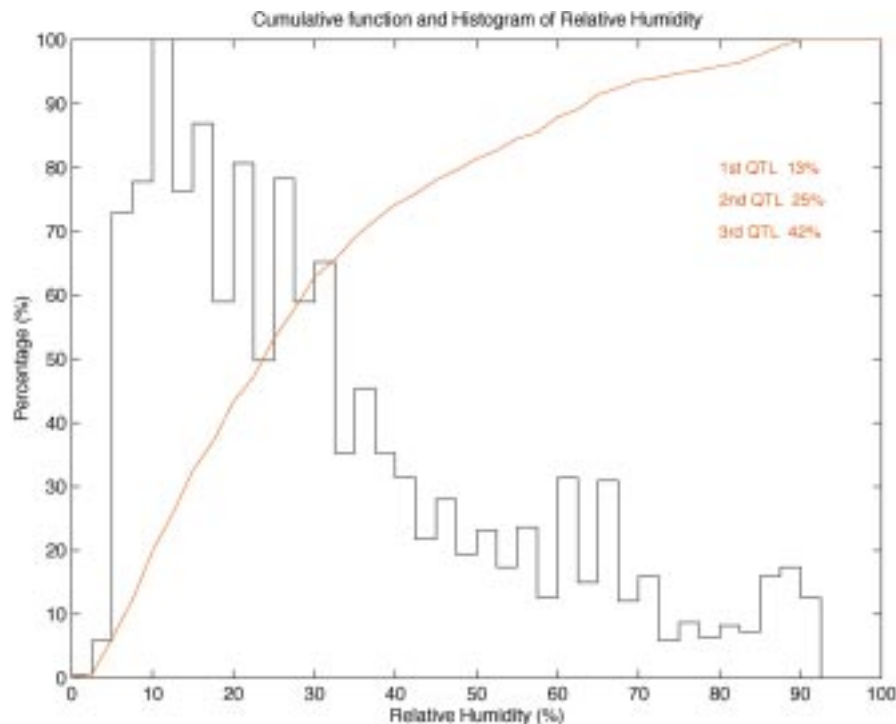


Figure 9: Cumulative function and histogram for the relative humidity over the period June–September 1998 in the Chajnantor area.

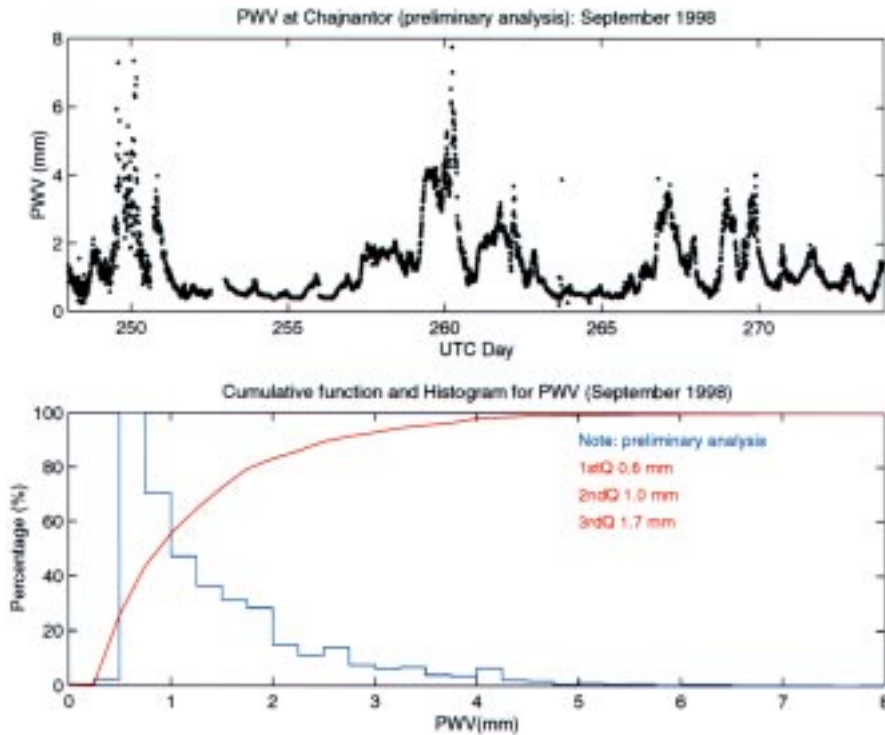


Figure 10: Amount of precipitable water vapour content during the month of September 1998 in the Chajnantor area (upper plot), and cumulative function and histogram for the same month (lower plot). Several storms affecting the area can be seen.

determined and used to improve the astronomical images. Both the 22 GHz and the 183 GHz line are candidates for this method, but it is not yet clear which is best for the conditions at Chajnantor.

Two radiometers for the 183 GHz water-vapour line have been built as a collaborative project between *Onsala Space Observatory*, through the *Group for Advanced Receiver Development* at *Chalmers University of Technology*, and the *Mullard Radio Astronomy Observatory (MRAO)*, *Cavendish Laboratory*, Cambridge. They have been installed at Llano de Chajnantor at the ends of the 300-m baseline of the 11.2 GHz interferometer. The plan is to compare the atmospheric phase fluctuations determined from the radiometers and from the interferometer as a test of the phase correction scheme. The radiometers also allow, under computer control, complete movement of the beam across the sky.

These radiometers are double-side band heterodyne receivers with three detection bands spaced 1.2, 4.5, and 7.5 GHz away from the line centre. The three-channel spectrum measures the water line shape and intensity. The amount of precipitable water vapour is then determined by fitting to an atmospheric model (Wiedner 1998).

The mixers are of the sub-harmonically pumped Shottky types developed at the *Rutherford and Appleton Laboratories*, in the UK. This design has two main advantages: it does not require an external bias and we do not need to double the Gunn oscillator frequency to pump the mixer. The resulting RF circuit is simpler and more reliable. In the laboratory, the receiver temperature was

measured to be about 1500 K. This has been confirmed during normal operation in the field.

The local oscillator (LO) is a free-running, 91.7-GHz Gunn oscillator. It is not phase locked because of the broadness of the water line and because the line is very symmetric. Hence any instability is compensated by the DSB detection. Also the frequency stability of the oscillator is better than 4 MHz/°C, so by regulating the LO temperature to within 1 °C, we obtain a negligible 0.004% frequency drift.

The radiometers are continuously calibrated by switching the beam between the sky and two reference black bodies at temperatures of 35 and 100 °C.

4. Results

Daily climatology data have been collected for the period June–September 1998 winter season in the Southern Hemisphere, and are presented as an average over this period. Figure 5 shows the diurnal cycle of the solar radiation for June–September 1998. The radiation peaks at about 1000 W/m², and the average maximum is around 800 W/m². The histograms in Figure 6 show that the wind is a constant in the area, with lower speeds during the night (median of about 6 m/s) and higher speeds during the day (median of about 10 m/s). This is a parameter that must be kept in mind during the design stage of mechanical structures to be built in the area, especially the antennas. Over 80% of the time the wind

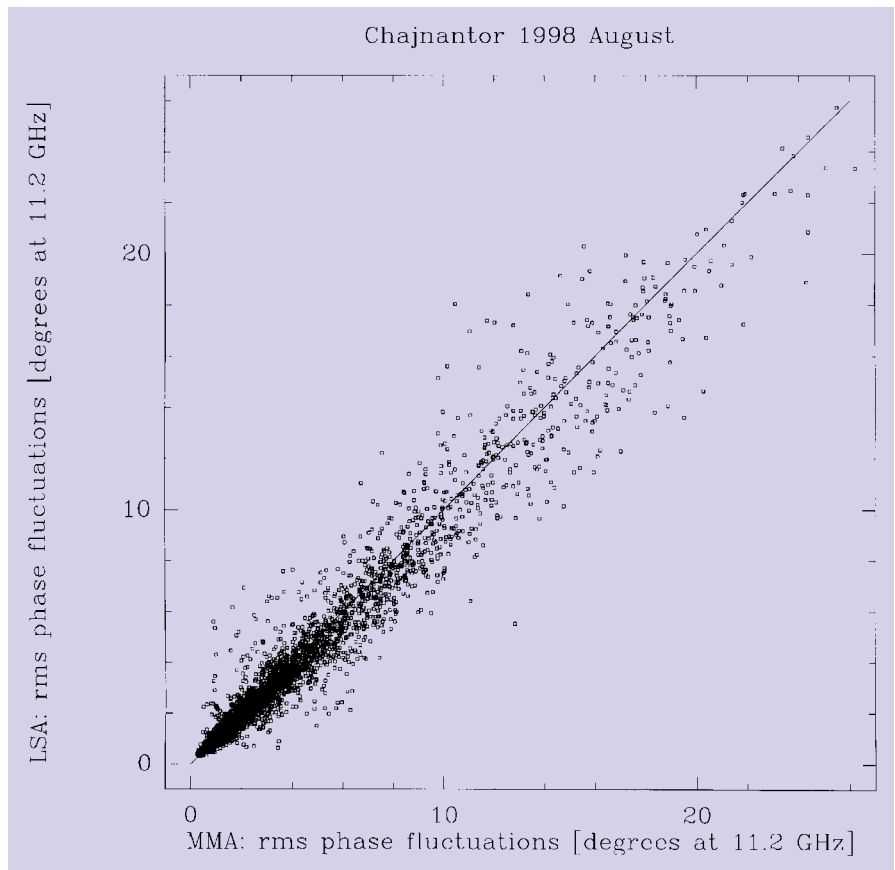


Figure 11: Data from the LSA and the MMA 11.2-GHz interferometers (phase stability monitors) for August 1998. The good correlation between both instruments shows that they perform identically.

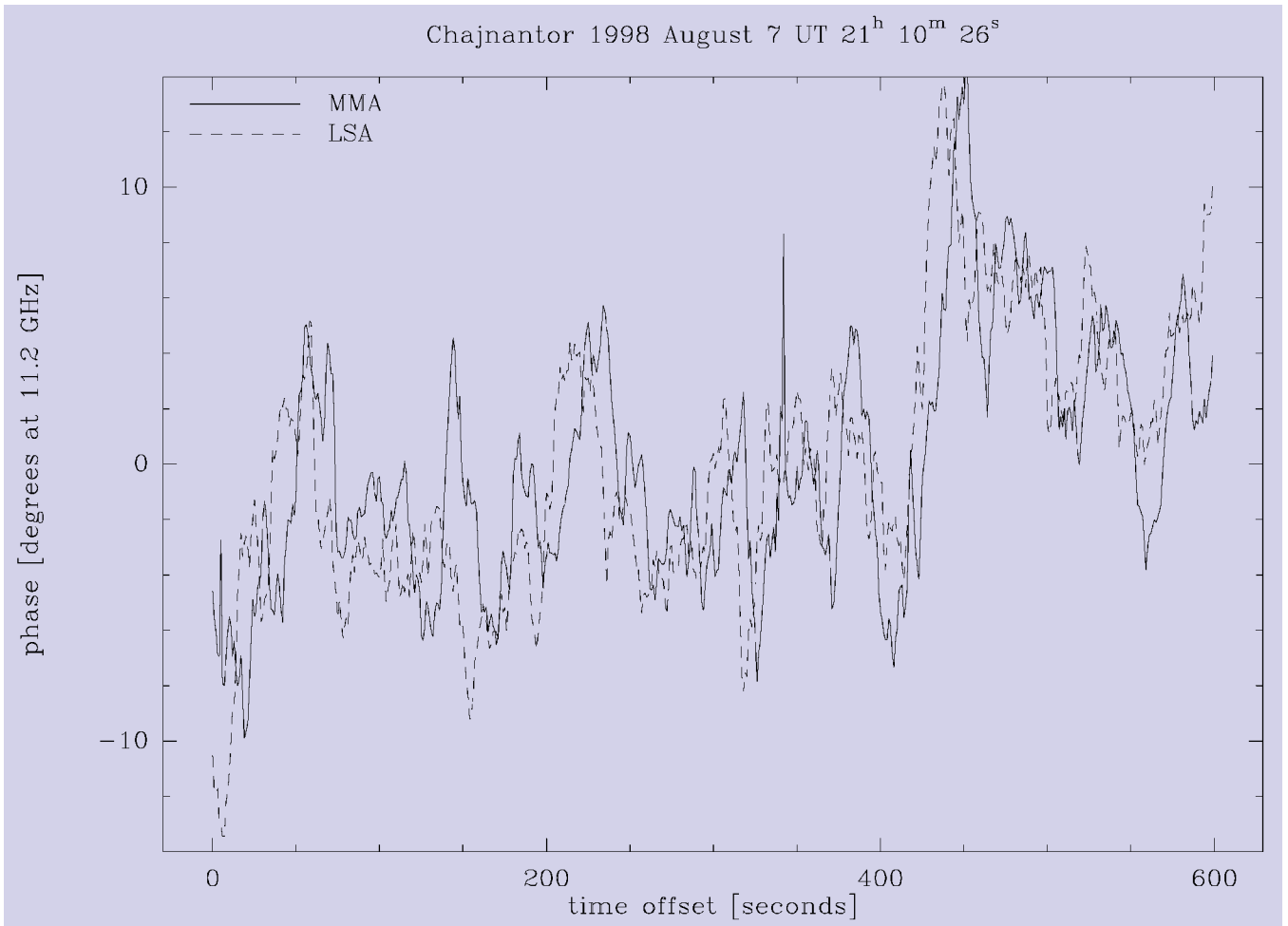


Figure 12: Example of the 11.2-GHz interferometers data showing the expected time delay as the atmospheric turbulence patterns cross over the interferometer line of sight. From these data a height of about 500 m for the turbulence layer can be inferred.

blows from the west (from the desert to the high mountains) as can be seen in Figure 7. The diurnal cycle of temperature is shown in Figure 8: during the night, the temperature becomes stable with the high solar radiation influencing it during the day.

Over the observation period the relative humidity did not change much during a diurnal cycle, being very stable during the night – at an average of around 38% – decreasing during the day to reach a minimum average of around 25%. Figure 9 shows the cumulative function and histogram for the relative humidity.

Data for the precipitable water-vapour (PWV) content of the atmosphere during September 1998 are shown in Figure 10, where some days with very bad weather can be seen as peaks distribution. It can also be seen that normally PWV is lower and stable during local night-time. In the same Figure the histogram for PWV shows that 50% of the time PWV is less than 1 mm and 75% of the time less than 1.7 mm. Since the first analysed month for Chajnantor (September) was a particularly bad month, with several storms over the area, due to a transition between the two global weather conditions known as “El Niño” and “La Niña”, better results are expected after some accumulated

statistics. It should be noted that above 3.5 mm of PWV, measurements are no longer linear due to instrumental limitations.

Data from the two interferometers for August 1998 show they perform identically. The rms phase fluctuations calculated over 10-minute intervals for each interferometer are compared in Fig. 11. Most of the scatter in this figure is due to atmospheric evolution on short time scales. Although the computers controlling the instruments are synchronised to better than 1 s, the 10-minute intervals used for analysis are only synchronised to 5 minutes. The MMA interferometer measures slightly larger fluctuations than the LSA instrument, largely because the MMA interferometer observes a satellite at lower elevation (Holdaway and Ishiguro 1995).

A detailed example of the interferometer data (Fig. 12) shows the expected time delay as the (quasi-static) atmospheric turbulence pattern passes sequentially through the interferometers’ lines of sight. In this example, the LSA signal leads the MMA signal by about 10 s. Together with the geometry and an estimate of the wind speed aloft, we can estimate the height of the dominant turbulent layer. Other

structures are also evident in the data, possibly due to layers at different heights or to fast evolution of the turbulent pattern.

5. Conclusions and Future Work

On Llano de Chajnantor we have installed weather stations, two 183 GHz water vapour radiometers, and a phase stability monitor (11.2 GHz interferometer). Data are recorded automatically and retrieved once a month during periodic visits to the site. Data processing and analysis are in their first stages. The meteorological data are analysed in Chile, the 183 GHz radiometer data are analysed in Chile and Sweden, and the interferometer data are analysed in collaboration with NRAO.

The site remains extremely promising for submillimetre interferometry although bad weather caused by the transition between the two global weather conditions known as “El Niño” and “La Niña” was experienced.

In the near future we will compare our data with those obtained through radio sonde launches – a campaign which started in October 1998 and will continue through 1999. This is a collaboration between ESO, NRAO, Cor-

nell University, and the Smithsonian Astrophysical Observatory. As a complement to the 183 GHz radiometers, we also plan to install a 22-GHz radiometer to observe another water vapour line and correlate measurements. The radiometer, on loan from R. Martin from Steward Observatory, will be installed next year. It has been extensively upgraded to make it more reliable and capable of automatic operation at the site.

In the data analysis, we will explore alternatives to the atmospheric model fitting of the retrieved line from the 183 GHz radiometer measurements, as well as to correlate these measurements with other ones done at different frequencies and/or techniques.

Together with IRAM engineers, we will start measurements of the wind sampled at a high rate in order to determine the power spectrum of the wind behaviour. Such information has an important bear-

ing on the design of the LSA/MMA antennas.

The data, results and all relevant information about the project can now be found in the web page <http://puppis.ls.eso.org/lisa/lisahome.html>

6. Acknowledgements

Many people around the world have made fundamental contributions to this project. We wish particularly to thank the ESO staff in Chile, Patricia Adiazola, Viviana Alcayaga, Mary Bauerle, Alfredo Carvajal, Manuel Hervias, Luís Morales, Patricia Parada, and Ivonne Riveros for their special assistance whenever we came with an urgent request.

References

- Aceituno P., Montecinos A., Departamento de Geofísica Universidad de Chile, 1996.
The Messenger, No. 91, March 1998.
 Fuenzalida R., ESO internal report, 1996.

- Fuenzalida H., Ruttlant J., in Proceedings of the II Congreso Interamericano de Meteorología, Buenos Aires, Argentina, 1987, 6.3.1.
 Holdaway M., Ishiguro M., MMA Memo 127, 1995.
 Holdaway M., Owen F., MMA Memo 136, 1995b.
 Holdaway M., Radford S., Owen F., Foster S., MMA Memo 139, 1995c.
 Holdaway M., Radford S., MMA Memo 196, 1998.
 Otárola A., Delgado G., Bååth L., in Proceedings of the ESO IRAM NFRA Onsala workshop 11–13/12/95, P. Shaver Ed., Springer Verlag, 1996, 358.
 Radford S., Reiland G., Shillue B., PASP, No. 108, 1996, 441.
 Schmidt D., PhD thesis, Friedrich-Alexander University, 1997.
 Wiedner M., PhD thesis, University of Cambridge, 1998.
 Woody D., Holdaway M., Lay O., Masson C., Owen F., Plambeck D., Radford S., Sutton E., MMA Memo 144, 1995.

gdelgado@eso.org



The ISAAC Team on Paranal After First Light on UT1

From left to right: J. Stegmeier, G. Finger, A. Moorwood, P. Biereichel, J. Brynell, J.-G. Cuby, J. Knudstrup, M. Meyer, J.-L. Lizon.

Probing the Cosmic Large-Scale Structure with the REFLEX Cluster Survey: Profile of an ESO Key Programme

H. BÖHRINGER¹, L. GUZZO², C.A. COLLINS³, D.M. NEUMANN⁴, S. SCHINDLER³, P. SCHUECKER¹, R. CRUDDACE⁵, S. DEGRANDI², G. CHINCARINI², A.C. EDGE⁶, H.T. MACGILLIVRAY⁷, P. SHAVER⁸, G. VETTOLANI⁹, W. VOGES¹

¹Max-Planck-Institut für Extraterrestrische Physik, Garching, Germany;

²Osservatorio Astronomico di Brera, Milano/Merate, Italy; ³Liverpool John-Moores University, Liverpool, U.K.;

⁴CEA Saclay, Service d'Astrophysique, Gif-sur-Yvette, France; ⁵Naval Research Laboratory, Washington, D.C., USA;

⁶Durham University, Durham, U.K.; ⁷Royal Observatory, Edinburgh, U.K.;

⁸European Southern Observatory, Garching, Germany; ⁹Istituto di Radioastronomia del CNR, Bologna, Italy

1. Introduction

To understand the formation of the visible structure in the Universe out of an ini-

tially almost homogeneous matter distribution is one of the most fascinating quests of modern cosmology. The first step to this understanding is of course an assessment of the matter distribution in the present Universe on very large scales extending over several hundred Mpc (for a Hubble constant of $50 \text{ km s}^{-1} \text{ Mpc}^{-1}$). Such large scales are interesting for two major

reasons: the present-day structures on this scale are directly comparable to the signature of the primordial structure detected in the microwave background by COBE with similar comoving sizes, and at these scales the observed density fluctuations are just linear amplifications of the initial conditions in the early Universe. While the study of the galaxy distribution has already given us very interesting insights into the structure on scales of a few hundred Mpc, an alternative approach using the next larger building blocks of the Universe, galaxy clusters, as probes for the cosmic structure can give us a ready access to even

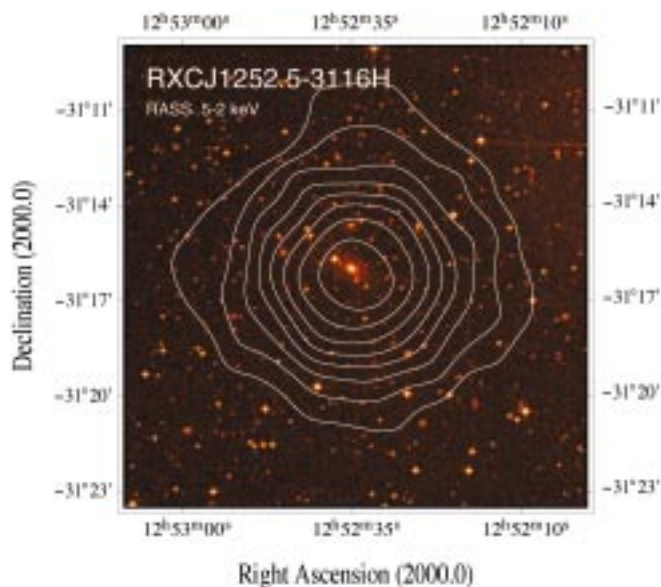
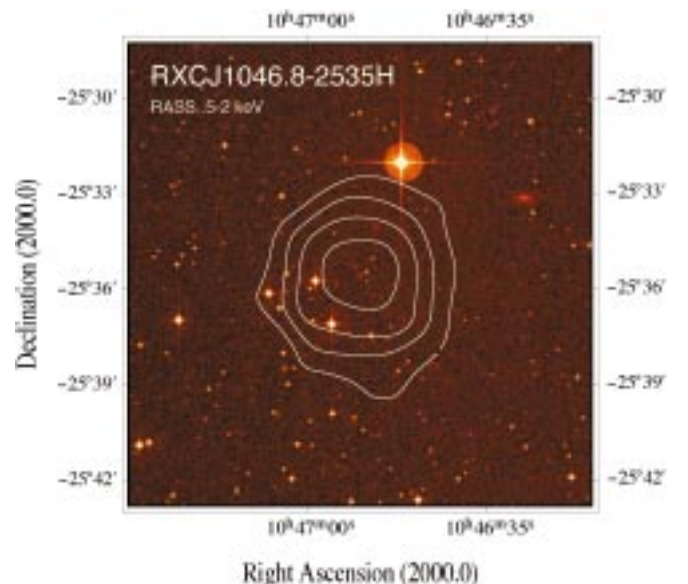
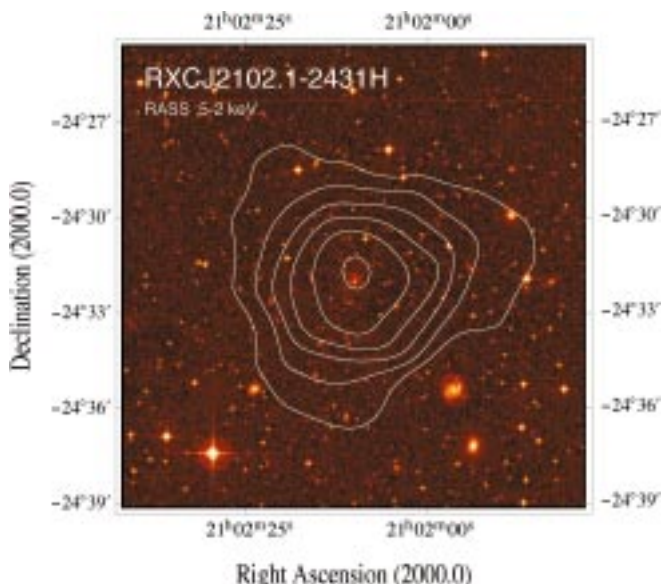


Figure 1: Three of the galaxy clusters not listed in the catalogue by Abell et al. (1989) found during the identification of X-ray cluster sources from the ROSAT All-Sky Survey in the frame of the ESO key programme. The clusters range from poor nearby objects with $z = 0.053$ (left), a cluster with $z = 0.188$ (bottom left), to rich distant clusters with $z = 0.243$ (bottom right). The figures have been produced from the STScI digital scans of the UK-Schmidt IIIaJ plates with X-ray contours from the ROSAT All-Sky Survey images superposed. The contours are 1.5, 2, 3, 4, ... sigma significance contours of the X-ray signal-to-noise within a Gaussian filter with a radius of 1 arcmin.



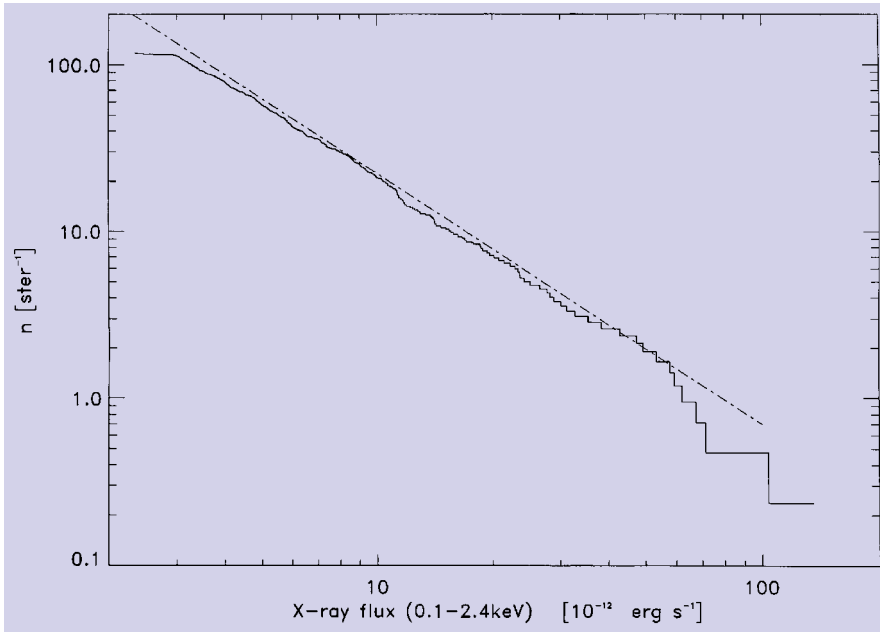


Figure 2: Cumulative number counts of X-ray clusters as a function of the limiting flux for the REFLEX sample.

larger scales (see also Tadros et al., 1998 for the APM cluster survey in the optical).

X-ray astronomy has offered a unique tool to efficiently detect and characterise galaxy clusters out to large distances. Originating in the hot intracluster plasma that fills the gravitational potential well of the clusters, the X-ray emission is an equally robust parameter for a first estimate of the size and mass of clusters as the velocity dispersion measured from the galaxy redshifts. But, while the X-ray luminosity can be readily detected for many clusters in an X-ray sky survey, the collection of velocity dispersions requires very large and time-consuming redshift surveys.

In the project described here we have embarked on a redshift survey of galaxy clusters detected in the ROSAT All-Sky Survey (Trümper 1993, Voges et al. 1996), the first complete sky survey conducted with an imaging X-ray telescope. In the frame of an ESO key programme (Böhringer 1994, Guzzo et al. 1995) we are seeking a definite identification of all possible cluster candidates found in the ROSAT Survey in the southern celestial hemisphere above an X-ray flux limit chosen such as to provide a reasonably homogeneous sensitivity coverage of the sky area. Within this survey programme, which we call the ROSAT ESO Flux Limited X-ray (REFLEX) Cluster Survey, we are investigating about 800 galaxy clusters and have obtained more than 300 new cluster redshifts.

The present article describes methods of the cluster detection and identification as well as first preliminary results on the statistics of the cluster population and a view on the large-scale distribution of the clusters. In a forthcoming issue of *The Messenger* we describe in more detail the strategy of the optical observations and the spectroscopic results.

2. Cluster Detection and Follow-up Observations

The X-ray sky atlas constructed from the ROSAT All-Sky Survey Mission with its more than 100,000 X-ray sources (Voges et al. 1996) contains thousands of mostly unidentified galaxy clusters. Since the majority of these sources are characterised by few photons, only the brightest, well-extended X-ray cluster sources are readily identified, while the main part of the identifications has to be based on further optical information. For the REFLEX Survey we made mainly use of the COSMOS optical object catalogue (e.g. Heydon-Dumbleton et al. 1989) produced from the digital scans of the photographic UK Schmidt Survey (providing star/galaxy separation for the sky objects

with high completeness down to $b_j = 20.5$ mag.). The cluster candidates are found as overdensities in the galaxy density distribution at the position of the X-ray sources (see Böhringer et al. in preparation). Not all the sources flagged by this technique are true galaxy clusters, however. The price paid for aiming at a high completeness in the final catalogue is a low detection threshold in the galaxy density leading to a contamination of the candidate list by more than 30% non-cluster sources. This large contamination can be reduced to about one-third by a direct inspection of the photographic plates, the detailed X-ray properties, and using all the available literature information.

The subsequent work is the observational task of the ESO key programme comprising a total of 90 observing nights distributed evenly among the 1.5-m, 2.2-m, and 3.6-m telescopes at La Silla. These follow-up observations have a two-fold purpose: we search for a definite identification for the unknown objects and collect redshifts for all clusters for which this parameter is not known. To make optimal use of the ESO telescopes, we observe nearby, poor clusters and groups in single-slit mode with the smaller telescopes and use the 3.6-m telescope with EFOSC in multi-slit operation to get multiple galaxy spectra of dense, rich clusters. Several coincident redshifts strongly support the cluster identification and the spectroscopy of central dominant early-type galaxies at the X-ray maximum plays a particularly important role in this study.

The observing programme will be completed end of 1998. Having observed the clusters with higher X-ray flux with highest priority, we can construct a first catalogue of clusters for the brighter part of the sample down to an X-ray flux limit of $3 \cdot 10^{-12} \text{ erg s}^{-1} \text{ cm}^{-2}$ (in the ROSAT band 0.1–2.4 keV) comprising

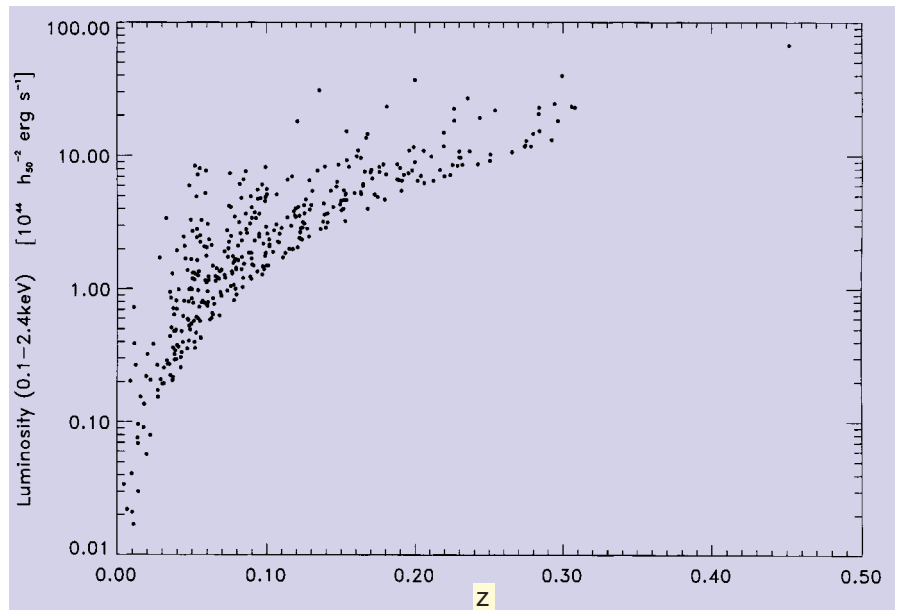


Figure 3: Distribution of the X-ray luminosities as a function of redshift for the galaxy clusters of the REFLEX sample.

475 objects. 53% of these clusters can be found in the main catalogues of Abell (1958) and Abell, Corwin, and Olowin (1989) and further 10% in the supplementary list. Most of the remaining clusters are previously unknown objects. This result highlights the importance of the selection process in the construction of the sample: a significant fraction of the X-ray bright and massive clusters would have been missed had the X-ray clusters only been identified on the basis of existing catalogues. The fraction of known Abell clusters decreases further if one goes to lower X-ray flux limits e.g. in the extended REFLEX sample. We should also note here, however, that one part of the objects missing in Abell's compilation are nearby, X-ray bright groups, which are not rich enough in their galaxy content to fulfil Abell's criteria.

The high completeness of this sample is demonstrated by a counter-test, in which we searched for X-ray emission at the position of all Abell and ACO clusters in the ROSAT Survey independent of a previous detection of these sources by the survey source identification algorithm. Only 5 clusters (~1%) were found to have been missed by the cluster search based on the COSMOS data. Figure 1 gives examples of three non-Abell clusters found at different redshifts ($z = 0.053, 0.188, 0.243$). A fraction of the X-ray sources in the cluster candidate list are found to have non-cluster counterparts in the follow-up observations including AGN in clusters where the AGN provide the main source of the X-ray emission. These sources are removed from the sample. We also find a small number of cluster X-ray sources in which AGN contribute to the overall X-ray luminosity. As far as the different sources of X-ray emission can be distinguished by their extended and point-like nature, we have disentangled these

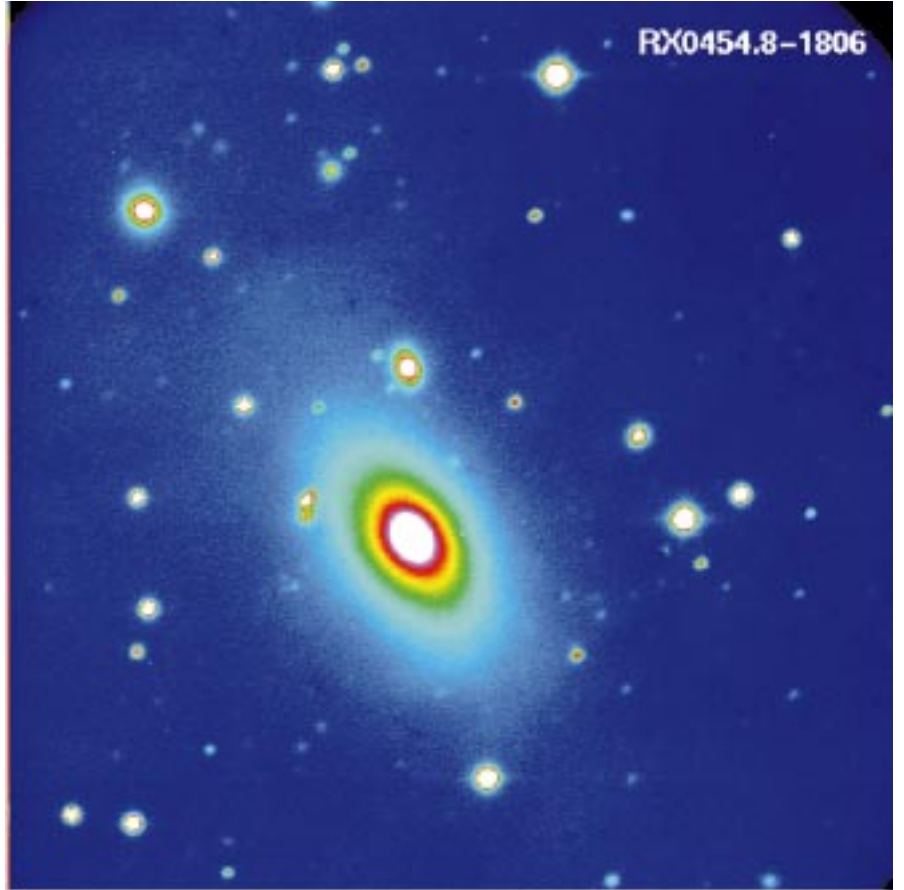


Figure 4: Galaxy group with an exceptionally dominant central cD galaxy at a redshift of $z = 0.0313$ in the REFLEX sample. The CCD image is a short routine exposure (without filter) to define the MOS slit mask taken with EFOSC1 at the 3.6-m telescope. The scale of the image is about 3.5 by 3.5 arcmin.

contributions. For an estimated very small fraction of sources of a few percent this contamination may remain undetected.

A few spectacular discoveries were made in the course of this programme

including the most X-ray luminous cluster discovered so far, RXJ1347-1145 (Schindler et al. 1995, 1996) and clusters featuring bright gravitational arcs, e.g. S295 (Edge et al. 1994).

3. Properties of the X-ray Clusters of Galaxies

In the following we are reporting results based on the X-ray bright sample of 475 galaxy clusters for which 413 cluster redshifts have been obtained and reduced so far or were collected from the literature. A plot of the number counts of the cluster population as a function of the limiting X-ray flux is shown in Figure 2. The logarithmic graph has a slope that is very close to an Euclidian slope of $-3/2$. This slope is easily explained by the fact that the majority of the clusters are not very distant – the peak in the redshift histogram is at $z \sim 0.06$ – and thus band-corrections and evolutionary corrections are not important. Figure 3 shows the distribution in redshift and X-ray luminosity. While most of the clusters detected are not very distant (median redshift is $z = 0.085$), a few very luminous clusters are found out to redshifts of $z = 0.3$ with one outstanding object at a redshift of $z = 0.45$, the most luminous cluster mentioned above. One also notes clearly the break at a redshift of $z = 0.3$, which is caused by the limited depth of the optical plate material

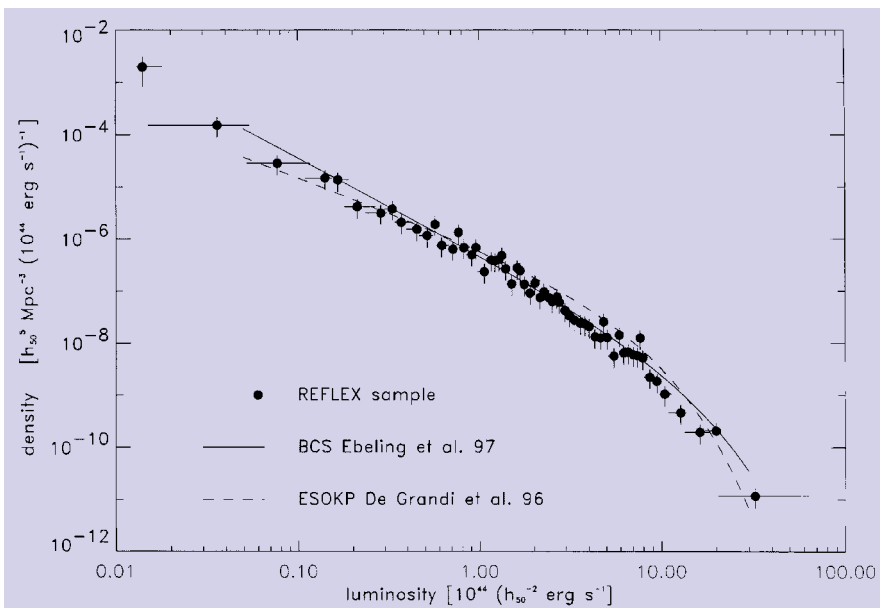


Figure 5: Differential X-ray luminosity function for the REFLEX sample (points with error bars; for details see Böhringer et al. in preparation) compared to the previous results by DeGrandi (1996) and Ebeling et al. (1997). A value of $H_0 = 50 \text{ km s}^{-1} \text{ Mpc}^{-1}$ is assumed for the scaling.

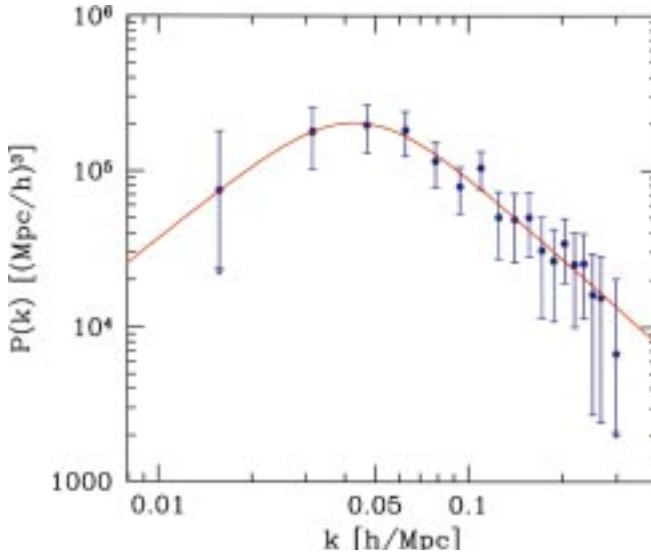


Figure 6: Power spectrum of the density distribution of the galaxy clusters in the REFLEX sample. For the analysis, only 188 clusters in a box of 400 Mpc side length is used (Schuecker et al. in preparation). The results are scaled to $H_0 = 100 \text{ km s}^{-1} \text{ Mpc}^{-1}$. The horizontal axis gives the wave vector of the Fourier components such that the corresponding physical scale is $2\pi/k$. The solid line is a parametric fit to the data not referring to a particular cosmological model.

used for the cluster pre-identification. Thus we can expect that there are more, in fact very interesting luminous clusters in the X-ray source list for this flux limit with redshifts between $z = 0.3$ to 0.5 . But a more extensive imaging search programme would be necessary to find these objects.

Another very interesting part of this X-ray cluster population is found among the nearby, low X-ray luminosity objects. These are groups of galaxies dominated by giant cD galaxies that are often found to be two or three magnitudes brighter than the next brightest galaxy in the system. A CCD image of such a group is shown in Figure 4.

The most straightforwardly obtained and important distribution function of the cluster sample is the X-ray luminosity function. This function is most closely related to the mass function of the clusters which is used as an important calibrator

of the amplitude of the density fluctuation power spectrum of the Universe (e.g. White et al. 1993). A preliminary version of the X-ray luminosity function of the sample is shown in Figure 5. Note that this function was derived for the sample when $\sim 80\%$ of the redshifts had been obtained. But in spite of this incompleteness, the luminosity function already recovers the densities reached in previous surveys (e.g. Ebeling et al. 1997, DeGrandi 1996) to which the present result is compared in the figure. The high quality of the present sample is also demonstrated by the fact that the slope of the number count function of Figure 2 is close to the expected Euclidian slope.

The most exciting aim of this programme is to assess the large-scale structure of the galaxy cluster and matter distribution in the Universe. The currently most popular and important statistical function for the characterisation of the

large-scale structure is the density fluctuation power spectrum. The form of the power spectrum depends on such basic features of our Universe as the mean density, the nature of the dark matter, and the physics of the inflationary process if such an event happened in the early Universe. Its knowledge provides therefore very important constraints on the possible cosmological models. A first preliminary result for this function obtained from 188 clusters of our sample in a box of $400 h_{100}^{-1}$ Mpc is shown in Figure 6 (details in Schuecker et al., in preparation). The function is featuring an interesting maximum at a scale of about $100\text{--}150 h_{100}^{-1}$ Mpc. The location of this maximum is related to the size of the horizon of the Universe at an epoch when the energy density of matter and radiation was equal and it is therefore a very important calibration point for the theoretical modelling of the evolution of our Universe. Note that the construction of the power spectrum shown in Figure 6 is based on a luminosity (mass) selection of the clusters which varies with redshift. Therefore, the quantitative interpretation of this result is not straightforward and more work is needed to relate this function to the power spectrum of the matter density fluctuation in the Universe.

From the power spectrum shown we can also derive another statistical function which is more illustrative to non-experts, the rms-fluctuation level on different scales as provided by a filtering of the cluster density fluctuation field by a simple Gaussian smoothing filter. This function is shown in Figure 7 where we note that at the scale of the maximum of the power spectrum (a scale of ~ 100 Mpc) the cluster density varies typically by about 10%, while at the largest scales (400 Mpc) a fluctuation level of the order of 1% is indicated. This sets a high standard of requirements on the cluster survey, and while we are confident that the present sample contains no systematic biases on the 10% level, further tests and simulations are needed to explore the reliability of the results on the largest scales.

4. Conclusions

It is obvious from the above arguments that studies of the large-scale structure using clusters as probes require great care in the preparation of the sample of test objects. The first results of the REFLEX Survey presented here and some further tests that we have conducted already demonstrate the high quality of the present sample. This is the result of a very homogeneous and highly controlled selection process used to construct the sample. The challenge of the selection work in this survey is to combine the complementary information from X-ray and optical wavelength in the most homogeneous way. Contrary to several earlier studies that we have conducted (Pierre et al. 1994, Romer et al. 1994, Ebeling et al. 1997, DeGrandi 1996) in which the

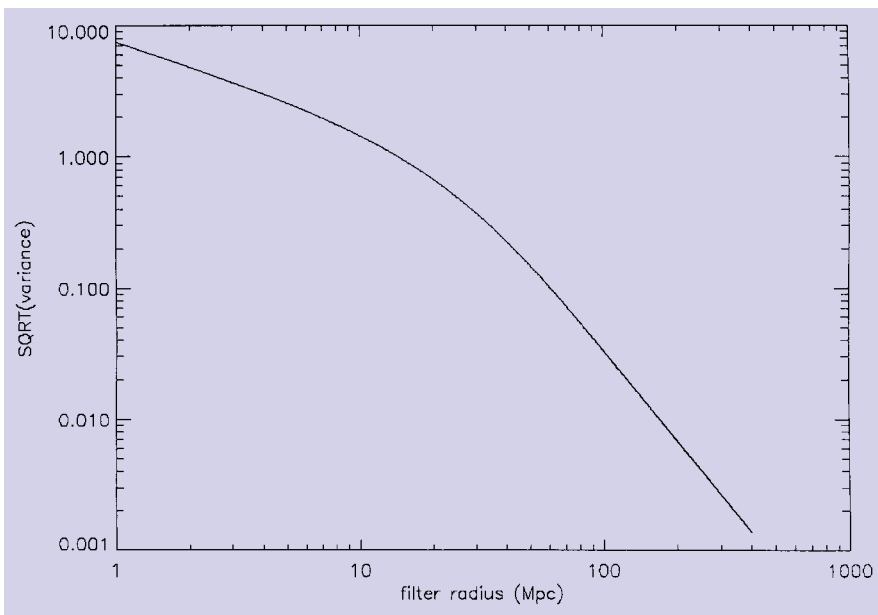


Figure 7: Square root of the variance of the fluctuations in the cluster density distribution as a function of scale (obtained with Gaussian filtering). A value of $H_0 = 100 \text{ km s}^{-1} \text{ Mpc}^{-1}$ is assumed for the scaling.

identification process was optimised to find as many clusters as possible by using all available sources of information, we have now achieved a highly complete cluster selection by just combining the ROSAT All-Sky Survey data and the COSMOS optical data base in a homogeneous way, completely controlled by automated algorithms. Additional information is only used in the final identification but does not influence the selection. This is a very important achievement in this survey work.

The data presented are still not fully complete in redshifts. But with data already obtained in January and September 1998 we can practically complete this data set (to 96%). An extended sample of REFLEX clusters down to a flux limit of $2 \cdot 10^{-12} \text{ erg s}^{-1} \text{ cm}^{-2}$ is already prepared and redshifts are available for more than 70% of the objects. This extended set of about 750 galaxy clusters will help very much to tighten the constraints for the power spectrum and extend it to larger scales. It will further enable us to investigate the cluster correlation function – in particular the X-ray luminosity dependence of the clustering amplitude, which is an issue not yet resolved. Finally, a

complementary ROSAT Survey cluster identification programme is being conducted in the Northern Sky in a collaboration of the Max-Planck-Institut für Extraterrestrische Physik and J. Huchra, R. Giacconi, P. Rosati and B. McLean which will soon reach a similar depth and provide an all-sky view on the X-ray cluster distribution.

References

- Abell, G.O., 1958, *ApJS*, **3**, 211.
 Abell, G.O., Corwin, H.G. and Olowin, R.P., 1989, *ApJS*, **70**, 1.
 Böhringer, H., 1994, in *Studying the Universe with Clusters of Galaxies*, H. Böhringer and S.C. Schindler (eds.), Proceedings of an astrophysical workshop at Schloß Ringberg, Oct. 10–15, 1993, MPE Report No. 256, p. 93.
 DeGrandi, S., 1996, in *Röntgenstrahlung from the Universe*, H.U. Zimmermann, J.E. Trümper, H. Yorke (eds.), MPE Report 263, p. 577.
 Edge, A.C., Böhringer, H., Guzzo, L., et al., 1994, *A&A*, **289**, L34.
 Ebeling, H., Edge, A.C., Fabian, A.C., Allen, S.W., Crawford, C.S., and Böhringer, H., 1997, *ApJ*, **479**, L101.

- Guzzo, L., Böhringer, H., Briel, U., et al., 1995, in *Wide-Field Spectroscopy and the Distant Universe*, S.J. Maddox and A. Aragón-Salamanca (eds.), World Scientific, Singapore, p. 205.
 Heydon-Dumbleton, N.H., Collins, C.A., and MacGillivray, H.T., 1989, *MNRAS*, **238**, 379.
 Pierre, M., Böhringer, H., Ebeling, H., Voges, W., Schuecker, P., Cruddace, R.G., and MacGillivray, H.T., 1994, *A&A*, **290**, 725.
 Romer, A.K., Collins, C.A., Böhringer, H., Cruddace, R.G., Ebeling, H., MacGillivray, H.T., and Voges, W., 1994, *Nature*, **372**, 75.
 Schindler, S.C., Guzzo, L., Ebeling, H., et al., 1995, *A&A*, **299**, L9.
 Schindler, S., Hattori, M., Neumann, D.M., and Böhringer, H., 1996, *A&A*, **317**, 646.
 Tadros, H., Efstathiou, G., and Dalton, G., 1998, *MNRAS*, **296**, 995.
 Trümper, J., 1993, *Science*, **260**, 1769.
 Voges, W., Boller, T., Dennerl, K., et al., 1996, in *Röntgenstrahlung from the Universe*, H.U. Zimmermann, J.E. Trümper, H. Yorke (eds.), MPE Report No. 263, p. 637.
 White, S.D.M., Efstathiou, G., and Frenk, C.S., *MNRAS*, 1993, **262**, 1023.

hxb@mpe.mpg.de

Timing, Spectroscopy and Multicolour Imaging of the Candidate Optical Counterpart of PSR B1509–58

R.P. MIGNANI¹, S. MEREGHETTI², C. GOUIFFES³ and P. A. CARAVEO^{2, 4}

¹ST-ECF, Garching, rmignani@eso.org

²Istituto di Fisica Cosmica “G. Occhialini”, Milan

³Service d’Astrophysique CEA/DSM/DAPNIA C.E Saclay

^{2,4}Istituto Astronomico, Università La Sapienza, Rome, Italy

1. Introduction

Optical counterparts have now been proposed for nine Isolated Neutron Stars (INSs). For some of them (the Crab and Vela pulsars, PSR B0540–69) the identifications have been confirmed through the detection of optical pulsations (with a tentative detection existing also for PSR B0656+14) or, in the case of Geminga, initially from the proper motion of the proposed counterpart. For the rest of the sample (PSR B1509–58, PSR B1055–52, PSR B1929+10 and PSR B0950+08), the optical identification still relies on the positional coincidence with a field object (see e.g. Caraveo 1998 and Mignani 1998 for a summary). Unfortunately, in most cases the intrinsic faintness of such objects hampers the timing of their optical emission, thus making necessary fast-photometry facilities attached to 4-m-class telescopes.

Among the uncertain cases, the best studied is certainly PSR B1509–58. With a dynamical age close to 1500 yrs, PSR B1509–58 is the youngest INS after the

Crab. While its period ($P=150 \text{ ms}$) is long compared with that of the similarly old Crab pulsar and PSR B0540–69, its spin down rate \dot{P} ($\sim 1.5 \cdot 10^{12} \text{ s}^{-1}$) is the highest in the pulsar family. This made it possible to obtain an accurate measurement of the \dot{P} and thus of the pulsar braking index (Kaspi et al. 1994). Since PSR B1509–58 lies close to the geometrical centre of the plerionic supernova remnant MSH15–52 (Strom 1994), it may be one of the very few cases of a pulsar/plerion association. However, the ages of the pulsar and of the remnant are significantly different (Gaensler et al. 1998), casting doubts on the association.

PSR B1509–58 was first detected in X-rays by the Einstein Observatory (Seward & Hardten 1982) and soon after in radio (Manchester, Tuohy and D’Amico 1982) with a single pulse profile preceding in phase the broad, asymmetric, X-ray peak. Pulsations in the 90–600 keV range have been detected by BATSE (Matz et al. 1994) and OSSE (Ulmer et al. 1993) on board GRO while only an upper limit on the source flux at $E \geq 100$

MeV was obtained with EGRET (Brazier et al. 1994).

In the optical, a candidate counterpart ($V \sim 22$), coincident with the pulsar coordinates reported by Taylor, Manchester and Lyne (1993) – TML93 – was proposed by Caraveo et al. (1994a). Were this object indeed the pulsar, at a distance of 4.4 kpc (TML93), its optical emission would certainly be magnetospheric, which is also expected from its young age. However, the corresponding luminosity exceeds by a few orders of magnitude the value expected on the basis of the Pacini Law (Pacini 1971) i.e. $L_{\text{opt}} \propto B^4 P^{-10}$ (where B is the pulsar magnetic field) which works for the other young pulsars (Pacini & Salvati 1987). A firm confirmation of the optical identification is thus of order. Of course, searching for optical pulsations at the radio period is the default way.

The results of timing of the candidate counterpart were first reported by Caraveo (1998) and soon after confirmed by the independent works of Chakrabarty & Kaspi (1998) and of

Shearer et al (1998). In all cases, no optical pulsations at the radio period were observed, thus leaving the problem of the identification open.

In the next sections we will discuss the results of detailed optical investigations of the PSR B1509–58 candidate counterpart performed by our group with the ESO telescopes. Apart from the fast photometry observations of Caraveo (1998), presented here in detail, the data set consists of both multicolour imaging and spectroscopy.

2. Data Overview

2.1 Timing

Optical timing of the Caraveo et al. counterpart was performed in May 1994 from the ESO 3.6-m telescope (Caraveo et al. 1994b). The telescope was equipped with the ESO fast (0.1 ms time resolution) photometer, a single-channel device with a GaAs photocathode sensitive in the range 3500–9000 Å, mainly used to search for an optical pulsar in SN1987A but also for the timing of PSR B0540–69 (Gouiffes, Finley and Ögelman 1992) and of the Vela Pulsar (Gouiffes 1998). A total of 9 observations, split in two adjacent nights, were performed (see Table 1) with two different filters i.e. a standard R and the *og590* which cuts at wavelengths shorter than 5800 Å. According to the seeing conditions, two different apertures were used with diameters of 7 and 4 arcsec, respectively.

Photon arrival times have been corrected for the Earth rotation and revolution (barycentric correction) using the JPL/DE200 FORTRAN code. The periodicity search was performed applying the standard folding technique. First, the whole procedure was tested using as a reference the ~ 5000 -s observation of the slightly fainter ($V \sim 22.5$) PSR B0540–69 (see Fig. 1). The procedure was then applied to the data of PSR B1509–58. Due to the better seeing and atmospheric conditions, we decided to concentrate our analysis on data taken the second night. For each observation, photon counts have been resampled in bins of 4 and 8

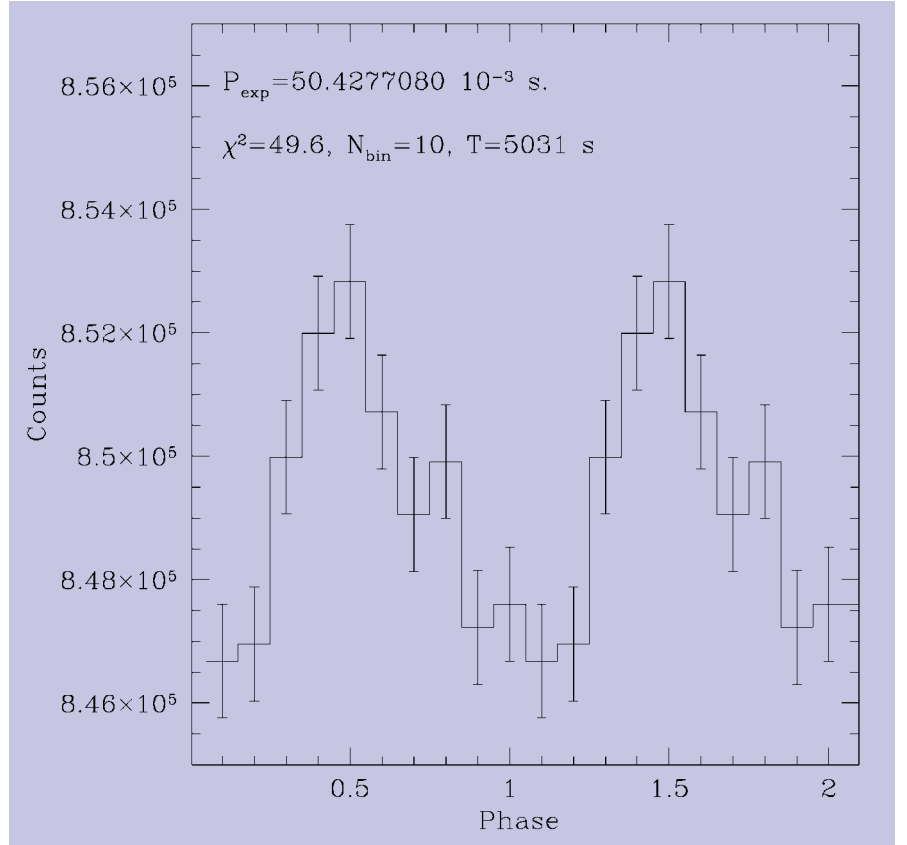


Figure 1: Light curve (≈ 5 ms/bin) of PSR B0540–69 folded over the expected period (P_{exp}) computed by time-propagating at the observing epoch the pulsar’s $P - \dot{P}$ according to the ephemeris of Gouiffes, Finley and Ögelman (1992). Two cycles are shown for clarity. A single broad peak is clearly visible in the light curve $\chi^2 \approx 50$, exactly as expected from previous fast photometry observations. The clear detection of the pulsar shows both the sensibility of the instrument and the correctness of our procedure.

ms. The time series have been folded at different trial periods stepping $\pm 10^{-8}$ s from the expected period, computed using the ephemeris of Kaspi et al. (1994). For each trial period the corresponding χ^2 has thus been computed but no significant maximum was observed in the χ^2 distribution. The periodicity search was repeated using the whole data set of the second night ($\approx 20,000$ s) but no significant improvement was achieved. Using as a zero point the observation of a standard star ($V = 16.125$) from an E5 region of a Graham field, we could derive an up-

per limit $R \sim 23$ –23.5 on the pulsed magnitude, which corresponds to a pulsed fraction $\geq 15\%$, similar to the value given by Chakrabarty & Kaspi (1998).

This means that if the optical candidate of Caraveo et al. is indeed the counterpart of PSR B1509–58, its pulsed fraction must be much smaller than for the Crab and Vela pulsar, which have pulsed fractions $\sim 100\%$ and $\geq 50\%$, respectively.

2.2 Spectroscopy and Imaging

To investigate the possibility of a wrong association with a fore/background object, in June 1995 we performed spectroscopy of the object from the NTT. Three 90-minute, medium-resolution (2.3 Å/pixel) spectra were obtained with EMMI-Red (ESO Multi Mode Instrument) in the wavelength range 3800–8400 Å. Unfortunately, the very low S/N made it impossible to perform any spectral analysis of the source, apart from excluding the presence of strong emission/absorption lines.

Multicolour images were also collected from the NTT during different observing runs (see Table 2 for a summary). To complement and improve the first measures in V and R of Caraveo et al. (1994a) we collected longer exposures with SUSI in B, V and the first exposure in I in 1995. A second deep observation

Obs.#	MJD	T (s)	r (arcsec)	CR (cts/s)	Filt	Obj
1	49478	1468	4	756	og590	PSR B1509-58
2		2821	4	825	og590	PSR B1509-58
3		462	7	2944	og590	PSR B1509-58
4		6305	7	3269	og590	PSR B1509-58
5		6097	7	1267	R	PSR B1509-58
6	49479	5031	4	1687	free	PSR B0540-69
7		3616	4	305	R	PSR B1509-58
8		2745	4	312	R	PSR B1509-58
9		6809	4	294	R	PSR B1509-58
10		6813	4	316	R	PSR B1509-58
11		4094	4	640	R	Graham std.

Table 1: Journal of fast photometry observations. Columns list the observing sequence, the observing epochs (MJDs), the duration of the single observations (s), the aperture diameter (arcsec), the count rate in the aperture (cts/s), the filter name and the target identifier.

in R was obtained in 1997. After cosmic-ray rejection, bias subtraction and flat fielding, a zero point was computed for each filter using photometric standards in the Stobie and Landolt fields. These new observations yielded more accurate V (22.1 ± 0.1) and R (20.8 ± 0.1) magnitudes together with the first measurements in B (23.8 ± 0.3) and I (19.8 ± 0.1). In order to assess the colours of the object, an unknown but potentially important amount of interstellar absorption should be considered. X-ray spectral fittings give an $N_H \approx 8 \times 10^{21} \text{ cm}^{-2}$ (Becker & Trümper 1997) with an, at least, 50% uncertainty which implies a difference of about one magnitude on the colour indexes. Assuming that the object be at the pulsar distance of 4.4 kpc, it could be thus anything from a G star (for the lowest value of the N_H) to a much highly absorbed O or B star. To search for other possible candidates we have used our deepest exposure of the field (the 1997 one) taken with SUSI under better seeing conditions (~ 0.7 arcsec). The revised radio co-ordinates of PSR B1509–58, reported in Taylor et al. (1995) have been registered on the image using the UK STARLINK software ASTROM (Wallace 1990) and a reference frame given by several USNO stars identified in the SUSI field (2×2 arcmin). Adding in quadrature to the pulsar positional error (1.3 arcsec) an average uncertainty of 0.25 arcsec attached to the absolute position of the USNO stars, and the r.m.s. of the plate solution fit (0.42 arcsec) we can estimate a conservative error of 1.4 arcsec on our astrometry. The radio position of the pulsar is thus shown in Figure 2, marked by a yellow cross. As already noted by Caraveo (1998), the revised radio co-ordinates of PSR B1509–58 are slightly different from the old ones reported in TML93, also marked in Figure 2 (in blue). However, the associated errors (± 1 arcsec in both dimensions) leave room for a substantial agreement. The object inside the overlapping error circles is the candidate counterpart of Caraveo et al. (1994a).

As evident from Fig.2, no other source is visible inside the uncertainty regions, down to a lower limit of $R \sim 25$.

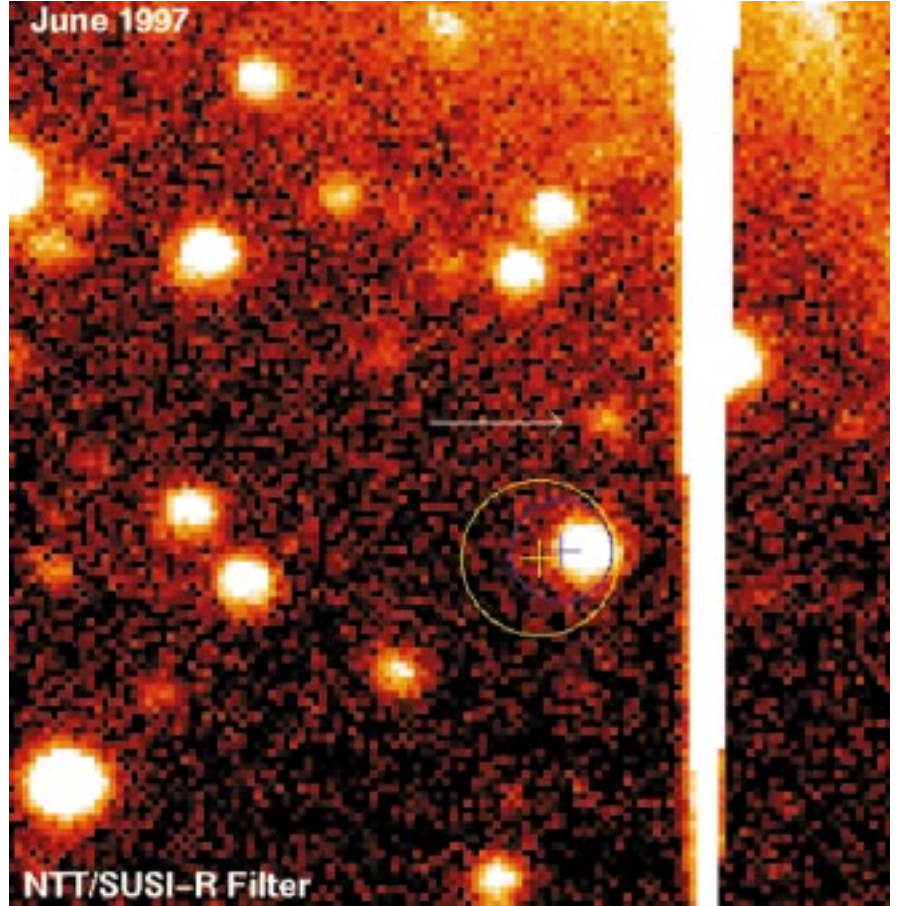


Figure 2: 16×16 arcsec 2 R-band image of the field of PSR B1509–58, taken in June 1997 with the ESO/NTT. The image has been obtained with the SUperb Seeing Imager (SUSI) under sub-arcsec seeing conditions (Q 0.7 arcsec). The exposure time was 45 min. The pixel size of the CCD is 0.13 arcsec. The yellow cross marks the position of PSR B1509–58 computed according to the revised radio coordinates of Taylor et al (1995). The circle ($r = 1.4$ arcsec) corresponds to the uncertainty region associated to the pulsar position, resulting from the combination of the error on the radio coordinates ($r \sim 1.3$ arcsec), the average uncertainty on the absolute coordinates of the USNO stars (~ 0.25 arcsec) and the σ of the astrometric fit (~ 0.42 arcsec). The candidate optical counterpart of the pulsar proposed by Caraveo et al. (1994a) is visible inside the error circle. For completeness, the old pulsar position from TML93 ($r \approx 0.9$ arcsec) is also shown in blue. The faint object ($R \approx 24$) seen about 2 arcsec north of the pulsar position and marked by the arrow is too far to claim any association.

3. Conclusions

No pulsations were detected from the proposed optical counterpart of PSR B1509–58, thus adding more weight to the results obtained by Chakrabarty & Kaspi (1998) and Shearer et al. (1998). Unless

invoking a peculiar-emission geometry, the lack of optical pulsations strongly argues against the identification of Caraveo et al. (1994a). Given the high interstellar absorption towards the pulsar, multi-colour imaging does not help to constrain the real nature of the object. Spectroscopy, to be performed with the UT1 of the VLT, is thus needed. Were the optical identification of Caraveo et al. be disproved, the real counterpart of PSR B1509–58 is to be searched somewhere in the close surroundings. In this case, it must be fainter than $R \sim 25$. This is in agreement with the Pacini law (1971) which would predict for PSR B1509–58 a magnitude ~ 27 .

Although this values is certainly within reach of the VLT (Mignani et al. 1999), if located a fraction of arcsec from the present candidate, such a faint object would be hardly visible from the ground even under exceptional seeing conditions. The situation would thus be similar to the case of PSR B1055–52, close (≤ 4 arcsec) to a ~ 14.6 magnitudes

Date	Det	Filt.	T	mag
July 93	EMMI-Red	V	5m	22.0 ± 0.2
	EMMI-Red	R	10m	20.8 ± 0.3
	EMMI-Red	B	5m	≥ 23
Jan 95	SUSI	B	20m	23.8 ± 0.3
	SUSI	V	25m	22.1 ± 0.1
	SUSI	I	5m	19.8 ± 0.1
Jul 97	SUSI	R	45m	20.8 ± 0.1

Table 2: Summary of the available photometry of the PSR B1509–58 candidate counterpart performed with the NTT from 1993 to 1997. Columns list the observing epochs, the detector used, the filters, the exposure times and the observed (not-dereddened) magnitudes. The July 1993 observations are the ones also reported in Caraveo et al. (1994a).

brighter field star and unresolved by the NTT/SUSI (Mignani et al. 1997). As in that case, high-resolution imaging of the region with the HST would be the only way to pinpoint the pulsar.

Acknowledgements

We acknowledge the support software provided by the Starlink Project, which is funded by the UK SERC. C. Gouiffes greatly acknowledges the support of the technical staff at La Silla for his invaluable and constant help in the use of the fast photometer.

References

Becker, W. & Trümper, 1997, *A&A* **326**, 682.
 Brazier, K.T.S. et al, 1994, *MNRAS*, **268**, 517.

Caraveo, P.A., Mereghetti, S. and Bignami, G.F., 1994a, *ApJ* **423**, L125.
 Caraveo, P.A., Bignami, G.F., Mereghetti, S., Mignani, R. and Gouiffes, C., 1994b, *BAAS* **184**, 2104C.
 Caraveo, P.A., 1998, *Adv. in Sp. Res.* Vol. **21**, 187.
 Chakrabarty, D. & Kaspi, V., 1998, *ApJ* **498**, L37.
 Gaensler, B.M., Brazier, K.T.S., Manchester, R.N., Johnston, S. and Green, A.J., 1998, *Memorie della Società Astronomica Italiana* – in press.
 Gouiffes, C., Finley, J.P. and Ögelman, H., 1992, *ApJ* **394**, 581.
 Gouiffes, C., 1998, *Neutron Stars and Pulsars: Thirty years after the discovery.* ed. N. Shibazaki, N. Kawai, S. Shibata and T. Kifune, p. 363, Universal Academic Press.
 Kaspi, V.M. et al., 1994, *ApJ* **422**, L83.
 Manchester, R.N., Tuohy, I.R. and D'Amico, N., 1982, *ApJ* **262**, L31.

Matz, S.M. et al, 1994, *ApJ* **434**, 288.
 Mignani, R., Caraveo, P.A. and Bignami, G.F., 1997, *ApJ* **474**, L51.
 Mignani, R., 1998, *Neutron Stars and Pulsars: Thirty years after the discovery.* ed. N. Shibazaki, N. Kawai, S. Shibata & T. Kifune, p335, Universal Academic Press.
 Mignani, R., Caraveo, P.A. and Bignami, G.F., 1999, *A&A* – in press.
 Pacini, F., 1971, *ApJ* **163**, L17.
 Pacini, F. & Salvati, M., 1987, *ApJ* **321**, 447.
 Seward, F.D. & Hardnen, F.R., 1982, *ApJ* **256**, L45.
 Shearer, A. et al, 1998, *A&A* **333**, L16.
 Strom, R.G., 1994, *MNRAS* **268**, L5.
 Taylor, J. H., Manchester, R. N. and Lyne, A. G., 1993, *ApJS* **88**, 529.
 Taylor, J.H., Manchester, R.N., Lyne, A.G. and Camilo, F., 1995 (<http://pulsar.princeton.edu/pulsar/catalog.shtml>)
 Ulmer, M.P. et al, 1993, *ApJ* **417**, 738.
 Wallace, P.T., 1990, *Starlink User Note 5.11*, Rutherford Appleton Laboratory.

The First X-ray Emitting Brown Dwarf

F. COMERÓN, *ESO, Garching, Germany*

R. NEUHÄUSER, *MPE, Garching, Germany*

A.A. KAAS, *Stockholm Observatory, Stockholm, Sweden*

The increasing number of brown dwarfs discovered in the last few years is rapidly opening the possibilities of studying a wide range of their properties and the ways in which these depend on essential parameters, such as the mass, the age, the rotation, or the environment. One of these properties is the magnetic field, which in principle should be expected to be important in fully convective objects such as brown dwarfs. The chromospheric X-ray emission, widely observed in M-type dwarfs (Neuhäuser 1997), has its origin in this magnetic activity. As such, it offers an observational tool to probe the interior of these objects, the mechanisms for the generation and maintenance of their magnetic fields, and the way in which the magnetic activity is affected by the basic parameters of the object. The detection of X-ray emission from brown dwarfs is thus of great importance to extend our understanding of the properties of stellar magnetic fields to the substellar domain, as well as to ascertain to what extent a small, substellar

mass, and the consequent lack of a permanent nuclear energy source, can have an impact in the production and the evolution of a magnetic field.

Until recently, no conclusive evidence for X-ray emission from brown dwarfs had

been found, as shown by an extensive search in ROSAT archive observations near the position of known bona-fide and candidate brown dwarfs (Neuhäuser et al. 1999). However, a newly identified member of the Chamaeleon I star form-

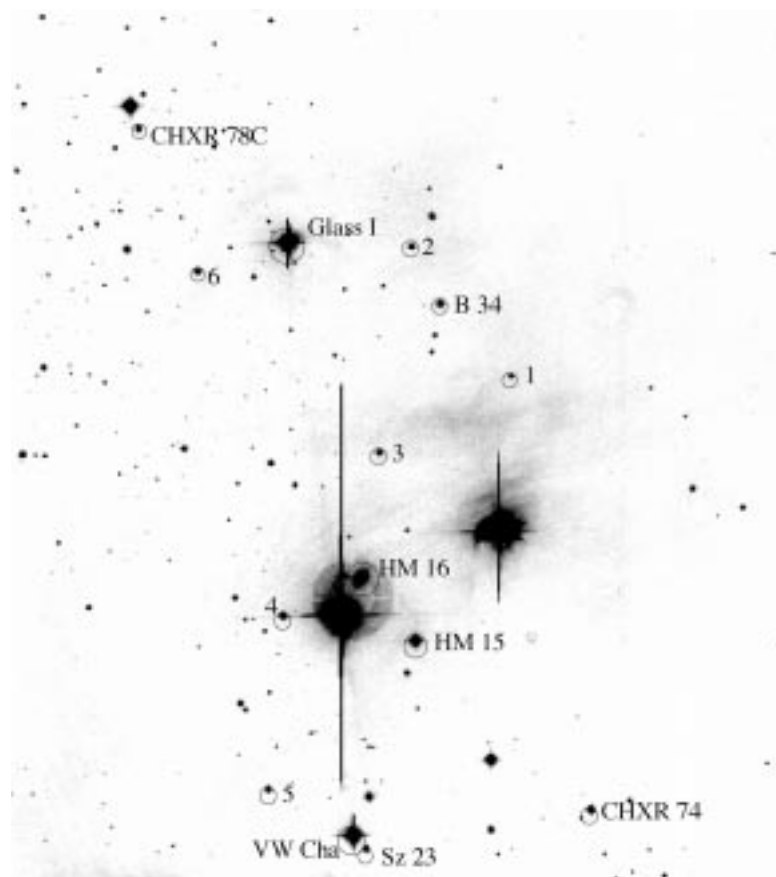


Figure 1: A 13' × 13' image of the centre of the Chamaeleon I aggregate in the I band. Labels identify previously known members of the aggregate, and numbers 1 to 6 denote the low-mass members newly found in the H α survey by Comerón et al. 1999, i.e. Cha H α 1 to 6. This image was obtained using DFOSC at the 1.5-m Danish telescope on La Silla, and includes the area surveyed in the infrared using IRAC2b at the ESO-MPI 2.2-m telescope. The area covered by the X-ray and ISOCAM observations is considerably larger.

ing cloud, whose temperature and luminosity clearly identify it as a brown dwarf younger than one million years, is clearly detected by a deep ROSAT observation with a 9σ detection significance (Neuhäuser & Comerón 1998). This object is only the second bona-fide brown dwarf to be detected in a star-forming region (Luhman et al. 1997), and the first one known to emit in X-rays.

The identification of the X-ray emitting brown dwarf in Chamaeleon I, hereafter referred to as Cha H α 1, is the result of three parallel efforts aimed at finding brown dwarfs in this star-forming region by means of different characteristics typical of low-mass young stellar objects. The first of them was a research on deep observations in the ROSAT archive, amounting to 37.8 ksec of effective observing time at the position of Cha H α 1, looking for faint, previously unidentified Chamaeleon I members revealed by their X-ray emission. The second one consisted of the combination of a JHK survey of 100 arcmin² of the centre of the aggregate, carried out with IRAC-2b at the ESO-MPI 2.2-m telescope on La Silla in May 1997, and an objective-prism survey of approximately the same field using DFOSC at the 1.5-m Danish telescope, also on La Silla, in March 1998. The aim in this case was to identify new faint members by means of their possible near-infrared excess or by their emission in H α . A third set of observations came from a large-area star-formation survey carried out with ISOCAM at 6.7 and 14.3 μ m (Nordh et al. 1996). The aim of this survey was to identify young stellar objects by means of their mid-IR excess in the colour index [14.3/6.7] and obtain a more complete census of the young stellar population for IMF studies. From an empirical correlation between the flux at 6.7 μ m of the excess sources and bolometric lu-

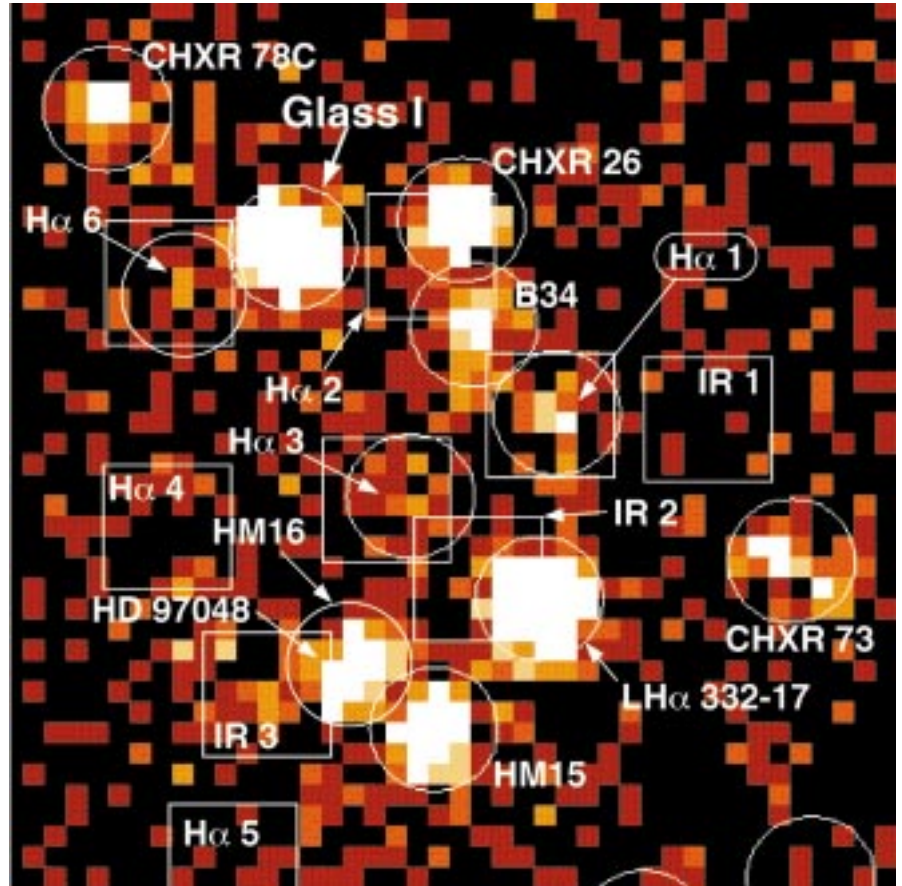


Figure 2: Deep ROSAT X-ray image of the centre of the Chamaeleon I aggregate, covering an area similar to that of Figure 1. The position of all the known and newly identified members is indicated.

minosities (Prusti et al. 1992) extrapolated to faint sources, as well as adopting the median age of T Tauri stars of 3×10^6 yr (Lawson et al. 1996) as a common age for these, the theoretical models of D'Antona & Mazzitelli (1997) predict that about 25% of the ISOCAM selected

young stellar objects in Cha I are substellar (Olofsson et al. 1998), a result that must be confirmed spectroscopically.

Cha H α 1 is identified in all these surveys. Figure 1 shows it in an I-band image of the field surveyed in H α , obtained also with the 1.5-m Danish telescope. Also indicated are the previously known members of the aggregate (e.g. Lawson et al. 1996), as well as five other new members identified by their H α emission whose masses are near, and possibly below, the limit separating stars from brown dwarfs (Comerón et al. 1999). The X-ray image of the same field is shown in Figure 2. The initial spectrum of Cha H α 1 from the DFOSC survey revealed a prominent emission at H α and a late M spectral type, but given the faintness of the object in the H α region, it was not possible to precisely determine the spectral subtype, an essential element to ascertain its temperature and therefore its mass. For this reason, additional spectroscopic observations at visible and near-infrared wavelengths were carried out in May 1998 using EMMI and SOFI at the NTT.

The visible spectrum of Cha H α 1 obtained with the NTT is shown in Figure 3, where it is compared to late M spectral standard stars. The overall appearance of the spectrum clearly indicates a late M type, as confirmed as well by several indicators which measure the strengths of temperature-sensitive spectral features.

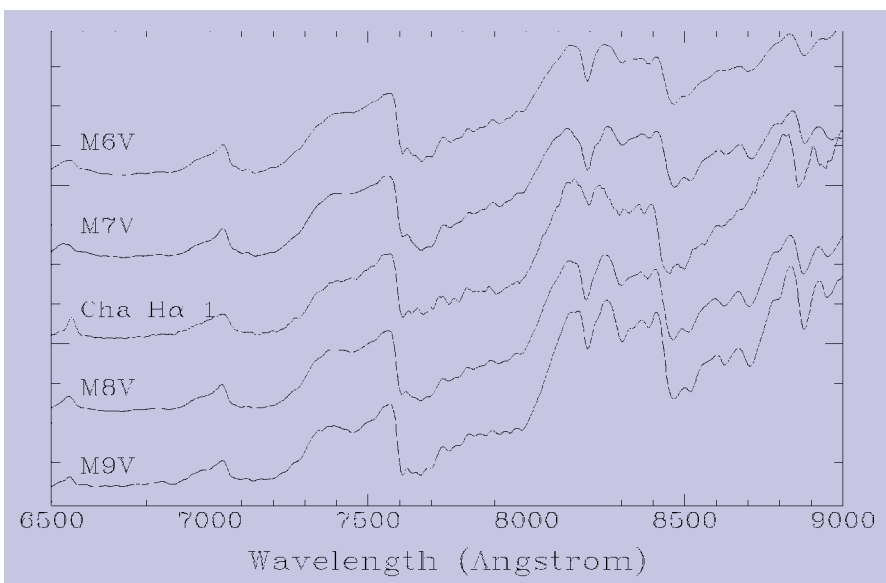


Figure 3: The visible spectrum of Cha H α 1 obtained with EMMI at the NTT. The M6V comparison spectrum is that of Gl 406; M7V, of vB 8; M8V is the combination of LHS 2243, LHS 2397 A, LP 412-31, and vB 10; and M9V, of BRI 1222-1222, LHS 2065, LHS 2924, and TVLM 868-110639. The spectral classification of the standard stars is from Kirkpatrick et al. 1995.

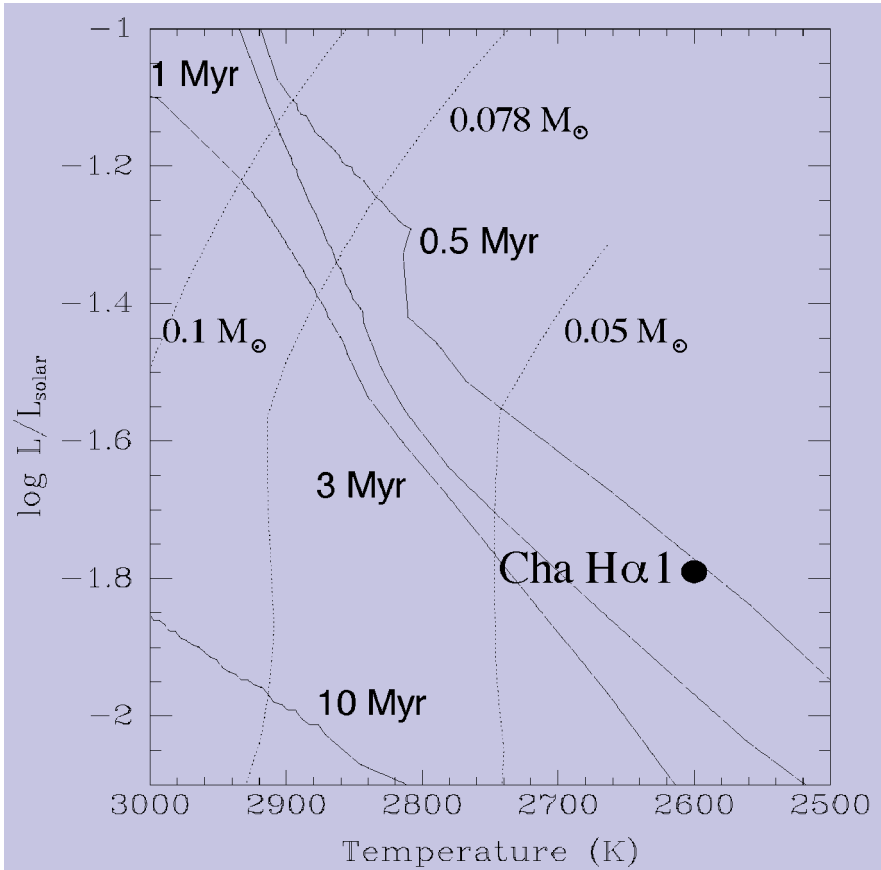


Figure 4: H-R diagram showing the position of Cha H α 1. The lines give the position of the isochrones (solid lines) and lines of equal mass (dotted lines) for late M spectral types according to Burrows et al. 1997. The line labelled as $0.078 M_{\odot}$, separates brown dwarfs from low mass stars.

Based on these elements, we classify Cha H α 1 as M7.5–M8. Some differences with the standard field M dwarfs are apparent as well: the principal one is the smaller depth of the Na I absorption feature at 8190 Å, which is known to be sensitive to gravity. The smaller depth is in fact a confirmation of the youth of Cha H α 1, as an object in the early stages of contraction should have a surface gravity intermediate between that of a dwarf (where Na I is strong) and a giant (where Na I is weak).

The precise spectral classification obtained from the NTT visible spectrum makes it possible to derive the surface temperature of Cha H α 1, using existing spectral type-temperature calibrations (Leggett et al. 1996). In this way, we obtain a temperature of 2600 K. On the other hand, the luminosity can be determined from the visible and near-infrared photometry obtained with our DFOSC and IRAC2b observations respectively: we adopt for Cha H α 1 the distance of 160 pc to Chamaeleon I recently derived from Hipparcos data and extrapolate to M7.5 the bolometric corrections and intrinsic colours of Kenyon and Hartmann (1995) in order to find the reddening-corrected luminosity of the object. In this way, we obtain $\log(L/L_{\odot}) = -1.79$. The derived temperature and luminosity allow the direct comparison with the results of pre-main-sequence evolutionary tracks, thus allowing an estimate of the age and

mass of Cha H α 1. Using pre-main-sequence tracks by Burrows et al. (1997), we obtain a mass of $0.03 M_{\odot}$ and an age of 5×10^5 years. The position of Cha H α 1 in the H-R diagram, and the lines of equal mass and age in that diagram predicted by the isochrones, are shown in Figure 4. The results are essentially unchanged by using tracks by D’Antona & Mazzitelli (1997), whose main difference is the allocation of a somewhat younger age for our objects, $\sim 3 \times 10^5$ years. Strictly, the temperature scale adopted is valid only for field dwarfs, whose surface gravities are higher; M giants of the same spectral subtype tend to be hotter, what may imply that our temperature for Cha H α 1 is actually an underestimate. However, even allowing for a total underestimate of 200 K which would include errors due to surface gravity effects and uncertainties in the temperature calibrations through model-atmosphere fitting, Cha H α 1 still remains safely in the substellar realm, with a mass below $0.06 M_{\odot}$.

Cha H α 1 displays most of the typical signatures of youth commonly associated with low-mass young stellar objects. The X-ray luminosity derived from the ROSAT observations is $\log L_X(\text{erg s}^{-1}) = 28.3 \pm 0.1$, implying an X-ray to bolometric luminosity ratio of $\log(L_X/L_{bol}) = -3.44$, well within the range occupied by low-mass stars in young clusters. This result suggests that there is no essential difference in the X-ray emission properties of very

young stellar objects when crossing the threshold separating stars from brown dwarfs. The prominent H α emission, with an equivalent width of 59 Å, is also typical of classical T Tauri stars. On the other hand, and unlike in the case of higher-mass members of Chamaeleon I and other young aggregates, this strong H α emission is not accompanied by a noticeable excess emission in the K near-infrared band; excess emission is nevertheless observed at 6.7 and 14.3 μm , as revealed by the ISOCAM measurements. The ISOCAM colour index $[14.3/6.7] = 0.15$ corresponds to $\alpha_{ISO} = -0.55$ ($\alpha = d \log(\lambda F_{\lambda}) / d \log \lambda$), which is in agreement with it being a Class II object. This colour is in rough agreement with theoretical models of flared circumstellar disks (Kenyon & Hartmann 1995). Excess is also found in the $K - m(6.7 \mu\text{m})$ colour index. In principle, the lack of excess in the K band is to be expected: neither viscous heating at the presumably low rates of accretion on a very low mass object like Cha H α 1, nor the irradiation by such a cool central star, should produce in a circumstellar disk any significant emission in the K band, although such excess emission could become important at longer wavelengths. However, we note that other very low mass objects with comparably low temperatures do display emission of circumstellar origin in the K-band (Comerón et al. 1998, Wilking et al. 1998). Our discovery of X-ray emission from Cha H α 1, while revealing brown dwarfs as a new class of X-ray emitting objects, seems to suggest that the transition from the stellar to the substellar domain does not imply a dramatic change in the properties of very young low-mass, fully convective objects. This seems to be reinforced by the very recent identification of X-ray emission from GY 202 (Neuhäuser et al. 1999), one of the probable brown dwarfs found in the ρ Ophiuchi cluster by Comerón et al. (1998 and references therein), whose substellar character has received recent support by spectroscopic observations by Wilking et al. (1998). The characteristics of this object (mass, age, $\log(L_X/L_{bol})$) seem to be very similar to those of Cha H α 1. The magnetic properties of massive young brown dwarfs may therefore be simply an extension of those already well studied in their more massive counterparts, M-dwarf stars. Nevertheless, a number of questions remain open: why no X-ray emission is seen from other, more evolved brown dwarfs, despite the availability of observations (Neuhäuser et al. 1999) that put rather severe limits on the $\log(L_X/L_{bol})$ ratios of some of them? Is X-ray emission a feature restricted to the very early stages of the evolution of brown dwarfs, perhaps decreasing at later times as a consequence of the lack of a stable source of energy in their interiors? What is the dependence of X-ray emission of brown dwarfs on parameters such as the mass, the age, the luminosity, the rotation, or the existence of circumstellar material? More detailed studies of objects such as Cha

H α 1, and better constraints on the X-ray emission of other brown dwarfs, will be necessary to answer these questions.

Acknowledgements: We thank the staff at ESO-La Silla for assistance with the observations, and Dr. Kevin Luhman for the comparison spectra presented in Figure 3. This work was supported by NATO Collaborative Research Grant CRG 940671. RN wishes to thank the Deutsche Forschungs-Gemeinschaft for financial support in their Star-Formation programme. AAK thanks for the financial support from the Swedish National Spaceboard. ROSAT is supported by the Max-Planck Society and the German Government (BMBF/DLR). ISO is an ESA project with instruments funded by ESA Member States and with the participation of ISAS and NASA.

References

- Burrows, A., Marley, M., Hubbard, W.B., Lunine, J.I., Guillot, T., Saumon, D., Freedman, R., Sudarsky, D., Sharp, C., 1997, *ApJ*, **491**, 856.
- Comerón, F., Rieke, G.H., Claes, P., Torra, J., Laureijs, R.J., 1998, *A&A*, **335**, 522.
- Comerón, F., Rieke, G.H., Neuhäuser, R., 1999, *A&A*, in press.
- D'Antona, F., Mazzitelli, I., 1997, *Mem. S. A. It.*, **68**, 807.
- Kenyon, S.J., Hartmann, L., 1995, *ApJS*, **101**, 117.
- Kirkpatrick, J.D., Henry, T.J., Simons, D.A., 1995, *AJ*, **109**, 797.
- Lawson, W.A., Feigelson, E.D., Huenemoerder, D.P., 1996, *MNRAS*, **280**, 1071.
- Leggett, S.K., Allard, F., Berriman, G., Dahn, C.C., Hauschildt, P.H., 1996, *ApJS*, **104**, 117.
- Luhman, K.L., Liebert, J., Rieke, G.H., 1997, *ApJ*, **489**, L165.
- Neuhäuser, R., 1997, *Science*, **276**, 1363.
- Neuhäuser R., Comerón F., 1998, *Science*, **282**, 83.
- Neuhäuser R., Briceno, C., Comerón, F., Hearty, T., Martín, E.L., Schmitt, J.H.M.M., Stelzer, B., Supper, R., Voges, W., Zinnecker, H., *A&A*, submitted.
- Nordh, L., Olofsson, G., Abergel, A., et al., 1996, *A&A*, **315**, L185.
- Olofsson, G., Kaas, A.A., Nordh, L., et al., 1998, In: *Brown Dwarfs and Extrasolar Planets*, eds. Rebolo R., Martín, E.L., Zapatero Osorio, M.R., *ASP Conf. Ser.* **134**, p. 81.
- Prusti, T., Whittet, D.C.B., Wesselius, P.R., 1992, *MNRAS*, **254**, 361.
- Wilking, B.A., Greene, T.P., Meyer, M.R., 1998, *AJ*, in press.

fcomeron@eso.org

CALL FOR IDEAS FOR FUTURE PUBLIC IMAGING SURVEYS

Based on the experience gained with EIS, and to prepare for the full exploitation of future imaging facilities such as the VST, ESO is ready to co-ordinate efforts to provide the community with imaging survey data taken at the La Silla Telescopes (2.2-m and NTT).

To this end, and following the recommendation of the Working Group for Surveys (WGS), ESO is issuing the present CALL FOR IDEAS for future public imaging surveys.

Scientists in the community are invited to fill out the form available in the ESO EIS Web page with their suggestions for future surveys (http://www.eso.org/science/eis/eis_ideas/wf2.2_form.html). The compiled responses will be forwarded to the chairman of the WGS (Joachim Krautter, J.Krautter@lsw.uni-heidelberg.de).

DEADLINE FOR SUBMISSION: FEBRUARY 15, 1999

In elaborating their suggestions interested scientists should consider the following guidelines.

A Public survey should primarily be aimed at the maximisation of the scientific outcome of the VLT, and should consist of observations not likely to be covered by "private" proposals.

Public surveys should also have a broad scientific goal, provide data that could be fruitfully used by astronomers working in different astronomical areas, e.g. solar system, stellar populations, observational cosmology, etc., and should be easily complemented by 'private' proposals aimed at more specific scientific goals. As a consequence, in general, public surveys may concentrate on broad-band imaging, leaving e.g. narrow-band follow up or second-epoch observations to 'private' proposals.

The Working Group will collect the submitted ideas, and elaborate one or more detailed proposals to be submitted to the OPC, including a description of the survey products, distribution policy and schedule.

It is expected that a Survey Team, following the model of the EIS team, will be charged to execute the survey, combining in it ESO scientists and Visiting scientists from the community. In the future, as standard survey tools become available throughout the community, one may also envisage public surveys being conducted by Teams assembled in a member state institute with demonstrated experience and required infrastructure. Shortly after OPC approval of a survey, ESO will issue an announcement of opportunity for the recruitment of the Visiting Scientists who will participate in the effort.

Please read also the EIS Working Group Recommendations regarding future surveys.

EUROPEAN SOUTHERN OBSERVATORY ATLAS OF THE NORTHERN SKY

In 1990 the Palomar Observatory (California Institute of Technology) and the European Southern Observatory (ESO) started the joint production of the Palomar Observatory - European Southern Observatory Atlas of the Northern Sky, also called the POSS II SURVEY.

The Atlas is based on photographic plates obtained with the Oschin Schmidt Telescope on Mount Palomar. It consists of 894 fields each in Blue (B), Red (R) and near Infrared (I), covering the entire northern sky. The film copies are produced at ESO/Garching. The first copies were made in 1990 and the Survey will be completed by the end of 2001.

We now have a few sets available for sale, either complete sets in all three colours or one-colour-sets. The amount of available sets is limited and there will be no further edition of the Atlas produced.

For more information, prices and orders please contact Christine Telander, ctelande@eso.org.

Technical information can be obtained from Jean Quebette, jquebatt@eso.org.

EUROPEAN SOUTHERN OBSERVATORY
Karl-Schwarzschild-Str. 2, D-85748 Garching bei München, Germany
Tel: +49-89-32006-0 – Fax: +49-89-32006-480 – <http://www.eso.org>

Observations with Adaptive Optics: Getting There

A REPORT ON THE ESO/OSA CONFERENCE, SONTHOFEN, 7-11 SEPTEMBER 1998

M.-H. ULRICH, ESO

Adaptive Optics on Large Telescopes has opened up the new field of ground-based IR and optical astronomy on scale of less than $0.5''$. The resolution routinely achieved is better than $0.15''$ – as if the observer had jumped more than 3 times closer to the observed object – a dream! Advances are occurring in all fields, from the solar system to high z galaxies.

The first Conference centred on astrophysical results obtained with Adaptive Optics (AO) "Astronomy with Adaptive Optics: Present Results and Future Programs" was organised jointly by ESO and the Optical Society of America and took place 7–11 September 1998, in the Bavarian resort of Sonthofen.

Here, I highlight the points that appeared to me as the most pressing and important of those discussed in and also out of sessions at the Conference.

These points revolve around the central question on how to use AO most effectively and implement the powerful tools needed to proceed efficiently from raw data to astrophysical papers.

To make the reading of this report easier, I do not give references to any of the papers presented at the Conference except for the figures. Full versions of the papers can be found in the proceedings, which are now available on the Web and will appear in print in early 1999 (see Section 6 for Web address).

1. How to Make AO Observations Efficient

In astrophysics, the scientific value of the output of any instrument is the combination of the astrophysical questions driving the observing programmes and the number and technical quality of the published papers.

Leaving aside for a moment the question of the scientific driver, one can ask the question: What is the most efficient way to obtain astrophysical results with Adaptive Optics now that this technique has been shown to work?

The best way is to have goals that are in line with what the instrument can deliver – a trivial statement when applied to decades-old techniques such as direct imaging and spectrography. It implies, in fact, having a full understanding of the AO data acquisition, calibration and analysis process at the time of the proposal preparation since this process

defines the achievable limits of performance.

The AO observations have to be understood as an ensemble formed by the simulations, the planning of the data reduction, the scientific tactical aspects of the optimisation at the telescope, the data acquisition itself, and finally the data processing, analysis and publication. *The proposal preparation must aim at an effective coupling of this entire procedure with sound astrophysical objectives.*

It follows that the observer must become familiar with the various parts of this ensemble and have at his disposal:

- a powerful system of simulation where one can choose as input (i) a variety of real or modelled science objects, (ii) different values of the parameters which characterise AO performance i.e. τ_0 , τ_1 , and θ_0 (isoplanicity) relevant to the Observatory, and (iii) different magnitudes and radial distances of the reference star.

- procedures to calculate the Point Spread Function (PSF) and its noise from the values in (ii) and (iii) plus the required exposure time needed to achieve a given S/N on the science object.

- a library of deconvolution algorithms with illustrative examples of their application.

- an observatory data bank with raw and processed data with calibrations and PSF with which the observer can acquire a first-hand knowledge of the potential and limits of the AO instrument.

- examples of successful data acquisition and processing.

- catalogues of artefacts and spurious effects.

Moreover, at the telescope, the visiting observer should have some possibility to modify a pre-registered observing plan in order to (1) adapt to changing seeing conditions since the performance of AO is so dependent on them (in some conditions, the Strehl ratio depends on the seeing to the sixth power), and (2) immediately repeat or expand observations for which an on-line quick look reveals exciting/unexpected results – it is especially important to have this possibility in a new field such as high angular resolution because the results are often difficult to predict and artefacts can appear. This needs an on-line pipeline for the data reduction. This would result in a more agile observational procedure, enabling the ob-

server to follow through and concentrate on a winning trail.

Finally, it must be recalled that there are different types of AO science to be extracted from the AO observations: photometry, astrometry, mapping of extended objects, mapping around bright sources, detection of faint companions to bright stars, polarisation, and spectra at low and high resolution. They differ rather significantly by the data characteristics which they require, such as angular resolution, Strehl ratio, accuracy in flat-fielding, extent of the corrected field, and S/N and, therefore, call for different observing strategies.

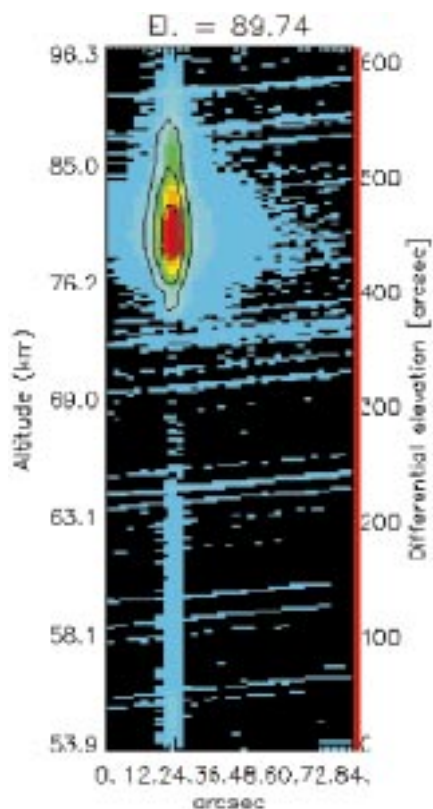


Figure 1: Image of the laser plume in the mesospheric sodium layer and the top of the Rayleigh scattering cone. In this experiment (August 1998) the laser beam emitted by the AO+LGS ALFA system on the 3.5-m telescope at Calar Alto is observed from the side with the 2.2-m telescope located at 343 m from the 3.5-m telescope. The lines across the figure are star trails. Abscissae: apparent width of the beam in arcsec. Ordinates: left altitude in km and right elevation from the bottom of the image in arcsec (F. Delplanque et al.).

2. Determination of the PSF and Deconvolution

Central to the AO data analysis is the determination of the PSF and the subsequent deconvolution. This question is being vigorously investigated and a number of new developments and results were presented at the Conference. The effort is directed towards the precise mapping of the PSF envelope in radius and azimuth. The method used initially, when there is no star in the field bright enough to provide an accurate PSF, was to observe a nearby bright star before and after the science object observations. This has proven to be unsatisfactory in most cases because of significant changes in the seeing conditions (and thus in the PSF profile) occurring between calibration and science exposures. New approaches are being actively explored alone and in combination:

– The "synchronous PSF" method (developed by J.-P. Véran) makes use of the wavefront sensor, WFS, data to determine the on-axis PSF. The PSF so determined becomes a poorer match with fainter reference stars, increasing distance from the reference star, and, of course, worsening seeing.

The synchronous PSF method can, in principle, be extended to off-centre positions but only if a SCIDAR is on site to measure the dependence on the profile of the turbulence with altitude.

– A method particularly suited to photometry in crowded fields e.g. globular clusters, consists in starting from a given (initially imprecisely known) PSF and using the relatively isolated stars in the field to improve the determination of the PSF. In the myopic deconvolution one can also make use of *a priori* knowledge of the source's shape (point-like, sharp edge, etc...).

– Myopic deconvolution (developed by J. Christou, S. Jefferies and co-workers) makes use of multiple short exposures. The only unchanged pattern common to all exposures is the science object. The method has been applied to resolve images of bright close binaries obtained at 0.85 microns using the 941 actuators AO system on the 3.5-m telescope of the Starfire Optical Range (SOR). The closest resolved separation is 0.067 arcsec for a difference in magnitude of 0.58.

This is a rich and complex topic for which only a schematic overview is given here. Other aspects of post-processing were examined such as various flavours of deconvolution procedures – non-linear deconvolution, Magain, Courbin & Sohy method, Richardson-Lucy method, use of a different PSF at increasing radial distance from the reference star and more.

Other issues were discussed which were related to data-acquisition strategy, flat-field, calibration, tethering, oversampling, non-common path aberration, and how to remove the wings of the star image, which is behind the coronagraph.

Is there a best deconvolution procedure?

Could one procedure be better adapted to a given astrophysical programme than another? In an effort to answer these questions, ESO has proposed to make available a certain number of ADO-NIS data complete with their PSF(s) and WFS data to several interested groups. Each group will apply its algorithms and procedure to the same data. The results will be compared. Significant differences

will have to be understood, and their importance evaluated for different scientific objectives and different hardware implementation of AO. In a first phase, the exercise is applied to photometry in crowded fields. Then, it will be extended to other types of data and astrophysical projects: Fabry-Perot (FP) data, detection of companions, extended emission, spectrography, polarisation, etc... opening a long-range process of continuous improvement of AO data analysis.

Artefacts

Attention was drawn to the danger of artefacts and spurious effects. A startling illustration of this problem was presented in the form of images of the inner region of galaxies harbouring an AGN taken with the Adaptive Optics Bonnette (PUEO) of the CFHT. The artefacts for these particular observations take the form of cross pattern structures. These are misleading as they look like the *torus+spiral arms* structure expected, in some models, to be present in the immediate vicinity of AGN. The origin of these cross pattern structures is still unclear but the moral of the story is that extreme care and caution must be exercised in order to avoid this and other pitfalls. More efforts are needed to set up the procedure that will remove these effects.

The Superspeckles and the subtraction of images with identical PSF

There is exciting science, which requires the search, and discovery of very faint companions to bright stars i.e. brown dwarfs and planets. The sensitivity of the search depends on the S/N in the envelope of the AO corrected star image. (The figure of merit here is the magnitude dif-

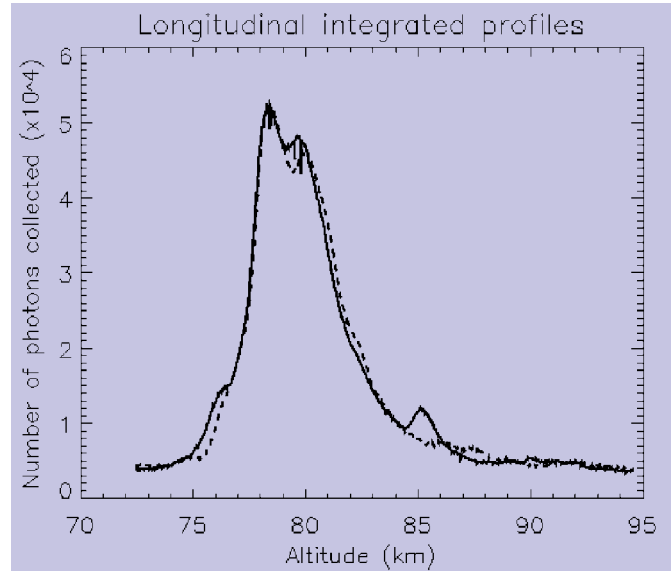


Figure 2: Two longitudinal profiles of the laser plume obtained at 20 minutes interval during the experiment of Fig. 1. One can note the changes in the profile near the maximum as well as the appearance of transient layers around 76 and 87 km (F. Delplanque et al.).

ference, Δm , between the star and the companion.) The speckles produce a correlated noise whose variance dominates the photon noise. To circumvent this difficulty, Racine, Walker and co-workers have devised the method of "Dual Imaging": A beam-splitter produces two images of the field on the detector and a narrow-band filter centred on a spectral band which has a different strength in the companion and the star, is inserted in one of the beams. The two images have identical PSF and differ only by the contrast between the companion and the bright star. By subtracting one image from the other, one obtains an image where the residual correlated speckle noise is reduced by several orders of magnitude correspondingly increasing the S/N of the companion. The performance expected from "Dual Imaging" is to increase Δm by 3 magnitudes and Δm could even reach 22 at 0.5 arcsec! The method of "Dual Imaging" can be used in other projects requiring the subtraction of two images: line/continuum observations, polarisation and speckle imaging.

Astrometry

In star-forming regions, dust absorption strongly modifies the distribution of the visible light as compared to that of the IR light resulting in differences between the maps in the two bands. Exactly aligning the two maps is often problematic (for example, in the absence of foreground stars) and in these cases, the colour and temperature of the sources cannot be measured with confidence. A simple solution is to have the possibility to observe simultaneously in both bands through two cameras, with a dichroic separating the visible and IR beams. For example, on NAOS a visible camera could be installed in the "parallel path".

RW Aur [S II]

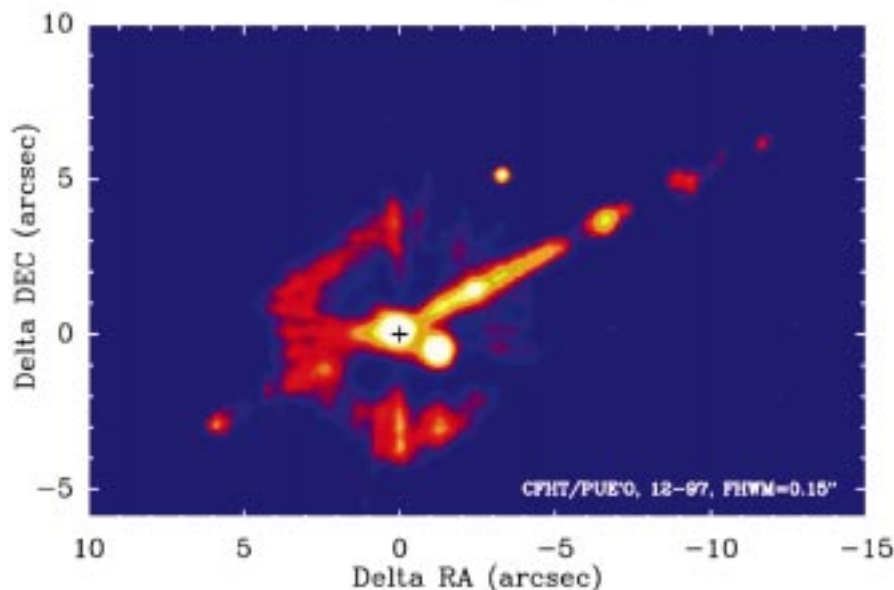


Figure 3: The jet of the pre-main sequence binary RW Aur imaged with PUEO at the CFHT, in the optical emission lines [SII]6717,6734. The jet is associated with component A, marked by a cross. Resolution (FWHM) is $0.15''$ and dynamic range 10^5 , 3σ (F. Ménard et al.)

3. AO Systems Coming into Operation in the Near Future on Very Large Telescopes

3.1 Systems commissioned next year, 1999, on 6- to 10-m telescopes

- The University of Hawaii AO system Hokupa'a (Curvature sensor and 36 actuators) will be set on the Gemini North 8.2-m telescope.

- Japanese 8.2-m Subaru telescope. (Curvature sensor and 36 actuators).

- Keck 10-m telescope II (Shack-Hartmann sensor with eventually 349 actuators) + laser guide star system, LGS.

- on Mt Hopkins, the "MMT" now retrofitted with a 6.5-m single mirror (Adaptive secondary with 330 actuators).

- It is recalled that the SOR 941 actuators system has started operation on the 3.5-m telescope although not primarily for astronomical observations.

Furthermore, two spectrographs where the entrance slit is in the AO-corrected focal plane have just started operation: the GraF Spectrograph on ADONIS at the ESO 3.6-m telescope and the OASIS integral field spectrograph for PUEO on the CFHT 3.6-m.

3.2 Systems commissioned in 2000+ on 6- to 10-m telescopes

In the year 2000 and shortly after, other very large telescopes will be equipped with AO systems, with LGS system in most cases:

- on the VLT, NAOS+CONICA on UT1, SINFONI on UT1, CRILES on UT4, MACAO for VLTI.

- on other very large telescopes: Keck I, the 2 LBT-8.4-m telescopes, the

8.2-m telescopes Gemini I and II, and the Magellan 6.5-m.

3.3 Ground-based Adaptive Optics and Space Telescopes

Around the year 2007, when NGST (diameter about 8 m, wavelength range 0.8 to 10 μ) is launched, about ten 6.5-m to 10-m telescopes equipped with AO imaging and/or spectroscopy will have carried out observations for 6–8 years, each with a larger collecting area and higher angular resolution than HST. There is currently an active debate to define HST's uniqueness space in the era of AO systems on 8-m telescopes. The result will be an important input in the definition of HST new instruments and programmes, wide-field deep survey in J for example, and of course UV and optical imaging and spectroscopy. (For more information on this debate one can contact Jim Beletic at jbeletic@eso.org and Bob Fosbury at rfofbury@eso.org.)

Each of the two techniques, space-based observations and ground-based AO observations, has its area of best performance. Complementarity is very fruitful (example in 5.1) – and some overlap is beneficial as a check.

The arguments of the debate in general, and also for the particular case of Ground-based AO versus NICMOS/HST are well known: With equal diameter telescopes and equal integration time, broad-band space observations go deeper than ground-based AO systems in the infrared bands where the sky background dominates. Other advantages of space are stable and uniform PSF, complete sky coverage, continuous wavelength coverage between 1 and 10 microns and beyond and possibility to have the entire telescope cooled. The advantages of

ground-based telescopes AO systems are the diversity of instruments (such as narrow-band filters, FP, spectrographs with a variety of resolutions), the easy upgrade of CCD, IR arrays and WFS, and the possibility to carry out large programmes and extensive surveys since a number of large-diameter ground-based telescopes are being equipped with AO systems. Sky coverage is limited to less than 50 per cent, the exact value depending on the Strehl ratio one could accept and on the galactic latitude. In a few years, LGS will bring routinely nearly complete sky coverage and good PSFs.

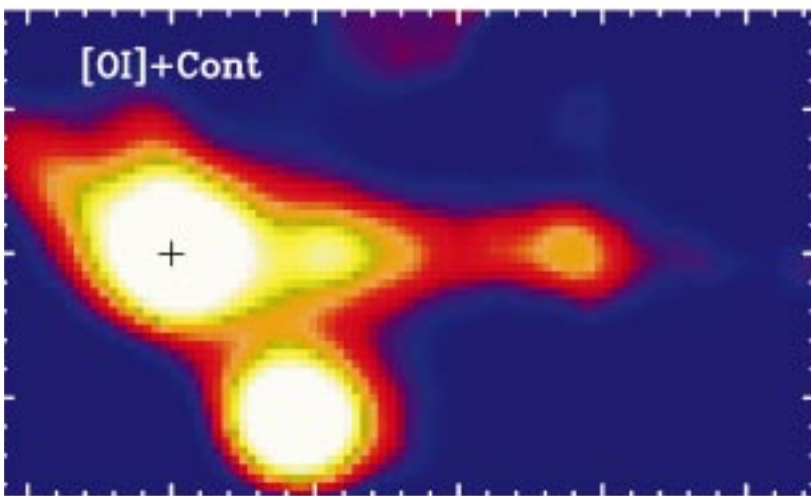
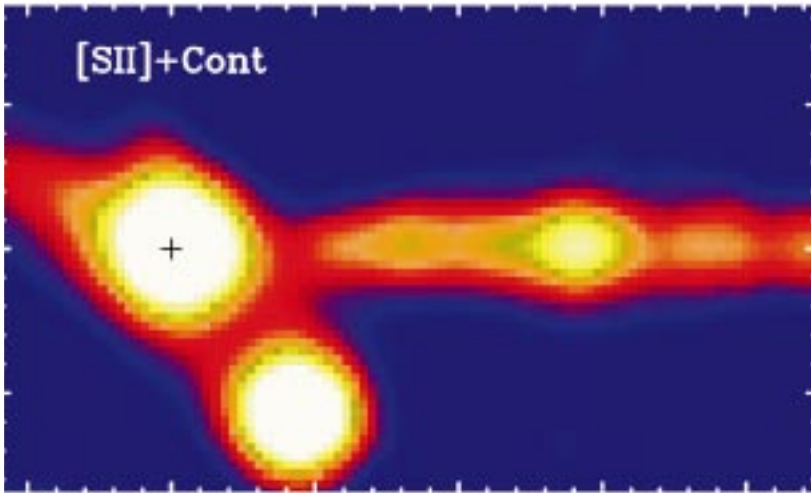
Ground-based telescopes in the 2-m diameter range could also be equipped with AO systems getting close to the diffraction limit in the visible. The large number of medium-size telescopes will make it possible to carry out large scale programmes and surveys.

4. Other Important Issues

4.1 Technologies – Laser Guide Star Systems

A number of technological advances and experimental results were presented on deformable mirrors, adaptive secondaries and laser guide-star systems (LGS). The first astrophysical results ever obtained in Europe with an AO+LGS system were presented (Section 5.2). Monitoring of the column density and effective altitude of the sodium mesospheric layer is planned or under way at all observatories building a LGS system and first results were presented. A large part of the LGS studies in Europe are coordinated through a network funded by the European Union within its "Training and Mobility for Researchers" (TMR) Programme. An example of such study is the observation of the laser beam of the ALFA system at Calar Alto. In this experiment, the beam is launched from the 3.5-m telescope towards the zenith and is observed from the side with the 2.2-m telescope located 343 m from the 3.5-m. The beam excites the mesospheric sodium layer of about 10 km thickness located at an average altitude of 80 km. From the side the excited region is seen as a bright "plume". The properties of this plume and their time variability are the object of the study. Some of the results obtained in August 1998 can be seen in Figures 1 and 2 (F. Delplanque et al.). The 5-min. exposure on Figure 1 shows the plume, and below and above it the trail caused by Rayleigh scattering, the intensity of the trail reaching 1% of the maximum intensity of the plume at 7 arcmin below the plume centroid. The two curves on Figure 2 are the longitudinal (i.e. along the laser beam direction) profiles of the plume measured 20 minutes apart. In this time interval, there are already noticeable variations of the longitudinal profile and, moreover, one can note the appearance of transient layers below and above the maximum intensity of the plume, here at 76 and 85 km. These changes in shape

RW Aur



◀
Figure 4: Comparison of the structure of the RW Aur A jet in the [SII] line and the [OI]6300 line. The line intensity ratio varies along the jet; the [OI] emission decreases very rapidly along the jet and the first [OI] knot has no counterpart in [SII] (C. Dougados et al. quoted in Ménard et al.).

and in effective altitude have consequences on the wave-front sensor operation. The shape modification increases the noise on the centroid measurements in a different way on each sub-aperture and requires an adapted modal control. The altitude variations require that a continuous measurement of the sodium spot effective altitude be made in order to correct for the induced defocus. Happily, these effects change relatively slowly allowing for efficient correction. The hindering effects of the light pollution for the other telescopes on the site, and possible solutions are also investigated.

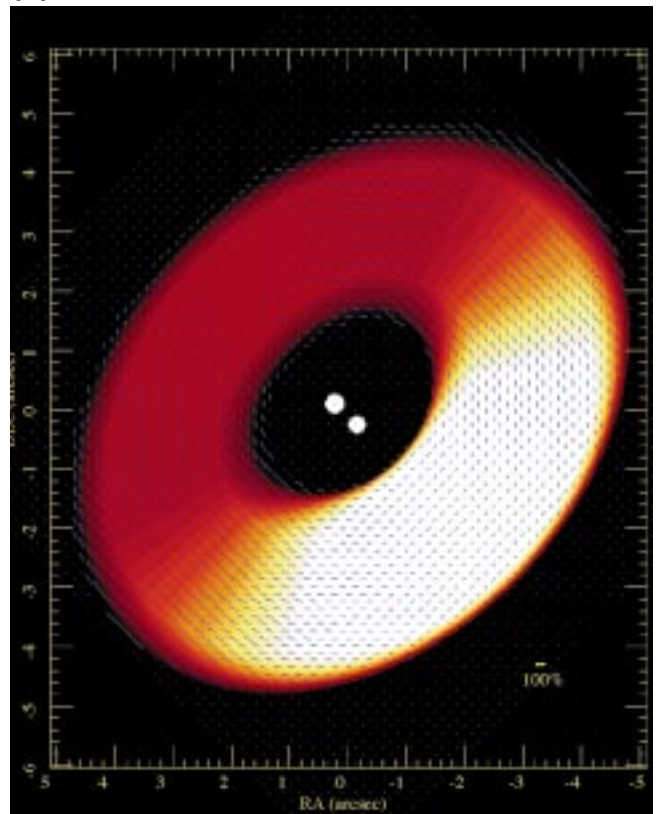
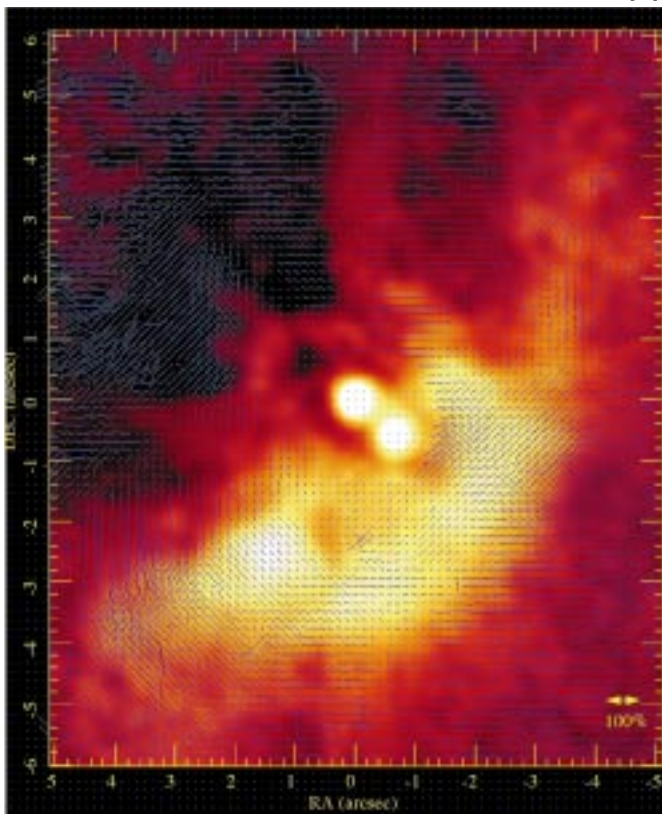
4.2 Flexible Scheduling

The performance of an AO system, the Strehl ratio in particular, improves

Figure 5: (a) The polarisation vectors of the envelope surrounding the double T Tauri system UY Aur superposed on an image in J (Hokupa'a on the CFHT 3.6-m, November 1997). Note the maximum in polarisation at PA 130 and -40 degrees, the centrosymmetric pattern in polarisation angle and the high front/back contrast of the background image in J.

(b) For comparison, a Mie scattering model of a flattened dust disk with a power law (-4.7) size distribution of dust grain which best fits the front/back ratio of intensity. Both figures from D. Potter et al. ◀▶

(a) (b)



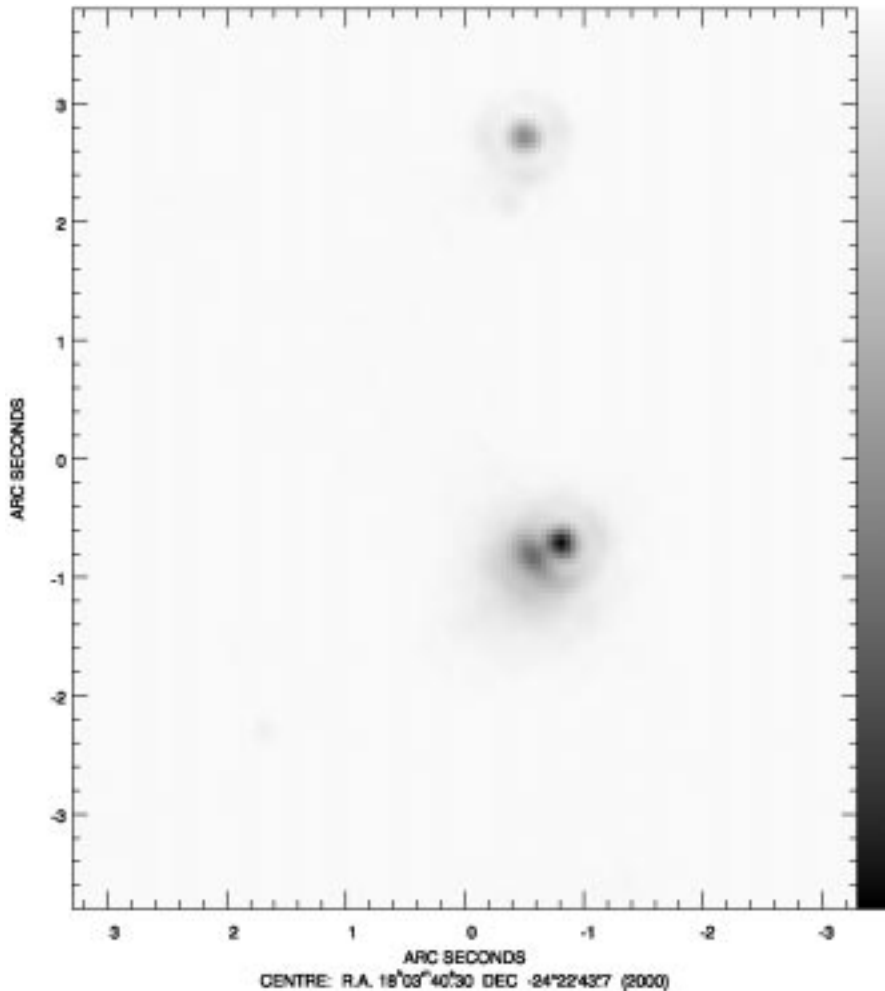


Figure 6: The young massive star Her 36 and the mysterious intense infrared source form the double object in the lower half of the image. The IR source is at $0.3''$, or 500 AU in projection, from Her 36; its nature is still unknown. Observations with ADONIS in L (B. Stecklum et al.).

strongly with improving seeing. For best return of money and time spent on building the AO system and the telescope, the AO system should be used in excellent atmospheric conditions. Flexible Scheduling and Queue Scheduling aim at assigning the best conditions to the instruments and programmes that need them the most. This is a complicated process, and requires to have on hand the statistical properties of the atmosphere (r_0 , τ_0 , θ_0) at the site on time scales ranging from hours to months. The advantage of splitting nights with other instruments will have to be clearly demonstrated, taking into account calibration time and overhead time to pass from the AO instrument to another and vice-versa. A recommended approach for early use of the next generation of AO instruments is to use it through entire (selected) nights, and execute the best AO programmes suited to the current conditions.

5. Astrophysical Results of AO Observations

10 papers on Circumstellar disks and jets, 8 on binaries and stars with faint companions, 7 on galaxies and quasars, and

2 on the Solar System were presented at the Conference.

5.1 Circumstellar disks, Jets, and Stars

Star formation and Planet formation

AO observing in the near IR is particularly well suited to this phenomenon which occurs in dust rich regions. The final mass of a star results from the combined effects of accretion through the disk and mass loss through jets and outflows. Detailed maps, polarisation and spectroscopy provide clues to the fundamental processes of star formation and early evolution, and disk and jet formation and evolution. The best laboratories in which to observe these phenomena are the Classical T Tauri stars because, in these systems, part of the dust has been cleared out making the base of the jets (and the disk) directly observable. Classical T Tauri are thus favourite targets to investigate jet formation. As an example, Figures 3 and 4 show the jet associated with component A of the binary Classical T Tauri star RW Aur, mapped in the optical range with PUEO at the CFHT (F. Ménard et al.). The fact

that the jet is very straight is an important finding about the location of the jet formation. Tidal torques being expected to disrupt or warp the disk, the jet's straightness suggests that the jet originates from the very central part of the disk which remains unperturbed by the companion star.

Only a handful of circumstellar disks around T Tauri stars have been resolved in their scattered light. There is very limited information on the composition and size distribution of the dust grains in these disks and on density inhomogeneities. This information, however, is crucial to the understanding of how planets form. The combination of infrared imaging and polarisation is a powerful tool to gather this information as is illustrated in the images of the circumbinary disk around UY Aurigae (Figure 5a, b from D. Potter et al.) obtained with Hokupa'a on the 3.6-m CFHT in November 1997. Figure 5a shows the high-contrast, high-resolution polarimetry map with the polarisation vectors overlaid on the deconvolved grey-scale image in J. The polarisation vectors show a centrosymmetric pattern in angle and intensity with peaks in polarisation intensity at position angle of 130 and -40 degrees. This pattern is entirely consistent (Figure 5b) with the extended IR surface brightness observed around UY Aur being a flattened dust disk with a large number of small grains. The front/back ratio of intensity constrains the power law size distribution of the grains. The alternative model of a spherical envelope of dust appears unlikely.

Results obtained on the young massive star Her 36 also illustrate the power of AO observations and give an example of the complementarity of AO, HST and radio observations (Figures 6 and 7 from B. Stecklum et al.). Her 36, spectral type O7V, is responsible for the ionisation of the "Hourglass" Nebula. Early photometric and polarimetric investigations yielded clear evidence that it showed unexpected peculiarities in polarisation and a strong infrared excess. High angular resolution in the IR, first by lunar occultation, then with ADONIS, revealed the intense IR source to be not Her 36 itself but a separate object located $0.3''$, or 500 AU from Her 36 in projection (Figure 6). This clarifies the nature of Her 36 as a normal young massive star, but the nature of the intense IR source remains a mystery. HST detected the source in H α and the VLA detected it as a weak point source at 2 cm (Figure 7). The search and non-detection in maser emission makes it unlikely that the IR source is a deeply embedded massive young stellar system. Could it be disk debris left from the formation of Her 36, or a proplyd object, or an evaporating gaseous globule?

Main Sequence Stars

Circumstellar disks are also observed around MS stars. The best known ex-

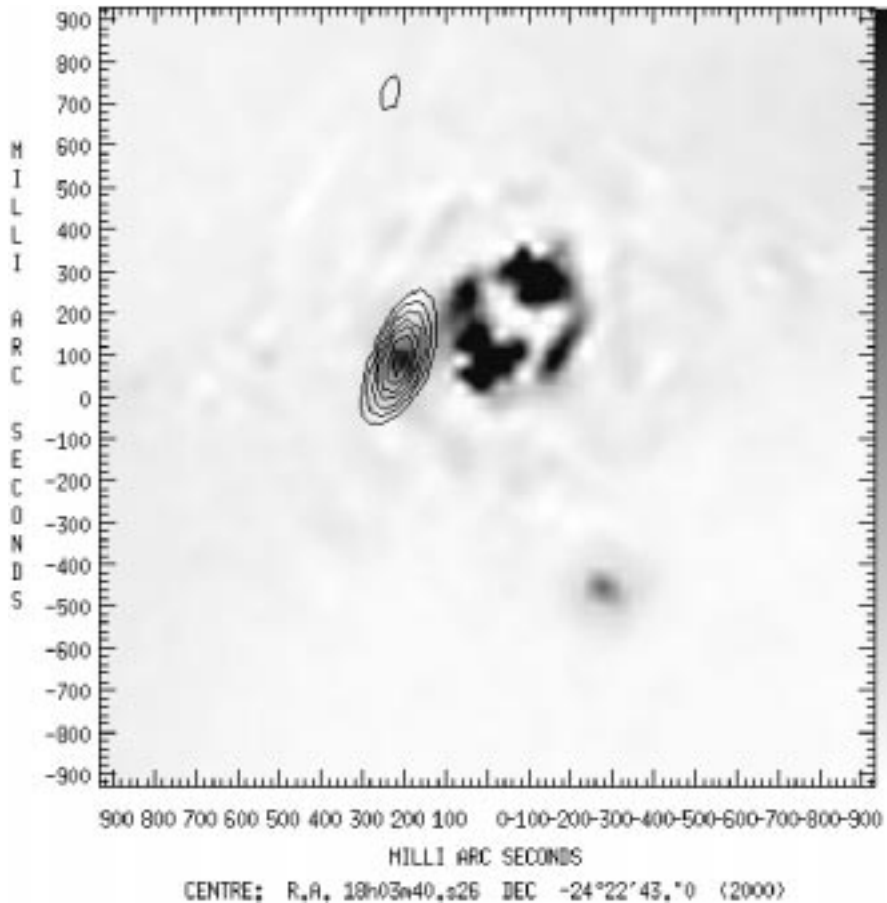


Figure 7: HST/WFPC2 $H\alpha$ image of Her 36 after PSF subtraction. The intense IR source is detected as a weak point-like source at 2 cm with the VLA (contour lines) but is not detected in maser emission making it unlikely that it is a deeply embedded young stellar object (B. Stecklum et al.).

ample is β Pictoris. By coronagraphy with ADONIS, the disk has been mapped to within 20 AU from the star, that is inside the planet orbits in our Solar System!

Several papers were also given on the frequency of occurrence of binary stars and its dependence on environment and age, and on the search for brown dwarfs and planetary companions. The image analysis strategy can take advantage of the *a priori* information that the sources

in the field are point-like. This is valid also for that uniquely important target, the Galactic Centre.

5.2 Extragalactic Studies

Results have been reported on gravitational lenses, intervening galaxies, and quasar companions. Attempts have been made at finding signs of accretion in the vicinity of AGN or at identifying structures which could be the molecular torus ex-

pected to be present around AGNs. Maps of luminous IR galaxies with unprecedented resolutions were presented. The compactness of the IR central source helps to distinguish between the presence of a dust embedded quasar or of a compact bright star-forming region.

At the Conference were presented the first images of galaxies ever obtained in Europe with an AO+LGS system (R. Davies et al.). They are part of a programme to observe the light distribution in the core of galaxies in clusters. In the clusters studied, there appears to be a correlation between the size of the core at the galaxies' centre *with* the radial distance of the galaxies from the cluster's centre and their HI content – the core being more compact in more centrally located galaxies. Davies et al. suggest that the crossing of the central part of the cluster by a galaxy depletes the galaxy of its HI (a long-known effect) and stimulates star formation in the gas left in the galaxy core, gas which is likely to be subjected to strong tidal effects.

5.3 Solar System

In the age of space probes, there remain important Solar System observations, which are most successfully carried out with AO on large telescopes. AO can detect and monitor faint, variable or transient objects/structures on the planetary surfaces, rings, and satellites. Furthermore, AO yields the most detailed maps of solar-system objects not targeted by the space probes. One of the impressive planetary observations presented in Sont-hofen is shown in Figure 8 (F. Roddier et al.). The three images of Neptune were taken 45 min apart on July 6, 1998. They were taken through a narrow-band filter centred inside a methane absorption band at 1.72μ , with Hokupa'a on the CFHT. The angular diameter of Neptune was $2.36''$. High-altitude clouds are seen here against a dark methane band atmospheric absorption and appear bright. During the Voyager encounter, most of Neptune's cloud activity was in the South

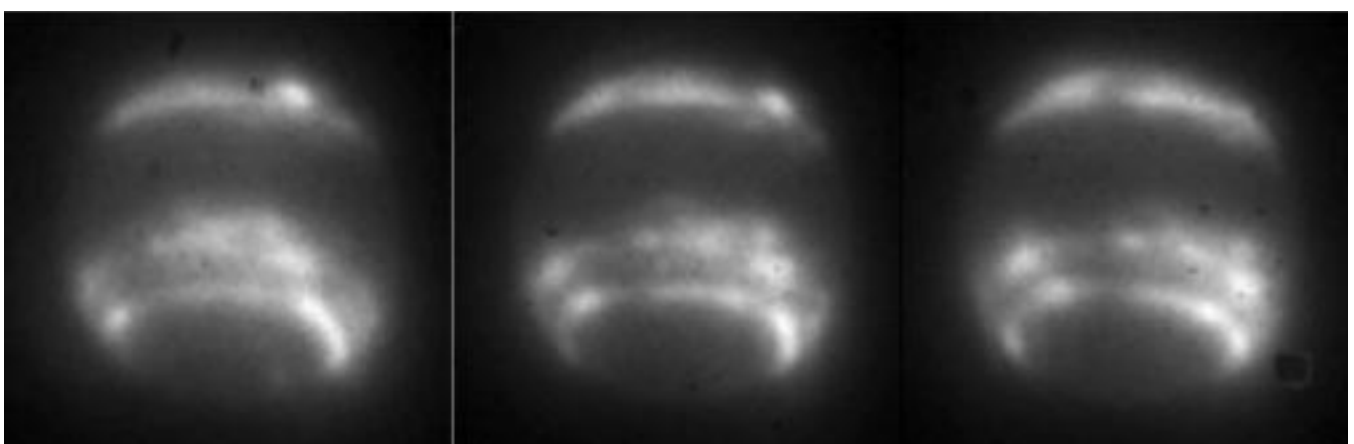


Figure 8: Cloud activity on Neptune. Images taken 45 min apart with Hokupa'a on the CFHT on July 6, 1998. High-altitude clouds appear bright against a dark methane band atmospheric absorption. Note the rapid planet rotation. The angular diameter of Neptune was $2.36''$ (F. Roddier et al.).

hemisphere. It then moved to the north where it peaked around 1994. In July 1998, as can be seen on the Figure, the cloud activity had grown again in the south. The causes of these changes are unknown.

6. Conclusions

This first Conference centred on Astrophysics with AO was a success, and the common wish at the end was to have such a Conference on "Astronomy

with Adaptive Optics" every 1.5 years.

The Adaptive Optics systems expected to be routinely operating in the near future are growing in number. The observers are getting more and more familiar and proficient with their "new tool" and define new strategies to observe efficiently. We can expect a large growth of striking results in the coming years as well as a continuation of the technology maturation process. This continues to motivate ESO's effort to equip the VLT with several AO systems in the near future.

Moreover, these efforts pave the way to the road to the Giant Optical Telescopes of the next century.

The paper version of the Proceedings can be obtained by writing to Christina Stoffer at ESO, cstoffer@eso.org. On-line version of the papers is available at <http://www.eso.org/gen-fac/meetings/eso-osa98>

mhulrich@eso.org

Award for the ESO VLT Project

Naturally, 'First Light' for the first of the VLT Unit Telescopes has not gone unnoticed by the astronomical community. However, also newspapers, magazines, radio and TV have reported widely about this new facility and about the first, fascinating pictures that were obtained with UT1. Another sign of the world-wide attention that the VLT has caught was the fact that the well-known US magazine Popular Science chose the project for one of the coveted "The Best of What's New Awards" for 1998, given to the 100 most important technology developments in the course of the year. The construction of the VLT was recognised as an "outstanding achievement" within the "Aviation and Space" category.

The Award was formally handed over to ESO, represented by Prof. Massimo Tarenghi, during a luncheon at the Tavern on the Green in New York on November 13. On the same occasion, about 500 invited guests from industry, the media and



M. Tarenghi, posing for the official photo at the ESO Stand.



Popular Science editor Cecilia Wessner speaking at the award ceremony.

government agencies had the opportunity to inform themselves about the individual prize winners through project and product presentations by means of small exhibitions. Here, ESO found itself in the company of a great variety of organisations and enterprises working in different high-tech areas, ranging from NASA (International Space Station and the Mars rover "Sojourner"), Airbus Industrie (A-340-500) and various experimental aircraft manufacturers, through IBM (copper-based computer chips), Apple Computer (iMac), and Iridium Satellite telephones to the latest products in medicine and medical research.

Given the audience and the extremely high technological level of the projects and innovations presented, this was undoubtedly a good occasion for ESO to inform US media and the technologically interested public about the VLT as major European science project.

C. MADSEN

ESO Director General to Become President of AUI

TEXT OF THE JOINT ESO-AUI PRESS RELEASE OF 3 NOVEMBER 1998 (EXCERPTS)

The appointment of Professor Riccardo Giacconi, Director General of the European Southern Observatory (ESO) since January 1, 1993, to the Presidency of Associated Universities, Inc. (AUI) in the USA, has been jointly announced by Professor Paul C. Martin, Chair of AUI's Board of Trustees and Mr. Henrik Grage, President of the ESO Council. Professor Giacconi will assume this new position at the end of his term at ESO as of July 1, 1999.

AUI is a not-for-profit science management corporation that operates the National Radio Astronomy Observatory (NRAO) under a Cooperative Agreement with the National Science Foundation (NSF). Corporate headquarters are located in Washington, D.C. The President is its chief executive officer.

Mr. Grage, President of the ESO Council, expressed the gratitude of the ESO Community for the leadership provided by Prof. Giacconi during these crucial years of development of the organisation and its La Silla and Paranal Observatories. In particular, the splendid achievements on the Very Large Telescope (VLT) are a tribute to the ESO staff and to his management and guidance. VLT is currently the largest single project in ground-based astronomy. It has met or exceeded all performance requirements while being built on time and within budget.

When reached for comment, Professor Giacconi pointed out: "I have enjoyed enormously the time I have spent here at ESO and I consider it one of the high points of my career. I feel confident that I am leaving ESO in very good condition. The fine performance of the entire staff has succeeded in bringing the organisation to an outstanding position in ground-based astronomy in the world. The prospects for the future are equally brilliant.

I will be happy and proud to assume the Presidency of Associated Universities, Inc. starting next summer. For more than fifty years, AUI has, in collaboration with universities and the national and international scientific community, overseen and managed national facilities which have made possible a wealth of important discoveries in physics, astronomy, and many other areas of science and technology. In the 21st century, new challenges and opportunities to serve the community await AUI."

"We are thrilled that Professor Giacconi has decided to take this position", said Professor Paul Martin, Chairman of the Board of AUI. "It is hard to imagine anyone better qualified to lead an organisation committed to managing facilities performing frontier science. His vision and foresight have been at the heart of pioneering projects including the Einstein Observatory, the Space Telescope, and the VLT. He is an extraordinary scientist and an outstanding manager whose accomplishments and values have earned him worldwide respect and admiration."

FIRST ANNOUNCEMENT

ESO Workshop on Black Holes in Binaries and Galactic Nuclei – *Their Diagnostics, Demography, and Formation*

6–8 September 1999

ESO Headquarters, Garching bei München, Germany

The aim of this workshop is to bring together astrophysicists working on the rather separate fields of stellar mass and supermassive black holes, with emphasis on the formation, population, physics, and environments of black holes. An overview will be given of the observational evidence for the existence of black holes in binaries and galactic nuclei. Related topics like the late stages of (binary) evolution and galaxy formation will be addressed.

Topics to be covered include:

- **Black-hole diagnostics**

Binaries (X-ray sources, neutron stars vs. black holes)
Centres of galaxies, including our own (AGN phenomenon, stellar and gas dynamics signatures)
Jets, disks and accretion tori; Variability and outbursts

- **Properties of black-hole populations**

Stellar-mass black holes; Supermassive black holes

- **Black-hole formation**

Progenitors of stellar-mass black holes: Supernovae/Hypernovae Models for the formation of supermassive black holes

Scientific Organising Committee:

R. Bacon (France), R. Bender (Germany), R.D. Blandford (USA), P.T. de Zeeuw (Netherlands), L. Kaper (Netherlands), G. Monnet (ESO), M.J. Rees (United Kingdom), A. Renzini (ESO), D.O. Richstone (USA), R. Sunyaev (Germany), E.P.J. van den Heuvel (Netherlands, Chair)

Local Organising Committee:

L. Kaper (Netherlands, Chair), C. Stoffer (ESO), P. Woudt (ESO)
European Southern Observatory
Karl-Schwarzschild-Str. 2
D-85748 Garching bei München, Germany
Tel: +49-89-320060; FAX: +49-89-32006480
Email: bh99@eso.org
See also: <http://www.eso.org/bh99/>

VLT OPENING SYMPOSIUM

Antofagasta, Chile, 1–4 March 1999

To mark the beginning of the VLT era, the European Southern Observatory is organising a VLT Opening Symposium that will take place in Antofagasta on 1–4 March 1999, just before the start of regular observations with the VLT.

The Symposium will occupy four full days and consist of plenary sessions (invited talks only) on “Science in the VLT Era and Beyond” and three parallel Workshops (invited and contributed talks) on “Clusters of Galaxies at High Redshift”, “Star-way to the Universe” and “From Extrasolar Planets to Brown Dwarfs”.

During the Symposium, participants will have the opportunity to see the VLT in operation. Special visits to the Paranal Observatory will be organised each afternoon and early evening. After the Symposium, there will be an Official Inauguration Ceremony at Paranal on March 5. The Ceremony is intended largely for official guests from the member states and Chile and will be by invitation only.

Plenary Sessions: SCIENCE IN THE VLT ERA AND BEYOND

Scientific Organising Committee: D. Alloin, I. Appenzeller, J. Bergeron (co-Chairperson), C. de Bergh, B. Fort, R. Kudritzki, M. Mayor, G. Miley, P. Nissen, H. Quintana, A. Renzini (co-Chairperson), R. Sancisi

List of topics:

- Cosmology: where do we stand? – *S. White*
 - The most distant galaxies – *M. Pettini*
 - Galaxy evolution and nuclear activity – *G. Miley*
 - Probing active galaxies in the infrared – *A. Moorwood*
 - Supernovae at high redshift – *R. Kirshner**
 - The cosmic history of star formation – *P. Madau*
 - The centres of nearby galaxies – *R. Bender*
 - Nucleosynthesis in the young Universe – *B. Gustafsson*
 - New frontiers in the solar system – *A. Barucci*
 - Science with the Large Southern Array – *K. Menten*
 - Synergy between the VLT and the NGST – *H. Stockman*
- * *Tentative speaker*

The last plenary session will include a presentation of the highlights of the three workshops:

- Clusters of Galaxies at High Redshift
- Star-way to the Universe
- From Extrasolar Planets to Brown Dwarfs

Parallel Workshop 1: CLUSTERS OF GALAXIES AT HIGH REDSHIFT

SOC: H. Böhringer, A. Cavaliere, B. Fort (co-Chairperson), P. Katgert, P. Rosati (co-Chairperson), P. Schneider, M. Tarengi

Preliminary list of topics:

- Clusters at $z > 1$ (optical, IR)
- X-ray clusters at high z
- SZ clusters and surveys
- LSS at high- z and cluster formation (theory)
- LSS at very high redshift (observations)
- Clustering from absorption systems
- Clustering around high- z radio galaxies
- Galaxy populations and galaxy evolution in high- z clusters
- Cluster masses and dynamics
- Weak lensing
- Probing very distant galaxies with lensing clusters
- ICM physics and evolution
- Fundamental plane at high z
- ESO Imaging Survey
- 2dF Survey

Parallel Workshop 2: STAR-WAY TO THE UNIVERSE

SOC: I. Appenzeller, C. Chiosi, R. Kudritzki (co-Chairperson), J.-C. Mermilliod, P. Nissen, L. Pasquini (co-Chairperson), M. Spite

Preliminary list of topics:

- The VLT-UT2: a unique machine for stellar studies
- Distance Indicators: Cepheids. Improvement of Cepheids as distance indicators. Eclipsing binaries as precise distance indicators. Eclipsing binaries. Supergiants. Extragalactic planetary nebulae and what to do with them. Novae and GC systems
- Age Indicators: Age of globular clusters. MC's clusters. Globular clusters in the Galactic bulge. Bulge of our Galaxy. Other galaxies. Star forming regions. WR stars in star forming regions. Age indicators in solar-type and low-mass stars
- Abundance Indicators: Massive stars and their role in spectra and abundances of high redshift galaxies. Massive stars: observation. Intermediate/low mass in Sagittarius. Intermediate/low mass in MC's. The deep thick disk as seen by UVES. Intermediate/low mass in the Bulge. Stars versus HII regions: extragalactic HII regions. Stars versus HII regions: extragalactic stars

Parallel Workshop 3: THE SEARCH FOR EXTRASOLAR PLANETS WITH THE VLT/VLTI

SOC: F. Allard, P. Artymowicz, M. Mayor (co-Chairperson), F. Paresce (co-Chairperson), M.-T. Ruiz, P. Sackett

Preliminary list of topics:

Formation and Evolution: Reviews

- Theory: Diversity of planetary systems: formation scenarios. Brown dwarfs formation and evolution theories. Unsolved problems and future directions in theory. Solar nebulae and replenished disks with planets. Pulsar planet theories. Evolution of brown dwarfs and giant planets: contribution to the Galactic mass budget. The stellar and substellar IMF: theory
- Observations: Reviews: Protoplanetary disks. Replenished dust disks. The low-mass stellar IMF. The substellar IMF. The spectra of giant planets and brown dwarfs

Techniques

- Radial Velocity Searches: The large planet survey with CORALIE at La Silla. The Keck radial velocity search for extrasolar planets and brown dwarfs. Visible or infrared VLT high-resolution spectrographs (UVES and CRIRES). Towards 1 m/s with the 3.6-m telescope at La Silla
- Astrometric Detections: From PTI to KECK Interferometer. Astrometry with the VLTI. Astrometry with the NPOI. Astrometry from space: GAIA. Astrometry from space: SIM
- Planetary Microlensing and Transits: Planetary microlensing: present status and long term goals. Planetary transits
- Direct Detections: Brown dwarfs with DENIS. Brown dwarfs with 2MASS. Brown dwarfs in open clusters. Interferometric detections of giant planets and brown dwarfs with the VLTI. Adaptive optics from the ground or from space. NAOS-CONICA. VIZIR. IRSI

Local Organising Committee: D. Alloin, D. Hofstadt

Closing date for registration is December 31, 1998. More details and a registration form can be found at: URL <http://www.eso.org/gen-fac/meetings/vltos99/> or contact vltos99@eso.org for further information.

PERSONNEL MOVEMENTS

International Staff

(1 October – 31 December 1998)

ARRIVALS

Europe

CLOSE, Laird (CDN), Adaptive Optics Instrument Scientist
DAY, Philippa (GB), Technical Documentation Archivist
SKOLE, Steen (DK), Software Engineer
ALVES, Joao (P), Fellow
CONTINI, Thierry (F), Fellow
ROMANIELLO, Martino (I), Fellow
SUCHAR, Dieter (D), Archive Operations Systems Administrator
ZAMPARELLI, Michele (I), Systems Engineering Group of DMD
TORDO, Sébastien (F), Coopérant
NAUMANN, Michael (D), WEB Administrator/Master
CAVADORE, Cyril (F), CCD Detector Specialist
PATIG, Markus (D), Fellow
FERRARI, Marc (F), Associate
LEVEQUE, Samuel (F), Photonics Physicist
PRIETO, Almudena (E), User Support Astronomer

Chile

GARCIA AGUIAR, Martina (D), Mechanical Engineer
CHEVASSUT, Jean-Louis (F), DENIS Project
ELS, Sebastian (D), Student
JOUGET, Benoit (F), Coopérant
HÖÖG, Torbjörn (S), Mechanical/Electrical Engineer-Deputy of the Head of Department
DELAHODDE, Catherine (F), Student
ENDL, Michael (A), Student
MARCHIS, Franck (F), Student
SEKIGUCHI, Tomohiko (Japan), Student

DEPARTURES

Europe

HOOK, Isobel (GB), Fellow
VAN DE SPRENG, Jacob (NL), Project Control Officer
WOLTERS, Otto (NL), Accounting Assistant
LEVEQUE, Samuel (F), Associate

DUDZIAK, Gregory (F), Student and Associate
DE MARCHI, Guido (I), Fellow
BERNARDI, Mariangela (I), Student
ERBEN, Thomas (D), Student and EIS Visitor
PULONE, Luigi (I), Associate DGDF

Chile

TIEFTRUNK, Achim (D), Fellow
CHIESA, Marco (D), Telescope Software Engineer
BOSKER, Albert (NL), Administrative Assistant
GONZALEZ, Jean-François (F), Fellow

ESO Workshop Proceedings Still Available

Most ESO Conference and Workshop Proceedings are still available and may be ordered at the European Southern Observatory. Some of the more recent ones are listed below.

No.	Title	Price
50	Handling & Archiving Data from Ground-based Telescopes. Trieste, Italy, April 21–23, 1993. M. Albrecht & F. Pasian (eds.)	DM 35.–
51	Third CTIO/ESO Workshop on "The Local Group: Comparative and Global Properties". La Serena, Chile, 25–28 January 1994. M. Albrecht and F. Pasian (eds.)	DM 35.–
52	European SL-9 Jupiter Workshop. February 13–15, 1995, Garching, Germany. R. West and H. Bönhardt (eds.)	DM 80.–
53	ESO/ST-ECF Workshop on "Calibrating and understanding HST and ESO instruments", Garching, Germany. P. Benvenuti (ed.)	DM 60.–
54	Topical Meeting on "Adaptive Optics", October 2–6, 1995, Garching, Germany. M. Cullum (ed.)	DM 80.–
55	NICMOS and the VLT. A New Era of High Resolution Near Infrared Imaging and Spectroscopy. Pula, Sardinia, Italy, May 26–27, 1998	DM 20.–

List of Scientific Preprints

(September–December 1998)

1293. A.R. Tiefertunk, R.A. Gaume, T.L. Wilson: High-Resolution Imaging of NH₃ Inversion Lines Toward W3 Main. *A&A*.
1294. F. Primas, D.K. Duncan, J.A. Thorburn: The Remarkable Boron-Depleted, Lithium-Normal Population II Star HD 160617. *ApJ* Letters.
1295. D.R. Silva, G.D. Bothun: The Ages of Disturbed Field Elliptical Galaxies: II. Nuclear Properties. *AJ*.
1296. S. Brillant, G. Mathys, C. Stehlé: Hydrogen Line Formation in Dense Magnetized Plasmas. *A&A*.
1297. C.R. Cowley and G. Mathys: Line Identifications and Preliminary Abundances from the Red Spectrum of HD 101065 (Przybylski's Star). *A&A*.
1298. S. Hubrig, F. Castelli and G. Mathys: Isotopic Composition of Hg and Pt in 5 Slowly Rotating HgMn Stars. *A&A*.
1299. G. Mathys: Direct Observational Evidence for Magnetic Fields in Hot Stars. *Variable and non-spherical stellar winds in luminous hot stars*, Proc. IAU Coll. B. Wolf, A. Fullerton, O. Stahl (eds.).
1300. B. Leibundgut and J.G. Robertson: Emission Within a Damped Lyman α Absorption Trough: The Complex Sight Line Towards Q2059–360. *MNRAS*.
1301. R.A. Ibata, G.F. Lewis and J.-P. Beaulieu: Re-examination of the Possible Tidal Stream in Front of the LMC. *ApJ* Letters.
1302. G.F. Lewis et al.: Submillimeter Observations of the Ultraluminous BAL Quasar APM 08279+5255. *ApJ* Letters.
1303. R. A. Ibata and G. F. Lewis: Optimal Proper Motion Measurements with the Wide Field and Planetary Camera. *AJ*.
1304. P. Andreani et al.: The Enhancement and Decrement of the Sunyaev-Zeldovich Effect Towards the ROSAT Cluster RXJ0658-5557. *ApJ*.
1305. E.M. Corsini et al.: Dark Matter in Early-Type Spiral Galaxies: The Case of NGC 2179 and of NGC 2775. *A&A*.
1306. M. Kissler-Patig et al.: Towards an Understanding of the Globular Cluster Over-Abundance Around the Central Giant Elliptical NGC 1399. *A&A*.
1307. L. Pulone, G. De Marchi and F. Paresce: The Mass Function of M4 from Near IR and Optical HST Observations. *A&A*.
1308. G. De Marchi, B. Leibundgut, F. Paresce, and L. Pulone: A Deep Optical Luminosity Function of NGC 6712 with the VLT: Evidence for Severe Tidal Disruption. *A&A*.
1309. A. Pasquali, A. Nota, M. Clampin: Spatially Resolved Nebulae Around the Ofpe/WN Stars S61 and Be381. *A&A*.
1310. F. Primas, D.K. Duncan, R.C. Peterson, J.A. Thorburn: A New Set of HST Boron Observations. I. Testing Light Elements Stellar Depletion. *A&A*.
1311. L. Kaper, H.F. Henrichs, J.S. Nichols, and J.H. Telting: Long- and Short-Term Variability in O-Star Winds. II. Quantitative Analysis of DAC Behaviour. *A&A*.
1312. F. Comerón, G.H. Rieke, R. Neuhauser: Faint Members of the Chamaeleon I Cloud. *A&A*.

SUBJECT INDEX

Organisational Matters

- R. Giacconi: The Role of ESO in European Astronomy **91**, 1
 R. Giacconi: First Light of the VLT Unit Telescope 1 **92**, 2
 The Final Steps Before "First Light" **92**, 3
 R. West: VLT First Light and the Public **92**, 4

Observing with the VLT

- B. Leibundgut, G. de Marchi, A. Renzini: Science Verification of the VLT Unit Telescope 1 **92**, 5
 Scientific Evaluation of VLT-UT1 Proposals. Observing Period 63 (April 1 – October 1, 1999) **92**, 9
 P. Quinn, J. Breysacher, D. Silva: First Call for Proposals **92**, 9
 R.G. Petrov, F. Malbet, A. Richichi, K.-H. Hofmann: AMBER, the Near-Infrared/Red VLT Focal Instrument **92**, 11
 The VLT-UT1 Science Verification Team: Science Verification Observations on VLT-UT1 Completed **93**, 1
 M. Sarazin: Astroclimate During Science Verification **93**, 2
 M. Tarenghi, P. Gray, J. Spyromilio, R. Gilmozzi: The First Steps of UT1 **93**, 4
 Portuguese Minister of Science at Paranal **93**, 7
 The Cost of the VLT **93**, 8
 B. Koehler: ESO and AMOS Signed Contract for the VLT Auxiliary Telescopes **93**, 11
 B. Koehler, F. Koch: UT1 Passes "With Honour" the First Severe Stability tests for VLT1 **93**, 11
 Signing of Contract for the Delivery of the Delay Line of the VLT1 **91**, 25
 Image from the VLT Science Verification Programme **93**, 29
 News from VLT Science Verification **94**, 9

Telescopes and Instrumentation

- A. Moorwood, J.-G. Cuby and C. Lidman: SOFI Sees First Light at the NTT **91**, 9
 S. D'Odorico: The New Direct CCD Imaging Camera at the NTT. SUSI2 gets the first FIERA CCD controller and a mosaic of two 2k × 4k, 15µ pixel, thinned, anti-reflection coated EEV chips **91**, 14
 J.G. Cuby and R. Gilmozzi: VIMOS and NIR-MOS: Status Report **91**, 16
 P.O. Lagage, Y. Rio, J.W. Pel, H. Toisma: VISIR at PDR **91**, 17
 D. Baade et al.: The Wide Field Imager for the 2.2-m MPG/ESO Telescope: a Preview **93**, 13
 I. Appenzeller, K. Fricke, W. Fürtig, W. Gässler, R. Häfner, R. Harke, H.-J. Hess, W. Hummel, P. Jürgens, R.-P. Kudritzki, K.-H. Mantel, W. Meisl, B. Muschiello, H. Nicklas, G. Rupprecht, W. Seifert, O. Stahl, T. Szeifert, K. Tarantik: Successful Commissioning of FORS1 – the First Optical Instrument on the VLT **94**, 1
 A. Moorwood, J.-G. Cuby, P. Biereichel, J. Brynnel, B. Delabre, N. Devillard, A. Van Dijsseldonk, G. Finger, H. Gemperlein, R. Gilmozzi, T. Herlin, G. Huster, J. Knudstrup, C. Lidman, J.-L. Lizon, H. Mehrgan, M. Meyer, G. Nicolini, M. Petr, J. Spyromilio, J. Stegmeier: ISAAC Sees First Light at the VLT **94**, 7
 S. Stanghellini and A. Michel: Performance of the First Two Beryllium Secondary Mirrors of the VLT **94**, 10

NEWS FROM THE NTT

- G. Mathys: News from the NTT **91**, 21
 G. Mathys: News from the NTT **92**, 14

THE LA SILLA NEWS PAGE

- S. Guisard: Image Quality of the 3.6-m Telescope (Part VIII). New Seeing Record of 0.47" **91**, 24
 R. Gredel and P. Leisy: EFOSC2 and VLT Autoguider Commissioned at the 3.6-m Telescope **91**, 24
 Ph. Gitton and L. Noethe: Tuning of the NTT Alignment **92**, 15
 M. Kürster: CES Very Long Camera Installed **92**, 18
 J. Brewer and J. Andersen: Improving Image Quality at the Danish 1.54-m Telescope **92**, 18
 O.R. Hainaut: News from the NTT **93**, 16
 C. Lidman: SOFI Receives its First Users **93**, 16
 M. Sterzik: 3.6-m Telescope Passes Major Upgrade Milestones **93**, 17
 The 2p2team: 2.2-m Telescope Upgrade Started **93**, 19
 O.R. Hainaut: News from the NTT **94**, 11
 T. Augusteijn: 2.2-m Telescope Upgrade: a Status Report **94**, 12
 M. Kürster: Performance of CES 3.6-m Fibre Link and Image Slicers **94**, 12

VLT Data Flow Operations News

- D. Silva: The NTT Service Observing Programme: Period 60. Summary and Lessons Learned **92**, 20
 A. Moorwood: SOFI Infrared Images of the "NTT Deep Field" **92**, 25

ESO and ST-ECF Archive News

- B. Pirenne, M. Albrecht, B. Leibundgut: ESO and ST-ECF Archive News **93**, 20
 M. Albrecht: The VLT Data Volume **93**, 21
 B. Pirenne, M. Albrecht: Using DVD Technology for Archiving Astronomical Data **93**, 22
 M. Dolenski, A. Micol, B. Pirenne, M. Rosa: How the Analysis of HST Engineering Telemetry Supports the WFPC2 Association Project and Enhances FOS Calibration Accuracy **93**, 23
 B. Pirenne, B. McLean, B. Lasker: ST-ECF Participation in the GSC-II Generation Project **93**, 25
 M. Dolenski, A. Micol, B. Pirenne: HST Archive Services Implemented in Java **93**, 26
 A. Micol, D. Durand, S. Gaudet, B. Pirenne: HST Archive News: On the Fly Recalibration (OTF) of NICMOS and STIS Data **93**, 27
 A. Micol, B. Pirenne: HST Archive News: WFPC2 Associations **93**, 28

Observations with the Upgraded NTT

- P. Bonifacio and P. Molaro: Upgraded NTT Provides Insights Into Cosmic Big Bang **92**, 26
 R. Neuhauser, H.-C. Thomas, F.M. Walter: Ground-Based Detection of the Isolated Neutron Star RXJ185635-3754 at $V = 25.7$ Mag with the Upgraded NTT **92**, 27
 I. Burud, F. Courbin, C. Lidman, G. Meylan, P. Magain, A.O. Jaunsen, J. Hjorth, R. Ostensen, M.I. Andersen, J.W. Clasen, R. Stabell, S. Refsdal: RXJ0911.4+0551: A

- Complex Quadruply Imaged Gravitationally Lensed QSO **92**, 29

The Large Southern Array

- P.A. Shaver and R.S. Booth: The Large Southern Array **91**, 26
 A. Otárola, G. Delgado, R. Booth, V. Belitsky, D. Urbain, S. Radford, D. Hofstadt, L. Nyman, P. Shaver, R. Hills: European Site Testing at Chajnantor **94**, 13

SEST Upgrades and Reports from SEST Observers

- L.-Å. Nyman and A. Tieftrunk: SEST Upgrades **91**, 28
 F. Combes and T. Wiklind: Molecular Lines in Absorption at High Redshift **91**, 29
 P. Andreani: Using SEST to Probe the Geometry of the Universe **91**, 35
 R. Chini and E. Krügel: Cold Dust in Galaxies **91**, 37
 J. Lequeux: Carbon Monoxide in the Magellanic Clouds **91**, 41
 C. Henkel, Y.-N. Chin, R. Wielebinski, R. Mauersberger: Cool Gas in Southern Galaxies **91**, 45

Science with the VLT/VLTI

- L. Da Costa, E. Bertin, E. Deul, T. Erben, W. Freudling, M.D. Guarnieri, I. Hook, R. Hook, R. Mendez, M. Nonino, L. Olsen, I. Prandoni, A. Renzini, S. Savaglio, M. Scoddeggio, D. Silva, R. Slijkhuis, A. Wicenec, R. Wichmann, C. Benoist: The ESO Imaging Survey: Status Report and Preliminary Results **91**, 49
 A. Renzini: Après EIS **91**, 54
 M. Arnaboldi, M. Capaccioli, D. Mancini, P. Rafanelli, R. Scaramella, G. Sedmak, G.P. Vettolani: VST: VLT Survey Telescope **93**, 30

Reports from Observers

- J. Sanner, M. Geffert, H. Bönhardt, A. Fiedler: Astrometry of Comet 46P/Wirtanen at ESO: Preparation of ESA's ROSETTA Mission **92**, 33
 L. Binette, B. Jougnet, J.C.L. Wang, G. Magris C.: NTT Archives: the Lyman α Profile of the Radio Galaxy 1243+036 Revisited **92**, 37
 A.R. Tieftrunk, S.T. Megeath: Star Formation Toward the "Quiescent" Core NGC 6334 I(N) **93**, 36
 M. Rubio, G. Garay R. Probst: Molecular Gas in 30 Doradus **93**, 38
 H. Böhringer, L. Guzzo, C.A. Collins, D.M. Neumann, S. Schindler, P. Schuecker, R. Crudele, S. Degrandi, G. Chincarini, A.C. Edge, H.T. Macgillivray, P. Shaver, G. Vettolani, W. Voges: Probing the Cosmic Large-Scale Structure with the REFLEX Cluster Survey: Profile of an ESO Key Programme **94**, 21
 R.P. Mignani, S. Mereghetti, C. Gouffes and P.A. Caraveo: Timing, Spectroscopy and Multicolour Imaging of the Candidate Optical Counterpart of PSR B1509-58 **94**, 25
 F. Comerón, R. Neuhauser, A.A. Kaas: The First X-ray Emitting Brown Dwarf **94**, 28
 Call for Ideas for Future Public Imaging Surveys **94**, 31

Other Astronomical News

- Photos from Science Writers' Symposium **92**, 39
 B. Nordström: A Fresh Look at the Future: "La Silla 2000+" **93**, 42

- M.-P. Véron, G. Meylan: 6th ESO/OHP Summer School in Astrophysical Observations **93**, 43
 C. Madsen, R. West: Sea & Space – A Successful Educational Project for Europe's Secondary Schools **93**, 44
 M.-H. Ulrich: Observations with Adaptive Optics: Getting There **94**, 32
 C. Madsen: Award for the ESO VLT Project **94**, 38

Announcements

- ESO Studentship Programme **91**, 58
 Second Announcement of the ESO/ST-ECF Workshop on NICMOS and the VLT: A New Era of High-Resolution Near-Infrared Imaging and Spectroscopy **91**, 58
 List of ESO Scientific Preprints **91**, 58
 The 34th Liège International Astrophysics

- Colloquium "The Next-Generation Space Telescope – Science Drivers and Technological Challenges" **91**, 59
 Personnel Movements **91**, 59
 Joint Committee Between ESO and the Government of Chile for the Development of Astronomy in Chile **92**, 40
 L. da Costa and A. Renzini: ESO Imaging Survey: Update on EIS-deep and the Hubble Deep Field South **92**, 40
 ESO Fellowship Programme 1999 **92**, 41
 First Announcement of an "ESO Conference on Chemical Evolution from Zero to High Redshift" **92**, 42
 The Astronomical Almanac to be Revised **92**, 42
 List of Scientific Preprints (March-May 1998) **92**, 42
 Preliminary Announcement of an "ESO Workshop on Minor Bodies in the Outer Solar System" **92**, 43

- Personnel Movements (1 April – 30 June 1998) **92**, 43
 List of New ESO Publications **93**, 46
 Pierre Léna: Jean-Marie Mariotti (1955–1998) **93**, 47
 Personnel Movements **93**, 47
 Atlas of the Northern Sky **94**, 31
 ESO Director General to Become President of AUI **94**, 39
 First Announcement of the ESO Workshop on "Black Holes in Binaries and Galactic Nuclei – Their Diagnostics, Demography, and Formation" **94**, 39
 VLT Opening Symposium **94**, 40
 Personnel Movements (1 October – 31 December 1998) **94**, 41
 List of Scientific Preprints (September – December 1998) **94**, 41
 ESO Workshop Proceedings Still Available **94**, 41

AUTHOR INDEX

A

- M. Albrecht: The VLT Data Volume **93**, 21
 P. Andreani: Using SEST to Probe the Geometry of the Universe **91**, 35
 I. Appenzeller, K. Fricke, W. Fürtig, W. Gässler, R. Häfner, R. Harke, H.-J. Hess, W. Hummel, P. Jürgens, R.-P. Kudritzki, K.-H. Mantel, W. Meisl, B. Muschielok, H. Nicklas, G. Rupprecht, W. Seifert, O. Stahl, T. Szeifert, K. Tarantik: Successful Commissioning of FORS1 – the First Optical Instrument on the VLT **94**, 1
 M. Arnaboldi, M. Capaccioli, D. Mancini, P. Rafanelli, R. Scaramella, G. Sedmak, G.P. Vettolani: VST: VLT Survey Telescope **93**, 30
 T. Augusteijn: 2.2-m Telescope Upgrade: a Status Report **94**, 12

B

- D. Baade et al.: The Wide Field Imager for the 2.2-m MPG/ESO Telescope: a Preview **93**, 13
 P. Bonifacio and P. Molaro: Upgraded NTT Provides Insights Into Cosmic Big Bang **92**, 26
 L. Binette, B. Jougnet, J.C.L. Wang, G. Magris C.: NTT Archives: the Lyman α Profile of the Radio Galaxy 1243+036 Revisited **92**, 37
 H. Böhringer, L. Guzzo, C.A. Collins, D.M. Neumann, S. Schindler, P. Schuecker, R. Crudece, S. Degrandi, G. Chincarini, A.C. Edge, H.T. Macgillivray, P. Shaver, G. Vettolani, W. Voges: Probing the Cosmic Large-Scale Structure with the REFLEX Cluster Survey: Profile of an ESO Key Programme **94**, 21
 J. Brewer and J. Andersen: Improving Image Quality at the Danish 1.54-m Telescope **92**, 18
 I. Burud, F. Courbin, C. Lidman, G. Meylan, P. Magain, A.O. Jaunsen, J. Hjorth, R. Ostensen, M.I. Andersen, J.W. Clasen, R. Stabell, S. Refsdal: RXJ0911.4+0551: A Complex Quadruply Imaged Gravitationally Lensed QSO **92**, 29

C

- R. Chini and E. Krügel: Cold Dust in Galaxies **91**, 37
 F. Combes and T. Wiklind: Molecular Lines in Absorption at High Redshift **91**, 29
 F. Comerón, R. Neuhäuser, A.A. Kaas: The First X-ray Emitting Brown Dwarf **94**, 28
 J.G. Cuby and R. Gilmozzi: VIMOS and NIR-MOS: Status Report **91**, 16

D

- L. Da Costa, E. Bertin, E. Deul, T. Erben, W. Freudling, M.D. Guarnieri, I. Hook, R. Hook, R. Mendez, M. Nonino, L. Olsen, I. Prandoni, A. Renzini, S. Savaglio, M. Scodreggio, D. Silva, R. Slijkhuis, A. Wicenec, R. Wich-

mann, C. Benoist: The ESO Imaging Survey: Status Report and Preliminary Results **91**, 49

- L. da Costa and A. Renzini: ESO Imaging Survey: Update on EIS-deep and the Hubble Deep Field South **92**, 40
 S. D'Odorico: The New Direct CCD Imaging Camera at the NTT. SUSI2 gets the first FIERA CCD controller and a mosaic of two $2k \times 4k$, 15 μ pixel, thinned, anti-reflection coated EEV chips **91**, 14
 M. Dolenski, A. Micol, B. Pirenne, M. Rosa: How the Analysis of HST Engineering Telemetry Supports the WFPC2 Association Project and Enhances FOS Calibration Accuracy **93**, 23
 M. Dolenski, A. Micol, B. Pirenne: HST Archive Services Implemented in Java **93**, 26

G

- R. Giacconi: The Role of ESO in European Astronomy **91**, 1
 R. Giacconi: First Light of the VLT Unit Telescope 1 **92**, 2
 Ph. Gitton and L. Noethe: Tuning of the NTT Alignment **92**, 15
 R. Gredel and P. Leisy: EFOSC2 and VLT Autoguider Commissioned at the 3.6-m Telescope **91**, 24
 S. Guisard: Image Quality of the 3.6-m Telescope (Part VIII). New Seeing Record of 0.47" **91**, 24

H

- O.R. Hainaut: News from the NTT **93**, 16
 O.R. Hainaut: News from the NTT **94**, 11
 C. Henkel, Y.-N. Chin, R. Wielebinski, R. Mauersberger: Cool Gas in Southern Galaxies **91**, 45

K

- B. Koehler: ESO and AMOS Signed Contract for the VLTI Auxiliary Telescopes **93**, 11
 B. Koehler, F. Koch: UT1 Passes "With Honour" the First Severe Stability tests for VLTI **93**, 11
 M. Kürster: CES Very Long Camera Installed **92**, 18
 M. Kürster: Performance of CES 3.6-m Fibre Link and Image Slicers **94**, 12

L

- P.O. Lagage, Y. Rio, J.W. Pel, H. Toisma: VISIR at PDR **91**, 17
 B. Leibundgut, G. de Marchi, A. Renzini: Science Verification of the VLT Unit Telescope 1 **92**, 5
 Pierre Léna: Jean-Marie Mariotti (1955–1998) **93**, 47
 J. Lequeux: Carbon Monoxide in the Magellanic Clouds **91**, 41
 C. Lidman: SOFI Receives its First Users **93**, 16

M

- C. Madsen, R. West: Sea & Space – A Successful Educational Project for Europe's Secondary Schools **93**, 44
 C. Madsen: Award for the ESO VLT Project **94**, 38
 G. Mathys: News from the NTT **91**, 21
 G. Mathys: News from the NTT **92**, 14
 A. Micol, D. Durand, S. Gaudet, B. Pirenne: HST Archive News: On the Fly Recalibration (OTF) of NICMOS and STIS Data **93**, 27
 A. Micol, B. Pirenne: HST Archive News: WFPC2 Associations **93**, 28
 R.P. Mignani, S. Mereghetti, C. Gouffes and P.A. Caraveo: Timing, Spectroscopy and Multicolour Imaging of the Candidate Optical Counterpart of PSR B1509–58 **94**, 25
 A. Moorwood, J.-G. Cuby and C. Lidman: SOFI Sees First Light at the NTT **91**, 9
 A. Moorwood, J.-G. Cuby, P. Biereichel, J. Brynnel, B. Delabre, N. Devillard, A. Van Dijsseldonk, G. Finger, H. Gemperlein, R. Gilmozzi, T. Herlin, G. Huster, J. Knudstrup, C. Lidman, J.-L. Lizon, H. Mehrgan, M. Meyer, G. Nicolini, M. Petr, J. Spyromilio, J. Stegmeier: ISAAC Sees First Light at the VLT **94**, 7

N

- R. Neuhäuser, H.-C. Thomas, F.M. Walter: Ground-Based Detection of the Isolated Neutron Star RXJ185635-3754 at $V = 25.7$ Mag with the Upgraded NTT **92**, 27
 B. Nordström: A Fresh Look at the Future: "La Silla 2000+" **93**, 42
 L.-Å. Nyman and A. Tieftrunk: SEST Upgrades **91**, 28

O

- A. Otárola, G. Delgado, R. Booth, V. Belitsky, D. Urbain, S. Radford, D. Hofstadt, L. Nyman, P. Shaver, R. Hills: European Site Testing at Chajnantor **94**, 13

P

- R.G. Petrov, F. Malbet, A. Richichi, K.-H. Hofmann: AMBER, the Near-Infrared/Red VLTI Focal Instrument **92**, 11
 B. Pirenne, M. Albrecht, B. Leibundgut: ESO and ST-ECF Archive News **93**, 20
 B. Pirenne, M. Albrecht: Using DVD Technology for Archiving Astronomical Data **93**, 22
 B. Pirenne, B. McLean, B. Lasker: ST-ECF Participation in the GSC-II Generation Project **93**, 25

Q

- P. Quinn, J. Breysacher, D. Silva: First Call for Proposals **92**, 9

R

- A. Renzini: Après EIS **91**, 54
 M. Rubio, G. Garay, R. Probst: Molecular Gas in 30 Doradus **93**, 38

ESO, the European Southern Observatory, was created in 1962 to "... establish and operate an astronomical observatory in the southern hemisphere, equipped with powerful instruments, with the aim of furthering and organising collaboration in astronomy ..." It is supported by eight countries: Belgium, Denmark, France, Germany, Italy, the Netherlands, Sweden and Switzerland. ESO operates at two sites. It operates the La Silla observatory in the Atacama desert, 600 km north of Santiago de Chile, at 2,400 m altitude, where fourteen optical telescopes with diameters up to 3.6 m and a 15-m submillimetre radio telescope (SEST) are now in operation. In addition, ESO is in the process of building the Very Large Telescope (VLT) on Paranal, a 2,600 m high mountain approximately 130 km south of Antofagasta, in the driest part of the Atacama desert. The VLT consists of four 8.2-metre and several 1.8-metre telescopes. These telescopes can also be used in combination as a giant interferometer (VLTi). "First Light" of the first 8.2-metre telescope (UT1) occurred in May 1998. UT1 will be available on a regular basis for astronomical observations from April 1999 on. Over 1000 proposals are made each year for the use of the ESO telescopes. The ESO Headquarters are located in Garching, near Munich, Germany. This is the scientific, technical and administrative centre of ESO where technical development programmes are carried out to provide the La Silla and Paranal observatories with the most advanced instruments. There are also extensive astronomical data facilities. In Europe ESO employs about 200 international staff members, Fellows and Associates; in Chile about 70 and, in addition, about 130 local staff members.

The ESO MESSENGER is published four times a year: normally in March, June, September and December. ESO also publishes Conference Proceedings, Preprints, Technical Notes and other material connected to its activities. Press Releases inform the media about particular events. For further information, contact the ESO Education and Public Relations Department at the following address:

EUROPEAN
SOUTHERN OBSERVATORY
Karl-Schwarzschild-Str. 2
D-85748 Garching bei München
Germany
Tel. (089) 320 06-0
Telefax (089) 3202362
ips@eso.org (internet)
URL: <http://www.eso.org>

The ESO Messenger:
Editor: Marie-Hélène Demoulin
Technical editor: Kurt Kjär

Printed by
Druckbetriebe Lettner KG
Georgenstr. 84
D-80799 München
Germany

ISSN 0722-6691

S

- J. Sanner, M. Geffert, H. Böhnhardt, A. Fiedler: Astrometry of Comet 46P/Wirtanen at ESO: Preparation of ESA's ROSETTA Mission **92**, 33
M. Sarazin: Astroclimate During Science Verification **93**, 2
P.A. Shaver and R.S. Booth: The Large Southern Array **91**, 26
D. Silva: The NTT Service Observing Programme: Period 60. Summary and Lessons Learned **92**, 20
S. Stanghellini and A. Michel: Performance of the First Two Beryllium Secondary Mirrors of the VLT **94**, 10
M. Stertzik: 3.6-m Telescope Passes Major Upgrade Milestones **93**, 17

T

- M. Tarengi, P. Gary, J. Spyromilio, R. Gilmozzi: The First Steps of UT1 **93**, 4
A. R. Tieftrunk, S. T. Megeath: Star Formation Toward the "Quiescent" Core NGC 6334 I(N) **93**, 36

U

- M.-H. Ulrich: Observations with Adaptive Optics: Getting There **94**, 32

V

- M.-P. Véron, G. Meylan: 6th ESO/OHP Summer School in Astrophysical Observations **93**, 43

W

- R.M. West: VLT First Light and the Public **92**, 4

Contents

I. Appenzeller, K. Fricke, W. Fürtig, W. Gässler, R. Häfner, R. Harke, H.-J. Hess, W. Hummel, P. Jürgens, R.-P. Kudritzki, K.-H. Mantel, W. Meisl, B. Muschelok, H. Nicklas, G. Rupprecht, W. Seifert, O. Stahl, T. Szeifert, K. Tarantik: Successful Commissioning of FORS1 – the First Optical Instrument on the VLT	1
A. Moorwood, J.-G. Cuby, P. Biereichel, J. Brynnel, B. Delabre, N. Devillard, A. Van Dijsseldonk, G. Finger, H. Gemperlein, R. Gilmozzi, T. Herlin, G. Huster, J. Knudstrup, C. Lidman, J.-L. Lizon, H. Mehrgan, M. Meyer, G. Nicolini, M. Petr, J. Spyromilio, J. Stegmeier: ISAAC Sees First Light at the VLT	7
News from VLT Science Verification	9

TELESCOPES AND INSTRUMENTATION

S. Stanghellini and A. Michel: Performance of the First Two Beryllium Secondary Mirrors of the VLT	10
--	----

THE LA SILLA NEWS PAGE

O.R. Hainaut: News from the NTT	11
T. Augusteijn: 2.2-m Telescope Upgrade: a Status Report	12
M. Kürster: Performance of CES 3.6-m Fibre Link and Image Slicers	12

NEWS FROM THE LSA

A. Otárola, G. Delgado, R. Booth, V. Belitsky, D. Urbain, S. Radford, D. Hofstadt, L. Nyman, P. Shaver, R. Hills: European Site Testing at Chajnantor ..	13
--	----

REPORTS FROM OBSERVERS

H. Böhringer, L. Guzzo, C.A. Collins, D.M. Neumann, S. Schindler, P. Schuecker, R. Cruddace, S. Degrandi, G. Chincarini, A.C. Edge, H.T. Macgillivray, P. Shaver, G. Vettolani, W. Voges: Probing the Cosmic Large-Scale Structure with the REFLEX Cluster Survey: Profile of an ESO Key Programme	21
R.P. Mignani, S. Mereghetti, C. Gouiffes And P. A. Caraveo: Timing, Spectroscopy and Multicolour Imaging of the Candidate Optical Counterpart of PSR B1509–58	25
F. Comerón, R. Neuhauser, A.A. Kaas: The First X-ray Emitting Brown Dwarf Call for Ideas for Future Public Imaging Surveys	31
Atlas of the Northern Sky	31

OTHER ASTRONOMICAL NEWS

M.-H. Ulrich: Observations with Adaptive Optics: Getting There	32
C. Madsen: Award for the ESO VLT Project	38

ANNOUNCEMENTS

ESO Director General to Become President of AUI	39
First Announcement of the ESO Workshop on "Black Holes in Binaries and Galactic Nuclei – Their Diagnostics, Demography, and Formation"	39
VLT Opening Symposium	40
Personnel Movements (1 October – 31 December 1998)	41
List of Scientific Preprints (September–December 1998)	41
ESO Workshop Proceedings Still Available	41

MESSENGER INDEX 1998 (Nos. 91–94)	42
---	----